Sublethal effects of nanodiamonds and copper oxide on the freshwater shrimp, *Caridina africana*

NS Donough

orcid.org 0000-0002-4090-3373

Dissertation accepted in fulfilment of the requirements for the degree *Master of Science in Environmental Sciences* at the North-West University

Supervisor: Prof V Wepener

Co-supervisor: Dr TL Botha

Graduation July 2023

36065625

ACKNOWLEDGEMENTS

Being the first in my family to set my sights on post graduate studies, achieving it has been a life-changing blessing. I owe it all to my family, supervisors, NWU and to the NRF.

To my supervisors, Prof. Wepener and Dr. Botha. It has been a privilege to complete this degree under your guidance and support. Thank you for your mentorship and advice for the past two years that I will carry with me wherever I go. Thank you for believing in me and standing by me especially when everything began to feel too much. It got a little bit intense with the submission date drawing near, and would like to express my appreciation for the valuable feedback and assistance I received during this critical time. Without your valuable guidance, this dissertation would not be possible. I am truly appreciative for having you as my supervisors.

I would also like to thank the following entities/people at North-West University:

- To the preclinical drug development program (PCDDP) for the use of their Malvern ZetaSizer machine to obtain my DLS data.
- A huge thank you to the NABF personnel for allowing me to make use of their exposure rooms and equipment for the completion of this project.
- Thank you to the Water Research Group for the countless opportunities to grow and work towards equipping myself for the academic future, in addition to the conferences/workshops attended where we were able to present our findings on a national scale.
- Armagh Cook, thank you for your assistance, kindness and patience throughout this project.
- Dr. Hannes Erasmus, thank you for helping me with my results that required the AAS, and for always being hands-on, especially when the deadlines were creeping up and load shedding was not on our side for analysis.
- Dawid Coetsee, thank you for taking me sampling every time I'd ask and your willingness to help me sample. I truly appreciate your assistance and the time you would take out of your days to assist me.
- To Dr. Ilse du Preez, Monique Opperman and Luciano Willemse, thank you for your assistance and guidance with metabolomics.

- Thank you Artimisia Monjane-Mabuie and Coret van Wyk for your assistance in DNA/RNA extractions.

To my pillars of strength, my mom and dad. Thank you everything, for raising me to become the person I am today, for teaching me to shoot for the stars and for the sacrifices you've made for me to better myself. Your endless love and support are something I will cherish forever, and I am truly blessed to have you as my parents. A special thank you to my mom for always being there for me and for keeping me on track in the last few months of my write-up, you are my rock. To my brother, Leigh. Thank you for your words of wisdom when I really needed it, you truly are a blessing.

Thank you to God for continuing to give me the strength when I felt I couldn't carry on anymore, as well as blessing me with the opportunity to further my studies, and for allowing my path to cross with the wonderful individuals mentioned above.

Lastly, thank you to the National Research Foundation of South Africa (NRF). The financial assistance provided from the NRF is hereby acknowledged. This work is based on the research supported wholly by the National Research Foundation of South Africa (Grant UID: 131599). We acknowledge that any opinions, findings and conclusions or recommendations expressed in this dissertation generated by the NRF supported research, are those of the authors and are not necessarily attributed to the NRF. The NRF accepts no liability whatsoever in this regard. I would also like to extend thanks to the South African Department of Science and Innovation for making this research possible.

ABSTRACT

Nanomaterials are defined as materials where one dimension is sized 1 nm – 100 nm and are emerging technologies that are used for the benefit of mankind. Two noteworthy materials include nanodiamonds (NDs) and nano copper oxide (nCuO) as they have intrinsic properties that make them appealing for their uses in the medical and agricultural fields. However, once in an aquatic environment, they can negatively affect the organisms that inhabit it. The effects that contaminants exert on aquatic organisms can be organized into adverse outcome pathways (AOP), starting from the first anchor point, where the organism is affected on a molecular level, and in turn how this molecular initiating event is responsible for any changes in their physiological processes, influencing an apical endpoint within the organism or its population. Although these pathways are available for various contaminants, they are still scarce for nanomaterials. This study aimed to construct an AOP for NDs and nCuO and copper chloride for the freshwater shrimp, *Caridina africana*. Firstly, *C. africana* were acutely exposed to sublethal concentrations (LC_{10} and LC_{20}) of two nanomaterials and copper ion to assess the sublethal effects on the shrimp's physiological processes, such as their respiration rate, heart rate as well as behaviour. Thereafter, chronic toxicity tests were carried out to determine mortality rates after long-term exposure. The shrimp were subjected to metabolomic analyses to determine the anchor point responsible for the physiological changes exerted. Of the two nanomaterials, nCuO was more toxic than NDs at sublethal concentrations. The toxicity was expressed throughout the altered physiological processes, such as elevated respiration rates, decreased heart rate and reduced locomotor activity. The nCuO toxicity can be attributed to its particle size, agglomeration potential that results in the uptake of the particle, its adherence to the external surface of the shrimp and the uptake of copper ions following dissolution from the material by the shrimp. This resulted in nCuO causing the generation of reactive oxygen species. The copper chloride's toxicity resulted in an increase for all physiological endpoints. Its toxicity can also be caused by the dissolution of copper ions, which accumulates in the shrimp and generates reactive oxygen species, altering their physiological processes. Nanodiamonds toxicity is attributed to the same parameters as nCuO, and although considered inert, it caused the generation of reactive oxygen species, resulting in an elevated respiration rate and a decrease in locomotor activity. The different nanomaterials' effects on the endpoints were related to their physicochemical characteristics. These hierarchical biological responses were successfully integrated into the AOP construct.

Keywords: Nanomaterials, Nanotoxicology, Aquatic invertebrates, Adverse outcome pathways, Metabolomics, Physiology, Behaviour.

ABBREVIATIONS

Abbreviation	Description
% O_2	Percentage dissolved oxygen
°C	Degrees Celsius
µg/L	Microgram per litre
µL	Microlitre
ANOVA	Analysis of variance
AO	Adverse outcome
BPM	Beats per minute
$CaCl_2$	Calcium chloride
cm	Centimetre
Cu	Copper
$CuCl_2$	Copper chloride
DLS	Dynamic light scattering
g	Grams
GF-AAS	Graphite furnace atomic absorption spectrometry
h/hr	Hours
HCl	Hydrochloric acid
HNO_3	Nitric acid
KCl	Potassium chloride
KEs	Key events
LC	Lethal concentration
mg/L	Milligram per litre
$MgSO_4$	Magnesium sulphate
MIE	Molecular initiating event

min	Minutes
mL	millilitre
NABF	National aquatic bioassay facility
NaCl	Sodium chloride
nCuO	nano Copper oxide
NDs	Nanodiamonds
NMs	Nanomaterials
PLS-DA	Partial least square discriminant analysis
ROS	Reactive oxygen species
TEM	Transmission electron microscopy
VIP	Variable importance of projection
ZP	Zeta potential

TABLE OF CONTENTS

LIST OF TABLES

LIST OF FIGURES

CHAPTER 1 INTRODUCTION AND PROBLEM STATEMENT

1.1 Nanomaterials

Heiligtag & Niederberger (2013) reported that the use of nanotechnology first occurred in the fourth century to generate a glass cup that changes colours under different lighting conditions, using silver, gold and copper nanoparticles for this historic piece, indicating that nanomaterials (NMs) are the building blocks for this technology. Nanotechnology is considered one of the most promising technologies in the 21st century, and is used for the benefit of mankind through medical, agricultural and architectural applications, such as nano drugs and diagnostic tools, nano pesticides and surface coatings due to their unique properties (Pacheco-Torgal & Jalali, 2011; Nikalje, 2015; Bayda *et al*., 2019; Fadiji *et al*., 2022).

Nanomaterials can be produced anthropogenically (engineered/incidental) or found naturally. Anthropogenic NMs are produced via: industrial activities, construction sites, welding fumes, combustion particulates, roads, traffic and exhaust emissions, brake pads and fuel additives. These activities can produce metal oxides (e.g. Manganese, Iron, Copper, Zinc, Nickel, Aluminium, Cobalt and Titanium) nanoparticles (Sadik, 2013; Dolez, 2015; Jeevanandam *et al.*, 2018; Barhoum *et al*., 2022; Wang *et al*., 2022a). Naturally occurring NMs can be formed by volcanic activity, forest fires, weathering and other biogeochemical processes (Dolez, 2015; Jeevanandam *et al.*, 2018; Hochella *et al.*, 2019; Lespes *et al.*, 2020; Barhoum *et al*., 2022).

In nanomaterial engineering, there are two approaches to NM production: breakdown (top-down) or bottom-up. A top-down approach reduces the structural size of the materials towards the nanoscale, whereas a bottom-up approach is the formation of larger nanostructure from tiny atoms/molecules (*see Figure 1.1*) (Iqbal *et al.*, 2012; Suresh, 2013; Arole & Munde, 2014; Habiba *et al.*, 2014; Rawat, 2015; Ovais *et al.*, 2017; Singh *et al.*, 2020a; Abid *et al.*, 2022).

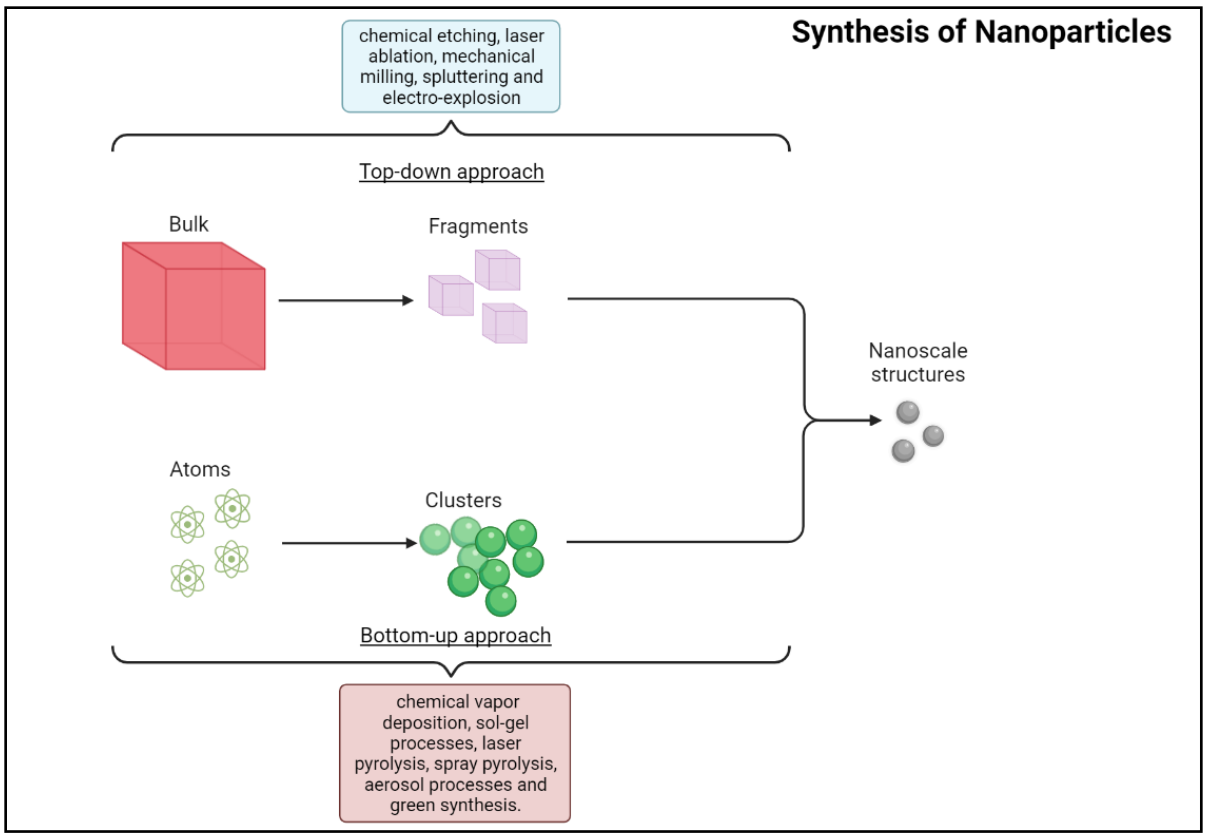

Figure 1.1 Approaches and processes utilized in the synthesis of nanoparticles**.**

As summarized from the European Commission (2022), a nanomaterial needs to fulfil at least one of the following criteria: 1) the particle has one or more external dimensions within 1 nm – 100 nm, 2) the particle has an elongated shape, like a rod, fibre or tube where two external dimensions are smaller than one nm and the other dimension is greater than 100 nm, 3) the particle has a plate-like shape where the dimensions fall within the same category as point 2.

They can be classified based on either their dimensions or their composition. For dimensions, there are four types: 0-D, 1-D, 2-D, or 3-D. For composition, there are also four types, such a carbon, metal, semi-conductor, or nanocomposite (*Figure 1.2*). *Figure 1.2.* shows the different categories that are used to classify nanomaterials Do & Pham (2010); Kim *et al.* (2012); Sweet *et al.* (2012); Cha *et al.* (2013); Kitching *et al.* (2013); Suresh (2013); Vitiello *et al.* (2015); Chen *et al.* (2018a); Chen *et al.* (2018b); Poh *et al.* (2018); Ghassan *et al.* (2019); Khan (2019); Neupane *et al.* (2019); Patel *et al.* (2019); Bertolacci *et al.* (2020); Din *et al.* (2020); Ebina *et al.* (2020); Singh *et al.* (2020a); Wang *et al.* (2020a); Yaqoob *et al.* (2020); Sabzehmeidani *et al.* (2021); Xu *et al.* (2021); Zuo *et al.* (2021); Abid *et al.* (2022), such as dimensions and composition.

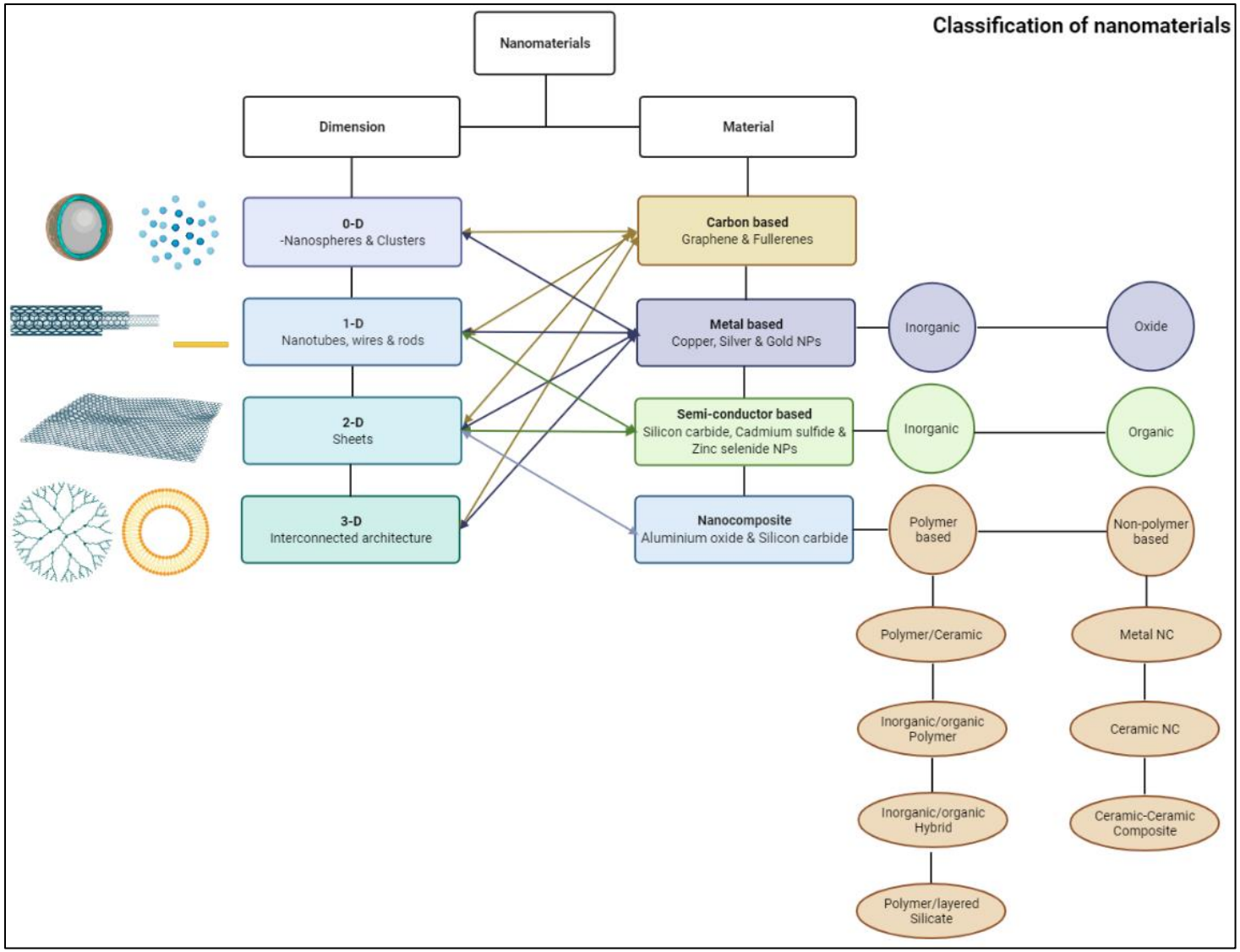

Figure 1.2 Classifications of nanomaterials based off their dimensions and composition.

Nanoparticles have various intrinsic properties (*see Table 1.1.*) which include: optical, electrical, mechanical, magnetic and thermodynamic properties which affects their application.

Due to the properties of NMs, nanotechnology has found many uses in agriculture, environmental and architectural applications, as well as for drug delivery and diagnostic tools in medicine. As with most emerging technologies, they have both advantages and disadvantages as outlined in *Table 1.2* (Anık *et al.*, 2019; Ghadimi *et al.*, 2020; Mushtaq *et al.*, 2020).

.

Table 1.1 Intrinsic properties of nanomaterials, how to measure the properties and what they are used for:

Property:	**Definition:**	**How their properties are affected:**	**Methods used to determine property:**	**Applications:**	**Reference(s):**
Optical	Optical absorption and fluorescence properties. It is dependent on size, shape and surface of NM Absorption and scattering of light	Dependent on surface atoms, electronic structure and size – specifically the quantum effect and surface plasmon resonance	Carlo method and spectroscopic techniques	Biological, cell imaging and photo thermal therapeutic applications	(Bhagyaraj & Oluwafemi, 2018; Adewuyi & Lau, 2021; Pooja *et al.*, 2021; Sahoo, 2022).
Electrical	Electrical conductivity, photoconductivity, and resistance	Dependent on size, NMs can exhibit great electrical conductivity properties when compared to their bulk counterparts.	Lennard Jones potential	Batteries, diodes and lasers	(Matsui, 2005; Min *et al.*, 2019; Coetzee *et al.*, 2020).
Mechanical	Toughness, hardness, super plasticity, brittleness, rigidity, ductility and porosity.	Dependent on size, as NMs can exhibit great mechanical properties that are not present within their bulk counterparts	Van der Waals forces, capillary forces, electrostatic forces, solvation and structural and hydration forces	Surface engineering and tribology	(Guo *et al.*, 2013; Wu *et al.*, 2020a; Adewuyi & Lau, 2021).

Magnetic	Magnetic properties due to electronic distribution (supermagnetism/superparamagnetic)	A non-magnetic element can become magnetic at a nanoscale.	Vibrating sample magnetometer / Direct current magnetometry techniques	MRI contrast, tissue repair and immunoassay of biological fluids	(Lu *et al.*, 2007; Akbarzadeh *et al.*, 2012; Guo *et al.*, 2013; Adewuyi & Lau, 2021; Arosio, 2021).
Thermal/Melting/ Thermodynamic	Melting entropy, enthalpy & melting point. This property gives rise to the stability of a NM suspension.	Dependent on size and shape. Melting point and melting entropy of nanofilms are greater than that of nanowires and for nanowires greater in size than the nanoparticles of the same material. Nanoscale materials have a large surface to volume ratio than their bulk counterparts, thus altering their thermal/thermodynamic properties	X-ray diffraction / electron diffraction can be used to determine this property and transmission electron microscopy	Thermal therapy	(Gao & Gu, 2015; (Kareem & Mawllod, 2020).

Table 1.2 Various uses of nanotechnology, examples and their advantages and disadvantages.

Use	Product/s	Nanomaterial	Advantages	References
Agricultural	Nanopesticides Nanofertilizers	Carbon-based Titanium dioxide	Controlled release, prevents premature degradation, enhance efficacy over a long time, lesser need for application	Prasad *et al.*, 2017; Jose & Krishnankutty, 2018; Mwaanga, 2018; He *et al.*, 2019; Shang *et al.*, 2019; Fadiji *et al.*, 2022).
Architectural	Steel Drywall Coatings	Nanocomposites/Copper oxide Nano-gypsum Titanium dioxide/Carbon-based	Stronger, free of corrosion, lighter, resistant to mould	(Pacheco-Torgal & Jalali, 2011; Niroumand *et al.*, 2013; El Alfy *et al.*, 2021).
Medical	Biosensors Drug delivery Medical Imaging (MRI)	Carbon nanotubes/Gold nanoparticles Abraxane/Nanodiamond Metal oxides/Quantum dots	Highly sensitive, ultrafast, biocompatible and highly stable, site specific delivery and controlled drug release	(Sun *et al.*, 2008; Boisseau & Loubaton, 2011; Gardner, 2015; Patra *et al.*, 2018; Zhou *et al.*, 2018; Farzin *et al.*, 2020; Siddique & Chow, 2020; Yazdi *et al.*, 2020; Sim & Wong, 2021).
Cosmetics	Sunscreen Lipstick Mascara	Zinc oxide/Titanium oxide Silicon dioxide Carbon black	Site-specificity, biocompatibility, transparency, long-lasting effects and stability	(Katz, 2007; Raj *et al.*, 2012; Effiong *et al.*, 2020; Fytianos *et al.*, 2020; Yadwade *et al.*, 2021; Gupta *et al.*, 2022).

1.2 Nanomaterials in Aquatic Environments

The continuous use of nanotechnology allows for it to be released into the environment. Since NMs are the building blocks for nanotechnology, this results in them being commercially available and continually developed. This then leads to its increased usage, thus allowing it to be discharged more frequently into aquatic environments through: direct entry, agrochemical spray drift, precipitation, emissions, wastewater treatment plants and industrial waste (Batley *et al.*, 2013; Renzi & Guerranti, 2015; Malakar *et al.*, 2021; Moloi *et al.*, 2021). This is an issue as bioaccumulation within aquatic organisms can occur and this may lead to biomagnification within the food web (Uddin *et al.*, 2020; Kuehr *et al.*, 2021a).

NMs can exert toxic effects on the organisms once it enters their habitats. The toxicity of a NM is dependent on a multitude of factors (*see Figure 1.3.*).

Figure 1.3 Characteristics of NMs. *Abbreviations used are Dissoln = Dissolution, Conc = Concentration, Agglom = Agglomeration.

It is noted that smaller sized NMs are more toxic than larger sized NMs. This is because the former can be transported into an organism's cells and tissues as a smaller size results in an increase in the percentage of atoms on the surface. These atoms drive the reactivity of the NMs (Sharifi *et al.*, 2012; Ovissipour *et al.*, 2013; Jennings *et al.*, 2015; Liu *et al.*, 2022).

The surface chemistry of a NM affects its catalytic activity, its ability to generate reactive species as well as its general cytotoxicity (Ovissipour *et al.*, 2013). The charge on the NMs surface relates to the surface chemistry and is also affected by the physicochemical properties of the media (Liu *et al.*, 2022). It is noted that the surface charge influences the absorption of ions and biomolecules that can affect the organism's response to the particle – selective adsorption, and ability to cross the blood-brain barrier (Sharifi *et al.*, 2012; Savage *et al.*, 2019; Sreya & Chitra, 2021). The surface charge of a NM plays a critical role in the aggregation of NMs, thus affecting its colloidal behaviour (Sharifi *et al.*, 2012; Jennings *et al.*, 2015).

Nanomaterials have different shapes, such as spheres, tubes, rings and fibres. Augustine & Hasan (2020) had reported that rod shaped NMs are more efficient in uptake than spherical shaped NM, due to their ability to effectively bind on cells, as the latter do not have many binding sites available to interact with the surface of cells (due to its curvature, leading to decreased surface available in comparison to rod shaped NMs) (Chowdhury *et al.*, 2019).

Sreya & Chitra (2021) reported that the pH, ionic strength, salinity, temperature, and dissolved oxygen of the medium can affect the charge of the NMs surface. It also influences the membrane permeability in organisms and affects the toxicity in cellular uptake pathways. It can also affect the agglomeration rate of the NM and its ability to adhere to an organism's tissue surface (Sharifi *et al.*, 2012; Ovissipour *et al.*, 2013).

Polyethylene glycol (PEG) is a coating used for some NMs. It is a steric stabiliser that aids in the NMs dispersion, but it can also affect the NM's stability in an aquatic environment, which in turn can affect the toxicity of the nanoparticle (Jennings *et al.*, 2015; Savage *et al.*, 2019; Liu *et al.*, 2022). Sharifi *et al.* (2012) noted that coatings can prevent dissolution of a NM, resulting in no release of toxic ions which make up the NM core. Coatings can also modify the surface charge of a NM, making it more toxic by altering its physicochemical properties (Sharifi *et al.*, 2012; Sreya & Chitra, 2021).

Avramescu *et al.* (2020) explains that solubility affects the stability of the NM in the biological media, influencing the agglomeration of the NM, which affects its interaction with the cells and the biological response.

Avramescu *et al.* (2020) states that metal based NMs can cause adverse responses due to either the metal ions released from the NM, and the dissolution can be influenced by the constituents of the exposure medium. If nanoscale particles are soluble, they will dissolute. Depending on a low or high surface dose, it can form toxic or non-toxic constituents, which can result in potential injury and/or excretion (Borm *et al.*, 2006).

The toxicity of NMs do no follow traditional dose dependency. At high concentrations, the NMs can result in high mortalities, but also have higher agglomeration rates, thereby less interaction with the organism. At low concentrations, sublethal effects occur, and these usually include physiological changes, but not mortality (Ovissipour *et al.*, 2013).

Nanomaterials undergo transformations to lower their surface energies. Agglomeration is a common form of this transformation (Egbuna *et al.*, 2021; Liu *et al.*, 2022). Agglomeration and aggregation are a process in which the primary nanoparticles generate a group of secondary nanoparticles, but agglomerates rely on van der Waals forces or electrostatic forces – weak interactions – whereas aggregates is the end result of agglomeration over a long period of time. This then results in aggregates being fused together by metallic or covalent bonds – strong interactions, making aggregation dependent on collision frequency and attachment efficiency (Bruinink *et al.*, 2015; Liu *et al.*, 2022). Collision frequency is dependent on the Brownian motion and differential settling (Floyd *et al.*, 2017). Agglomeration and/or aggregation is dependent on the exposure medium conditions, such as pH. It has been noted that the formation of larger aggregates results in reduced cell uptake due to its larger size and reduced surface area (Liu *et al.*, 2022). Another important phenomenon regarding agglomeration/aggregation potential is the Derajun-Landau-Verwey-Overbeek theory (DLVO). It refers to the interactions between colloidal particles and the aggregation behaviour of nanoparticles. It incorporates repulsive and attractive forces due to either van der Waal's attractive potential and Born's repulsive potential (Muneer *et al.*, 2020).

When NMs are present in a medium, biomolecules present within the media are able to adsorb onto the nanoparticle, forming a protein shell, which is then known as a protein corona (González-García *et al.*, 2022). This adsorption is aided by various forces that include hydrogen bonds and van der Waal's forces (Saptarshi *et al.*, 2013). Protein coronas result in the modification of a NMs physicochemical properties (Saptarshi *et al.*, 2013; Park, 2020; González-García *et al.*, 2022). For example, a NM that has a greater surface charge, will in turn attract more proteins (González-García *et al.*, 2022). Thus, the formation of protein coronas is dependent on the surface chemistry of the NM (Park, 2020). A protein corona can either increase or decrease the immune response of an organism (González-García *et al.*, 2022). A weakly bound layer is a soft corona and this is reversible, whereas a strongly bound layer is a hard corona, which is irreversible (Saptarshi *et al.*, 2013; Park, 2020).

1.3 Characterisation of Nanomaterials

There are techniques available to characterize NMs, which can aid in determining their properties that can give rise to their toxicity (*Figure 1.4*).

a) Transmission Electron Microscopy (TEM)

A beam of electrons is transmitted through a thin sample, interacting with it. This forms an amplitude contract image and the image can be magnified through the magnifying lens and focused/projected onto an imaging device (Kalantar-zadeh & Fry, 2008; Heera & Shanmugam, 2015; Boddolla & Thodeti, 2018; Joshi *et al.*, 2020; Malatesta, 2021).

Transmission electron microscopy reveals information about a NMs morphology and particle size distribution. This characterization technique is useful as it is able to focus on one nanoparticle in a sample, and can thus identify and quantify the nanoparticles chemical and electronic structure (Kalantar-zadeh & Fry, 2008). Since the physical and chemical components of NMs are dependent on their composition and structures, thus TEM is able to assist with that visualization and understanding (Kalantar-zadeh & Fry, 2008).

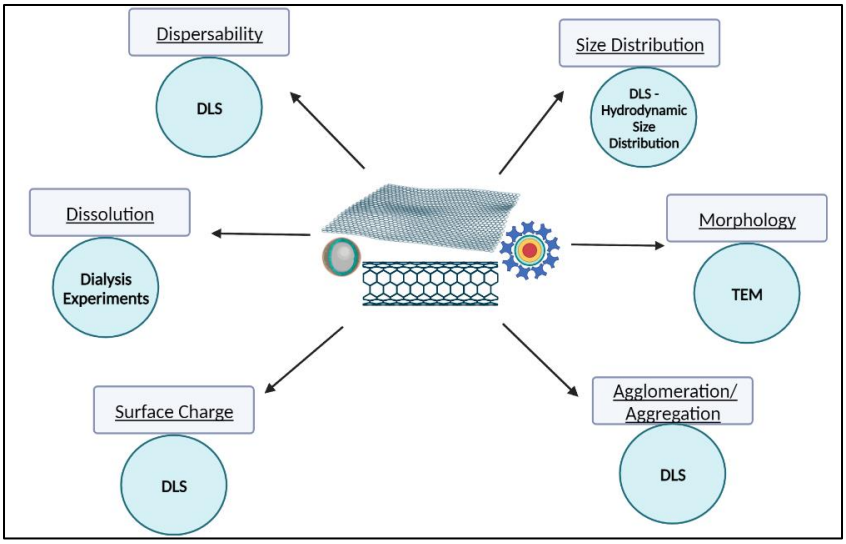

Figure 1.4 Characterisation techniques for determining the properties of nanomaterials, such as their size, shape, dissolution and agglomeration potential. *Abbreviations used are DLS = dynamic light scattering and TEM = transmission electron microscopy.

b) Dynamic Light Scattering (DLS)

The NM suspension is exposed to a beam of light. As the light reaches the sample, the intensity and direction of the light beam changes due to “scattering”. It can determine the hydrodynamic size distribution and the state of aggregation of the NM suspension (Kalantar-zadeh & Fry, 2008; Lim *et al.*, 2013; Joshi *et al.*, 2020). It is based off the Brownian motion of the nanoparticles – since the particles are constantly colliding with one another, energy is transferred inducing particle movement (Joshi *et al.*, 2020).

The DLS technique has a short measuring time, is non-invasive, not labour intensive and is extremely sensitive to towards small aggregates (Lim *et al.*, 2013; Joshi *et al.*, 2020). Thus, the aggregation state of NMs can be determined with this technique (Dhas *et al.*, 2018). It also assists with determining the surface charge of nanoparticles, by adding a solution to a folded capillary cell with two gold electrodes. When a voltage is supplied to the electrode, the particles will flow towards the electrode with the opposite charge (Raval *et al.*, 2019). This provides important information pertaining to the possible toxicity of the NM suspension being tested by evaluating the nanomaterial’s stability in a suspension, as well as confirming their size and surface charge, which is useful when looking at their interactions with biomolecules.

c) Dissolution

Clark *et al.* (2019) stated that dissolution can be determined by conducting dialysis experiments. It can be measured with atomic spectroscopy techniques, such as atomic absorption spectrometry (AAS) or inductively coupled plasma mass spectrometry (ICP-MS) (Hondow *et al.*, 2015; Zhang *et al.*, 2015). The dissolution rate provides information as to how a particle may interact with its biological and/or environmental components (Utembe *et al.*, 2015). If ions are released at a fast rate, the short-term toxic effect would be the same as the ionic form. On the other hand, if the ions are released at a slow rate, the more likely the chances that the adverse effects exhibited by the organism will be due to the particle itself (Utembe *et al.*, 2015; Zhang *et al.*, 2015). There are factors that influence the dissolution of a NM and these include all the factors mentioned in *Figure 1.4.* (Hondow *et al.*, 2015; Zhang *et al.*, 2015). Dissolution of a NM is important because it can affect cellular uptake, uptake pathway as well as mechanism of toxicity (Hondow *et al.*, 2015; Utembe *et al.*, 2015; Sohal *et al.*, 2018). Also, dissolution can still occur once within a cell (Utembe *et al.*, 2015).

d) CytoViva® Enhanced Darkfield Hyperspectral Microscopy

CytoViva® enhanced darkfield hyperspectral microscopy is used for the detection and characterization of engineered nanoparticles (Badireddy *et al.*, 2012). Scattered light from the organism enters the objective and forms an image (SoRelle *et al.*, 2016). The light scattered from the particles passes the objective, and this leads to a clear and dark background with bright appearing objects (Ishmukhametov & Fakhrullin, 2021). Using hyperspectral microscopy has been noted to identify both intracellular and extracellular nanoparticle clusters (Roth *et al.*, 2015).

1.4 Selection of nanomaterials used in this study.

Various types of NMs exist in anthropogenic activities and as mentioned in *Table 1.2,* examples of everyday nanomaterials includes nanodiamonds (NDs) and nano copper oxide (nCuO). Nanodiamonds are inert, but can still be functionalized, whereas nCuO toxicity can occur through the release of copper (Cu) ions (van der Laan *et al.*, 2018; Naz *et al.*, 2020).

a) Nanodiamonds (NDs):

Nanodiamonds are an example of a carbon-based NM (Lai *et al.*, 2020). They are a tetrahedral network with carbon as their core and can have various functional groups (Fusco *et al.*, 2020). They are usually produced through methods of detonation, high temperature-high pressure

milling, chemical vapor deposition as well as laser ablation (Basso *et al.*, 2020; Fusco *et al.*, 2020; Lai *et al.*, 2020). These specific NMs are known to have exceptional mechanical, optical and thermal properties as well as tuneable surface properties that make them suitable for biomedical applications, such as bioimaging and drug delivery (Domínguez *et al.*, 2018; Basso *et al.*, 2020; Fusco *et al.*, 2020; Qin *et al.*, 2021). They also find applications in tribology, cosmetics and sunscreen formulations, and have superior biocompatibility when compared to other nanocarbon materials, such as carbon nanotubes (Basso *et al.*, 2020; Fusco *et al.*, 2020; Qin *et al.*, 2021).

Nanodiamonds can be enhanced with PEG by covalent surface functionalization to increase its colloidal stability (Jung & Neuman, 2021). Polyethylene glycol is a hydrophilic polymer that is able to change the charge and chemistry of the NDs surface, making it useful in its various applications (Lai *et al.*, 2020).

Nanodiamonds are known to exhibit low toxicity, but the toxicity of this NM is dependent on its size as smaller sized NDs do exhibit some levels of toxicity, when compared to the larger size NMs (Domínguez *et al.*, 2018). This is demonstrated in an *in vivo* exposure in which freshwater clams were exposed to NDs of less than 6 nm. These clams experienced oxidative stress and lipid peroxidation (Cid *et al.*, 2015). In another *in vivo* study, nematodes were exposed to NDs larger than 50 nm, and these nematodes experienced no deleterious effects (Mohan *et al.*, 2010).

b) <u>nano Copper oxide (nCuO):</u>

Nano Copper oxide has excellent thermophysical and antibacterial properties which makes them useful in the production of electronics, sensors, paints, coatings and bactericides (Hanna *et al.*, 2014; Mansano *et al.*, 2018; Rotini *et al.*, 2018; Al Ghais *et al.*, 2019). They are formed via green synthesis, sol-gel and chemical vapor deposition (Eisermann *et al.*, 2012; Etefagh *et al.*, 2013; Keabadile *et al.*, 2020).

They present a relatively low dissolution rate in water, but are known to exert toxic effects on aquatic organisms due to the copper ions being released from the NM or from both the material and the ions (Pradhan *et al.*, 2012; Croteau *et al.*, 2014; Hanna *et al.*, 2014; Mansano *et al.*, 2018). The dissolved ions from the NM can interact with cells and cross cell membranes giving rise to reactive oxygen species (ROS), oxidative stress and apoptosis (Mansano *et al.*, 2018). Even though copper is an essential metal – plays an important role in oxygen transportation as part of hemocyanin and is an essential cofactor for various enzymes involved in metabolic activities - it can be toxic at elevated concentration, specifically in aquatic organisms, giving rise

to the negative effects mentioned prior including enzyme inhibition and decreased respiration (Hanna *et al.*, 2014; Muralisankar *et al.*, 2016; Al Ghais *et al.*, 2019; Malhotra *et al.*, 2020).

1.5 Determining the Toxicity of Nanomaterials using Toxicity Tests

There have been many acute toxicity tests conducted with carbon-based and nCuO NMs on freshwater organisms. Acute toxicity tests are a short term assessment utilised to assess the hazards of chemical contaminants to aquatic organisms (Arome & Chinedu, 2013). It is able to provide one with guidelines on the dose that can be utilized in longer experimental studies (Arome & Chinedu, 2013). Chronic toxicity tests measure the sublethal effects of a contaminant on the organism giving an indication of the possible effects that can be experienced by the organism long term (Muller *et al.*, 2011). Sublethal effects include behavioural and physiological changes, such as mobility, respiration and longevity (Mänd & Karise 2015; Passantino *et al.*, 2021) (*Table 1.3*).

Table 1.3 Exposure tests with nanomaterials on various organisms, focusing on different endpoints.

Organism:	**Nanomaterial:**	**Concentrations:**	**End point(s):**	**Reference:**
Danio rerio (Zebrafish)	CuO-NPs (nanorods & nanospheres)	50 – 200 µg/L	Oxygen consumption, swimming ability	(de Oliveira Eiras *et al.*, 2022).
Daphnia magna (Water flea)	Single wall carbon nanotubes	0.01 mg/L – 10 mg/L	Mortality	(Kim *et al.*, 2010).
Daphnia magna	CuO-NPs	10 µg/L – 1 mg/L	Immobilization	(Thit *et al.*, 2016).
Poecilia reticulata (Guppy)	CuO-NP Cu^{+} ions	20 µg/L	Uptake in gills , bioaccumulation	(Mansouri *et al.*, 2015).
Cyprinus carpio (Common carp)	CuO-NP	0.1 mg/L – 1 mg/L	Bioaccumulation , antioxidant enzyme activity	(Naeemi *et al.*, 2020).
Procambarus clarkia (Red swamp crayfish)	CuO-NPs	25 mg/L – 250 mg/L	Mortality, bioaccumulation and oxidative stress	(El-Atti *et al.*, 2019).

Freshwater organisms, specifically invertebrates, are utilized to study toxicity of materials in aquatic systems from individual to population levels (Chaumot *et al.*, 2014). They are well

established for the toxicological studies of engineered nanoparticles (Wang & Liu, 2022). Invertebrates are favoured for ecotoxicological studies because they are abundant, easily available and exhibit a variety of biological traits (Chaumot *et al.*, 2014; Wang & Liu, 2022). Crustaceans are one of the groups of invertebrates that are used for ecotoxicological studies as they are ecologically important in the freshwater ecosystem and are highly sensitive to environmental stressors (Baun *et al.*, 2008; Walters *et al.*, 2016; Siregar *et al.*, 2021). *Daphnia magna* is part of the branchiopoda class. It is one of the most common crustaceans used for ecotoxicity testing with national and international guideline standards (Baun *et al.*, 2008; Wang & Liu, 2022; Auffan *et al.*, 2012). Another class of crustaceans that are often used, are decapods.

1.6 Decapods

Decapod crustaceans belong to the family Atyidae. They have biological characteristics that make them important organism models for biochemical, physiological, and ecological research. These characteristics are suitable size, ease to culture in a laboratory, tolerance to handling as well as having individual traits that make them adapt to environmental conditions, and their advanced circulatory hormones (Passantino *et al.*, 2021). Shrimp is an example of the type of organism that falls within the decapod order. The behaviour, adaptability, physiology, and morphology of *Caridina (H. Milne-Edwards, 1837),* make them suitable for ecotoxicity testing. They also play an important role in the ecosystem's food webs (Mensah *et al.*, 2012b). *Caridina* is a common genus of shrimp that is used for ecotoxicity studies (*see Table 1.4 below*). Their adult body lengths can range from 12 mm – 26 mm (Leuven *et al*., 2008; Suchayo *et al*., 2008; Mirimin *et al*., 2015).

Table 1.4 Studies exposing various *Caridina* species to a range of toxicants.

Species & genus	**Contaminant**	**Reference**
Caridina africana	Atrazine	(van Rensburg *et al.*, 2022).
Caridina nilotica	Herbicides	(Mensah *et al.*, 2012a).
Caridina laevis	Pesticides	(Sucahyo *et al.*, 2008).
Caridina japonica	Fipronil	(Yang *et al.*, 2008).

Physiology

Caridina shrimps have five pairs of walking legs - pereiopods (*shown in green in Figure 1.5*). They have stalked eyes and have antennas, which function as sensory feelers (*shown in orange in Figure 1.5*). The thorax lies within the carapace which also encases the head (Hart *et al.*, 2001; Fransen, 2014). The abdomen of the shrimp is elongated. The shell of the shrimp is an exoskeleton containing calcium and is moulted. These organisms have six pairs of feeding appendages: the mandible; the maxillae (two pairs) and maxilliped (three pairs) (Hart *et al.*, 2001; Fransen, 2014). They possess five pairs of pleopods, which are used for swimming or reproduction. The uropod, together with the telson allows for backwards movement. Shrimps use their chelipeds for feeding (*shown in blue in Figure 1.5*). Atyid shrimp's chelipeds are more brush-like used to scrape and brush their food sources (Hart *et al.*, 2001; Fransen, 2014). There are chemoreceptors present on the antenna, and the pereiopods (Hobbs & Lodge, 2010).

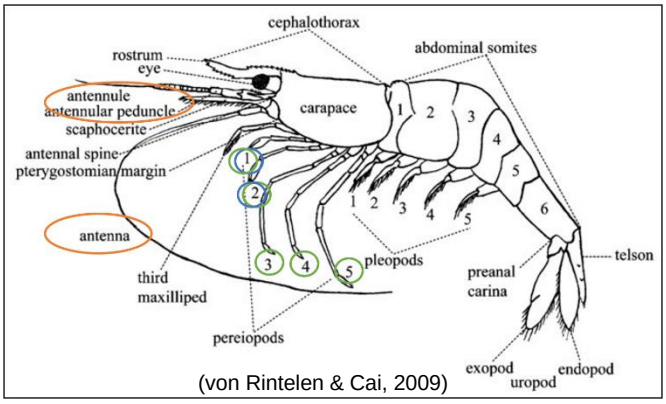

Figure 1.5 Shrimp Anatomy.

Cardiac system

Decapod crustaceans have an open circulatory system, where they have a single ventricle which they coordinate the opening and closing of the valves. Haemolymph is drawn through the ostia, pumped out and returned to the heart (McMahon & Wilkens, 1983; Guadagnoli *et al.*, 2007).

The prebranchial haemolymph is taken from the tissues into the infrabranchial sinuses and the haemolymph is guided to the gills via these sinuses to become reoxygenated (McLaughlin, 1983; Felgenhauer, 1992). Post-branchial haemolymph is transported into the branchio cardiac veins

and the oxygenated haemolymph surrounds the pericardial sinus of the decapod's heart. The haemolymph enters the heart via three pairs of ostia and leaves the heart through six aortic valves which is then distributed to the five arterial systems (*shown in purple in Figure 1.6*) (McLaughlin, 1983; Felgenhauer, 1992).

The heart rate varies in response to sensory stimulation and locomotion (McMahon & Wilkens, 1983).

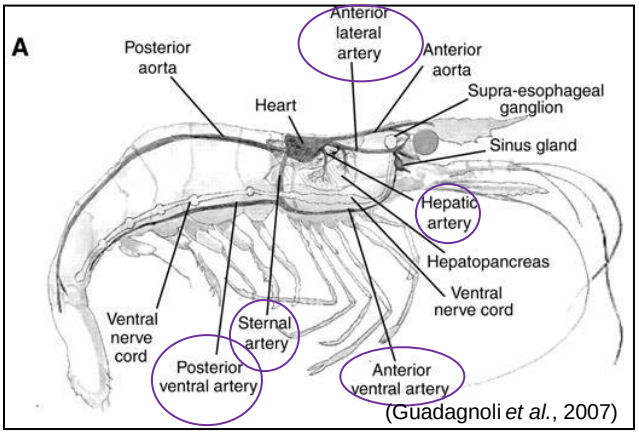

Figure 1.6 The cardiac system of shrimp.

Respiratory system

The ventilatory system of crustaceans is controlled with a ventilatory central pattern generation. This pattern generator is responsible for the uptake of oxygen across the crustacean's gills via a pumping action. The gills are located on the thoracic appendages – the base maxillipeds and pereiopods as well as on the side of the thorax in the branchial chamber, which is encased in the carapace (Felgenhauer, 1992; Hobbs & Lodge, 2010). It draws water across the gills through a rhythmic movement. This constant diffusion of water from the gills surfaces into the blood poses a challenge for the freshwater organisms as the pattern generation can be altered by environmental changes with crustaceans. (McMahon & Wilkens, 1983; Bierbower & Cooper, 2009; Hobbs & Lodge, 2010).

Behaviour

There are chemoreceptors that are present on the mouth, pereiopods and antenna of decapods. The eyes and the chemoreceptors play a very important role in their behaviour (Hobbs & Lodge, 2010).

Decapods spend time and energy grooming themselves. They use their maxillipeds and/or pereiopods to clean their other appendages/gill from organisms that may attach to their bodies and/or debris (Bauer, 1981). Shrimp locomotion involves swimming, walking as well as tail flipping. They are able to swim through the use of their pleopods (Li *et al.*, 2018a). Shrimp swim for migration, cruising and foraging purposes. They also have an elongated abdomen and uropods. With the use of these two they're able to flex the abdomen and have a powerful "tail flipping action". This mechanism is used for speed and acceleration. However, this action is energetically expensive, so it's only used for short periods of time (Arnott *et al.*, 1998; Zhang *et al.*, 2006; Yu *et al.*, 2009; Li *et al.*, 2018a).

Decapod crustaceans undergo moulting. The moulting process is controlled via the X-organ/sinus gland complex. This is located within the eyestalks. This complex secretes a peptide hormone – moult inhibiting hormone. The hormone is responsible for inhibiting the production of ecdysone that occurs in the Y-organs, which is located in the cephalothorax – under the carapace (Chang, 1995; Phlippen *et al.*, 2000; Nakatsuji *et al.*, 2009). When there is a reduction in the moult inhibiting hormone in the haemolymph, this decrease stimulates the Y-organs to synthesize and secrete ecdysone. The ecdysone is then converted to the active moulting hormone by the peripheral tissues, which then causes the crustacean to moult (Chang, 1995; Phlippen *et al.*, 2000; Nakatsuji *et al.*, 2009). An external environment may cause variation in behaviour within individuals (Takahashi, 2022).

1.7 Adverse Outcome Pathway

When an organism encounters a toxicant, it can alter their physiological responses on different levels. An adverse outcome pathway (AOP) is a construct that can be utilized to determine how a toxicant affects an organism starting from molecular levels.

An adverse outcome pathway (*Figure 1.7*) is a series of events that links a direct molecular initiating event to an adverse event at an biological organizational level relevant to risk assessment (Ankley *et al.*, 2010). It is an important tool for risk assessment. Toxicity is linked through different biological levels, causing sub-organism responses that can predict whole-organism effects. These effects can then be extrapolated across species (Gerloff *et al.*, 2017; Ma *et al.*, 2018; Goodchild *et al.*, 2019; Halappanavar *et al.*, 2019; Halappanavar *et al.*, 2021).

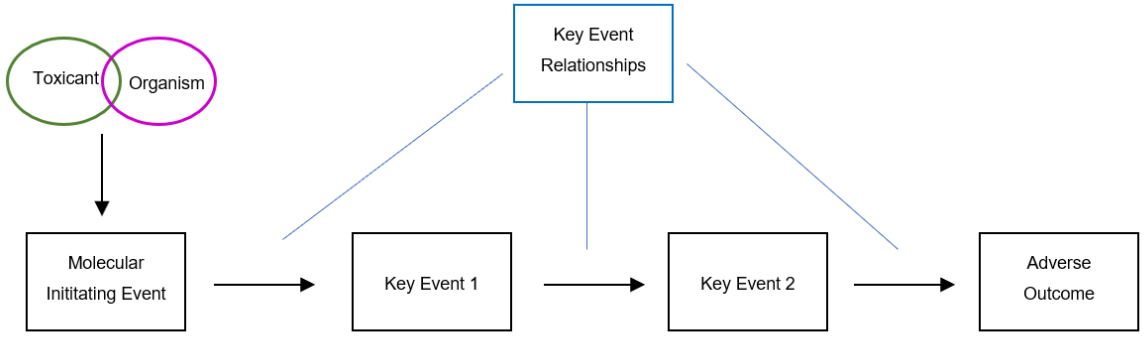

Figure 1.7 Simplified adverse outcome pathway - adopted and adapted from (Halappanavar *et al*., 2019).

i) Molecular Initiating Event (MIE): It is the first specialized key event of the pathway. Here the toxicant/chemical interacts with a biomolecule and causes a disturbance at a molecular level (Villeneuve *et al.*, 2014). This interaction can be specific – ligand-receptor, or non-specific – the toxicant physically sits on the biomolecule (Gerloff *et al.*, 2017).

ii) Key Event/s (KE/KEs): This can occur on a cellular, organelle and/or tissue level (Gerloff *et al.*, 2017). With key events, it is a measurable change in an organism's biological state that is considered essential, but not solely sufficient for its progression towards the final part of the pathway, which is the adverse outcome (Villeneuve *et al.*, 2014). Examples of

key events includes: gene expression, altered physiology and functions (Zhou, 2015; Carusi *et al.*, 2018).

a) *Metabolomics:* The quantitative and qualitative study of metabolites that are present in biological samples (Acosta-Tlapalamatl *et al.*, 2022; Carmen, 2022). These metabolites are dependent on the cellular response to environmental conditions (Acosta-Tlapalamatl *et al.*, 2022; Carmen, 2022). Metabolomics reflects the cellular state of an organism. It aids in understanding the biological mechanisms that are elicited by chemical toxicants (Davis *et al.*, 2016; Carmen, 2022). This information describes the main pathways that are affected by the toxicants and can thus be used for AOP construction and can identify previously unidentified key events (Davis *et al.*, 2016; Davis *et al.*, 2017; Carmen, 2022).

b) *Heart rate:* Measurement of an organism's heart rate provides a direct link to excitability, and readiness of its internal environment (Bierbower & Cooper, 2009). The heart rate of an organism reflects the physiological and psychological status of an organism. The rate is affected via signals from the environment (Singh *et al.*, 2020b; Agathokleous, 2022). The heart rate is linked to the metabolism and can be influenced by various factors: chemical exposure level, exposure medium, and time of exposure .

c) *Respiration:* Changes in respiration rates at sublethal concentrations of toxicants may result in long-term negative effects on an organism's community (Handy & Depledge, 1999; Lovern *et al.*, 2007). Respiratory distress is obvious in acute toxicant incidents, which makes it an important physiological change. Oxygen consumption rates show a dose-response relationship in many organisms and toxicants, and it can also be used instead of metabolic rate (Handy & Depledge, 1999; Lovern *et al.*, 2007).

d) *Behaviour:* Biological behaviour of an organism is an ecological relevant response of an organism at an individual level towards environmental changes (Wang *et al.*, 2020b; Ford *et al.*, 2021). Behaviour could reflect physiological alternations, like survival and can show the adaptation of the organism towards stressors (Dallas & Ross-Gillespie, 2015). The swimming activity of organisms is used as an indicator for survival (Wang *et al.*, 2020b).

iii) <u>Key Event Relationship/s (KER/KERs):</u> This illustrates a direct relationship between KEs It is based on empirical and plausible data (Villeneuve *et al.*, 2014; Gerloff *et al.*, 2017).

iv) Adverse Outcome (AO): An AO is how the toxicant affects the organ in an organism and how this consequently impacts the individual. Examples of AOs include growth inhibition and reduced survival (Villeneuve *et al.*, 2014; Gerloff *et al.*, 2017).

a) Lethality: Lethality/survival/mortality are often the endpoints/AOs that are utilized in AOPs (Ankley *et al.*, 2010; Russom *et al.*, 2014; Knapen *et al.*, 2018; Coady *et al.*, 2019).

Once a toxicant, such as a NM, enters an aquatic system, it can exhibit negative effects on the inhabitants. In the table below are a few studies that have created AOPs based on NM exposures. Various organisms and NMs that were utilized for the generation of AOPs (*Table 1.5*).

Table 1.5 Adverse outcome pathways generated from nanomaterial exposures.*Abbreviations used are NM = nanomaterial, MIE = molecular initiating event, KE(S) = key event(s), AO(S) = adverse outcome(s).

Organism	NM	MIE	KE(S)	AO(S)	Reference
Danio rerio	Silver NP	ROS generation on gonad tissue	Oxidative stress Germ cell apoptosis	Impaired reproduction	(Ma *et al.*, 2018).
Danio rerio embryos	Copper oxide NP	Impaired hatching	Starvation Delayed feeding & development	Embryo mortality Larval mortality	(Muller *et al.*, 2015).
Daphnia pulex	Nanoplastic	ROS generation	Oxidative stress	Decreased reproduction Growth inhibition	(Liu *et al.*, 2021).

Research pertaining to NMs and adverse outcome pathways on freshwater shrimps are limited. When using the key words (“shrimp” AND “adverse outcome pathway” AND “NM”), Google Scholar yields results where brine shrimp were used as a dietary supplement for other model organisms being used for adverse outcome pathway studies, but no results were yielded for freshwater shrimp being the model organism for NM adverse outcome pathway studies.

1.8 Problem Statement

Nanotechnology has become a topic of interest within the scientific community due to its multitude of applications. Nanomaterials – which are sized from 1 – 100 nm - are the precursors for the development of this type of technology, and are commercially available in over 1 600 products that includes - but are not limited to - medicine, personal care products, environmental remediation as well as industrial in fuel additives, imaging agents, sunscreen, remediation and food processing and packaging, respectively (Blaise *et al.*, 2008; Pradhan *et al.*, 2012; Exbrayat *et al.*, 2015; Jennings *et al.*, 2015; Bundschuh *et al.*, 2016; Vale *et al.*, 2016; Chaurasia, 2017; Khosravi-Katuli *et al.*, 2017; Li *et al.*, 2018b; Kandru, 2020). Thus, due to its continual development and increased usage, it will be discharged more frequently into aquatic environments (Blaise *et al.*, 2008; Pradhan *et al.*, 2012; Croteau *et al.*, 2014; Exbrayat *et al.*, 2015; Bundschuh *et al.*, 2016; Rotini *et al.*, 2018).

Since aquatic environments act as a sink for most discharged pollutants/contaminants, assessing the potential risks to aquatic wildlife is of utmost importance (Blaise *et al.*, 2008; Edokpayi *et al.*, 2017). The bioavailability as well as toxicity potential of NMs are dependent on the aquatic organism, such as their morphology, behaviour as well as the physicochemical characteristics of their habitat (Jennings *et al.*, 2015; Vale *et al.*, 2016). However, it is also dependent on the NM itself, such as its size, shape, solubility, structural properties as well as its chemical composition (Ivask *et al.*, 2014; Jennings *et al.*, 2015; Canesi & Corsi, 2016; Vale *et al.*, 2016).

Nanodiamonds and nCuO are just a few examples of NMs which are utilized in everyday life, ranging from biomedical to industrial and commercial applications (Mochalin *et al.,* 2012; Croteau *et al.,* 2014; Hanna *et al.,* 2014; Ivask *et al.,* 2014; Rotini *et al.,* 2018; Basso *et al.,* 2020; Fusco *et al.,* 2020). Nanodiamonds find use in drug delivery, tracing and therapeutic and diagnostic tools. and are seen as inert and less toxic than other carbon-based NMs (Mochalin *et al.*, 2012; Zhu *et al.*, 2012). The nano copper oxide has found use in antibacterial application, such as bactericides, as well as exhibiting anticancer activity and is toxic to aquatic organisms. It is responsible for enzyme inhibition, decreased immune function as well as decreased respiration rate within crustaceans (Hanna *et al.*, 2014; Bundschuh *et al.*, 2016; Muralisankar *et al.*, 2016; Al Ghais *et al.*, 2019; Chattopadhyay, 2020). An increase in their production and use will lead to a greater release into the environment. This is just one of the issues concerning NMs, as there can be a lack of information regarding their environmental safety (Hanna *et al.*, 2014). Also, little is

known of the toxicity of engineered nanoparticles in the aquatic environment. Thus, understanding the fate, bioavailability as well as the toxicity of NMs, will allow for its behavioural prediction and the impact it may have on aquatic organisms and their systems (Pradhan *et al.*, 2012; Croteau *et al.*, 2014; Hanna *et al.*, 2014).

Crustaceans, such as *Caridina africana (C. africana)* are potential standard toxicity test organisms as they are easily cultured and maintained within laboratory conditions, breeds throughout the year, have unique biological characteristics – which are vulnerable to contaminants – are widely distributed and have a relatively short life cycle. They also play an important role in the African freshwater system food web (Muller *et al.*, 2011; Mensah *et al.*, 2012b; van Rensburg *et al.*, 2020).

In the aquatic food web, predators feed on certain crustaceans, such as shrimp. If shrimp are exposed to NMs through dietary or water exposure, they are bound to accumulate these NMs. When the predators consume these shrimps, this gives rise to the phenomenon known as trophic transfer (Jennings *et al.*, 2015; Bundschuh *et al.*, 2016; Hu *et al.*, 2016). This will ultimately have a detrimental impact on predators further up in the food chain. Therefore, understanding the mechanisms and adverse effects of NM toxicity in smaller organisms is important.

Adverse outcome pathways (AOP) are a series of events that directly links a molecular initiating event to an adverse effect at an organizational level that is relevant to risk assessment (Lee *et al.*, 2015; Gerloff *et al.*, 2017; Ma *et al.*, 2018; Goodchild *et al.*, 2019; Halappanavar *et al.*, 2019; Halappanavar *et al.*, 2020). The AOP framework provides the necessary information required for deducing the effects across various species. Standard guideline tests are said to have sparse to limited information on the toxicity of a substance and provide minimal data as to why a substance is responsible for an adverse effect (Gerloff *et al.*, 2017). Thus, the aim of an AOP is to provide the knowledge base required to support the development of new testing methods (Gerloff *et al.*, 2017).

1.9 Hypothesis, Aims and Objectives

1.9.1 Hypothesis

H_0: The adverse outcome pathway will not be effective in testing the effects that nanodiamond and nano copper oxide have on *Caridina africana.*

H_1: The adverse outcome pathway will be effective in testing the effects that nanodiamond and nano copper oxide have on *Caridina africana.*

1.9.2 Aim and Objectives

The main aim of this project is to determine the effects of NDs and nCuO (through water borne exposures) on the freshwater shrimp, *Caridina africana* by utilizing the AOP framework. The aim can be achieved through the following objectives:

1. Characterizing the physico-chemical properties of the two NMs (NDs and nCuO) in exposure media.
2. Exposing *C. africana* to selected concentrations of NMs (i.e. the LC_{10} and LC_{20} calculated from LC_{50} of NDs and nCuO following standard tests and using bioaccumulation to confirm uptake).
3. Determine the effects of the two NMs on different components of the AOP framework– gene expression, such as metabolomics (MIE). This is followed by KEs that includes physiological effects (respiration and heart rate) and behavioural responses. The AOP is finalized by looking at the mortality/lethality of the shrimp as the AO.

CHAPTER 2 MATERIALS AND METHODS

2.1 Ethics Statement

This study was declared “no risk” by the Faculty of Natural and Agricultural Sciences (FNASREC) at North-West University, South Africa. The ethics number is NWU-00528-21-A9 (*see Appendix A).*

2.2 Shrimp Sampling and Husbandry

2.2.1 Sampling

Shrimp were sampled from Oog van Gerhard Minnebron (Mooi River Ecosystem Trials for Scientific Investigations - METSI) in Potchefstroom (-26.4798376, 27.1521772), South Africa. Sweep nets (frame dimensions of 300 X 300 mm with a mesh size of 500 µm) were used to collect the shrimp. Moss from the site was placed into the net and gently shaken to release the shrimps. The shrimps were then placed in 20 litre (L) buckets containing their field water and were transported back to the National Aquatic Bioassay Facility (NABF), North-West University, Potchefstroom, South Africa on the same day of collection.

2.2.2 ISO media Preparation

To make 50 L of ISO media, four different salt are added; 14.74 g of calcium chloride ($CaCl_2 \cdot 2H_2O$), 6.16 g of magnesium sulphate ($MgSO_4 \cdot 7H_2O$), 3.24 g of sodium hydrogen carbonate ($NaHCO_3$) and 0.28 g of potassium chloride (KCl) to 50 L of reverse osmosis (RO) water. The ISO media was aerated for 24 hrs prior to use (Truter, 1994; Heckmann & Connon, 2007).

2.2.3 Acclimation

A 100 L tank was set up with the shrimp’s field water, and upon the shrimp’s arrival at the NABF, the shrimps were left in the sample buckets to acclimate to the exposure room temperature for 48 hours (hr). They were then placed into the tank and acclimated for one week with ISO media in an exposure room within the NABF. This acclimation period consisted of adding 20% ISO media relative to the tank’s volume. Room parameters were adopted and adapted from Mensah *et al*. (2011); Muller *et al.* (2011) and Mensah *et al.* (2012b), as the room temperature remained

consistent at 23°C with a 12:12 light/dark cycle). After five days of acclimation, the shrimps that were of appropriate sizes (approximately 1 cm – 1.5 cm total length – measured using a Zeiss compound microscope (Carl Zeiss Microscopy, GmbH, Carl-Zeiss-Promenade 10 and Labscope 3.4.3 for Windows software) were sorted and placed into a 20 L tank, where they were acclimated further until needed for laboratory exposures. The shrimps that were not of appropriate size were placed into a separate tank 100 L tank for breeding purposes. The shrimp were fed either boiled cucumber, algae wafers, or Shrimp King™ (Baby, Colour, Mineral, Protein, Complete, and Snow pops granules/sticks) *Each product's composition is listed in Appendix B.

2.3 Shrimp Identification

Three shrimp were randomly sampled from the tank and placed in an ice bath for two hours. Thereafter, they were then placed in a beaker containing 70% ethanol (SIGMA) prior to DNA extraction (Darbyshire *et al*., 2019).

The shrimp were removed from the beaker and placed onto a paper towel where they were dabbed dry. The gut contents were excised from the shrimp to prevent cross-contamination with the algae's DNA (the shrimp's food source). The abdomen area was cut and removed from the rest of the organism and the tissue was cut into smaller pieces. This was done to break the exoskeleton to allow for easier access to the abdomen tissue to aid in the extraction of DNA. This was repeated for the other two shrimp. One of the shrimp's heads was also used for analysis. The tissue samples were then placed into separate vials and dried in a heat block to remove any remaining ethanol. This was done at 56°C for nine minutes. The vials were then placed under the microscope to ensure complete dryness. Genomic DNA was extracted using a Macherey-Nagel kit, following the manufacturer's instructions as outlined below. The DNA was verified using 1% agarose gel electrophoresis (Zhou *et al*., 2021).

2.3.1 Extraction

Buffer T1 (180 µL) and Proteinase K (25 µL) were added and vortexed until the sample was in solution (approximately five seconds/sample). The vials were then placed into a Provocell shaking incubator for 3 hrs and 33 minutes at 56°C at 300 revolutions per minute (rpm). The elution buffer was preheated in the heating block (70°C). Thereafter 200 µL of Buffer B3 was vortexed and incubated at 70°C for ten minutes. The samples were then vortexed again. 210 µL of 96% - 100% ethanol (SIGMA) was added to each sample vial followed by vigorous vortexing.

NucleoSpin® Tissue Columns were placed into collection tubes (1 per sample). 500 µL of the supernatant from each sample was added to their respective columns. The samples were then centrifuged ([11 000 x g (12 600 rpm) for 1 minute]). After centrifugation, the collection tubes were discarded, and the first set of columns was placed into new collection tubes. 500 µL of Buffer BW (Wash Buffer) was added to each of the NuceloSpin® Tissue columns. The samples were then centrifuged ([11 000 x g (12 600 rpm) for 1 minute]). The liquid was discarded, and the column was placed back into the collection tube. 600 µL of Buffer B5 (Wash Buffer 2) was added to the column and centrifuged ([11 000 x g (12 600 rpm) for 1 minute]). The flow tube was discarded, and the column was placed back into the collection tube. The samples were centrifuged again to remove any residual ethanol ([11 000 x g (12 600 rpm) for 1 minute]). The NucleoSpin® Tissue Columns were placed into 1.5 mL microcentrifuge tubes and 100 µL of Buffer BE (elution buffer) from the heat block.

The samples were then incubated at room temperature for one minute, then centrifuged (11 000 x g (12 600 rpm) for 1 minute). The NucleoSpin® Tissue Columns were then discarded, and the 1.5 mL microcentrifuge tubes containing DNA were stored in a -20°C freezer.

2.3.2 Amplification

The cox 1 gene was amplified using polymerase chain reaction (PCR). The forward primer was LCO1490 and the reverse primer was HCO2198. LCO1490: 5′-GGTCAACAAATCA TAAAGATATTGG-3′) and reverse primer (HCO2198: 5′-TAAACTTCAGGGTGACCAAAAAA TCA-3′) (Folmer *et al*., 1994). PCR was performed in a total volume of 25 µL that contained 7 µL of double distilled water, 1.25 µL of LCO1490: 5′-GGTCAACAAATCA, 1.25 µL of HCO2198: 5′-TAAACTTCAGGGTGACCAAAAAA TCA-3′, 3 µL of DNA and 12.5 µL of Master Mix (Dream tag). Thermal cycling started with one cycle of pre-denaturation at 94°C for five minutes, followed by 35 cycles of denaturation for 30 seconds (s), annealing for 45s at 50°C, extension at 72°C for 45 s, followed by the final extension holding at 72°C for 7 min as shown in Figure 2.1. PCR products were then separated by electrophoresis on 1% agarose gel.

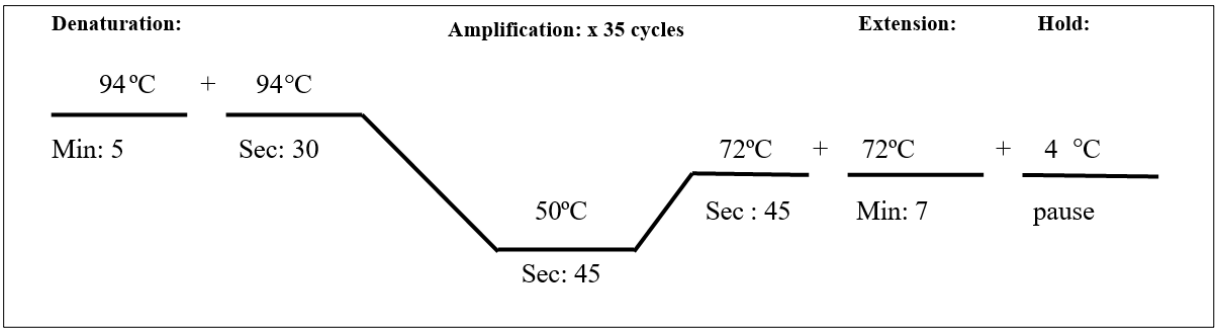

Figure 2.1 Simplified diagram of thermal cycling process.

2.3.3 Sequencing

Primer synthesis and DNA sequencing was done by Inqaba Biotechnical Industries (Inqaba Biotec).

The chromatograms sent by Inqaba Biotec were opened in FinchTV. The IUPAC code was used to sort through unfamiliar nucleotides (R, Y, S, W, K, M) to the appropriate nucleotide letter corroborating it with the peaks shown in FinchTV. The chromatogram was then trimmed on both sides and exported as a FASTA sequence. All sequences were then aligned and trimmed. These sequences were then exported as a "txt" file. These sequences were uploaded to NCBI's website using "Nucleotide BLAST" for analysis to determine the "most likely" organism.

To create a phylogenetic tree to confirm the relation to the most likely organism, various shrimp sequences were downloaded along with an outgroup sequence belonging to *Daphnia magna*.

MEGA X was then used to open all the FASTA sequences, in which the reverse sequences were converted to complement reverse sequences. These sequences were aligned and trimmed and exported as a MEGA file. They were then used to create a phylogenetic tree by first finding the best model. Models with the lowest BIC scores (Bayesian Information Criterion) are considered to describe the substitution pattern the best. For each model, AICc value (Akaike Information Criterion, corrected), Maximum Likelihood value (lnL), and the number of parameters (including branch lengths) are also presented (Nei & Kumar, 2000). Non-uniformity of evolutionary rates among sites may be modeled by using a discrete Gamma distribution (+G) with 5 rate categories and by assuming that a certain fraction of sites are evolutionarily invariable (+I). Whenever

applicable, estimates of gamma shape parameter and/or the estimated fraction of invariant sites are shown. Assumed or estimated values of transition/transversion bias (R) are shown for each model, as well. They are followed by nucleotide frequencies (f) and rates of base substitutions (r) for each nucleotide pair. Relative values of instantaneous r should be considered when evaluating them. For simplicity, sum of r values is made equal to 1 for each model. For estimating ML values, a tree topology was automatically computed. This analysis involved 14 nucleotide sequences. Codon positions included were 1st+2nd+3rd+Noncoding. There were a total of 513 positions in the final dataset. Evolutionary analyses were conducted in MEGA X (Kumar *et al.,* 2018).

2.4 Nanomaterial Stock Solutions

All the powders/salts were weighed on a Scaltech balance and suspended in 50 mL of Milli-Q® water in 50 mL falcon tubes (Labocare™). To prepare a stock solution, 100 mg of the "pure element" was desired for all materials.

a) Nanodiamond: 100 mg of Nanodiamonds-PEG, sized 3 – 5 nm (produced by PlasmaChem GmbH and supplied through Nanosolutions project).
b) Nano copper oxide: 125.18 mg of nano copper oxide, sized 14 ± 4 nm (PlasmaChem) yields 100 mg of copper.
c) Copper (II) chloride: 155.79 mg of copper chloride salt (Sigma-Aldrich) yields 100 mg of copper.

The nano-stock solutions were then placed in an ultrasonicator bath (Model E-UC6-HD-D, Scientech) containing reverse osmosis water. The solutions were sonicated at 25°C for one hr at 20 Hz prior to use. When the solutions were not in use, they were stored in a refrigerator at 4°C. For range finding, more stock concentrations were made.

2.5 Exposure Media Preparation

The composition of the media used for exposures are described in section 2.2.2 (Truter 1994; Heckmann & Connon, 2007). The stock solutions were first sonicated for one hour (Sanhueza *et al*., 2019). After sonication, solutions were left to cool for approximately five minutes. Concentrations ranging from 5 µg/L – 160 mg/L were micropipetted from the stock suspensions and dosed into the beakers for range finding. No manual mixing of the media occurred after dosing, but the aeration provided "mechanical' mixing.

2.6 Nanomaterial Characterization

2.6.1 Transmission Electron Microscopy (TEM)

Two concentrations of ND-PEG (20 mg/L and 100 mg/L) and 20 mg/L of nCuO stock solution were used for TEM analysis.

The solutions were sonicated, and a drop of each NM suspension was placed on a carbon-coated-copper grid. The excess fluid was soaked up by touching the paper towel on the edge of the droplet, which allowed them to dry. The samples were then viewed in a Tecnai G2 20 S-Twin transmission electron microscope at 200kV. The photographs of the NMs were captured with a Gatan bottom mount camera and Digital Micrograph software (Botha *et al.*, 2015).

2.6.2 Dissolution

The dissolution of engineered NMs by dialysis by Handy *et al*. (1989); Al-Bairuty *et al*. (2016) and Boyle *et al*. (2020) was adopted and adapted for the volumes utilized.

Stock solutions of nCuO (0.972 mg/L, 1.944 mg/L and 20 mg/L) were suspended in 50 mL of ISO media. These solutions were sonicated for one hr.

Twelve 600 mL (Schott Duran) beakers were filled with 292 mL of ISO media and twelve pieces of dialysis tubing of approximately 10 cm were cut and tied into a knot at one end.

Nine of the dialysis bags were filled with 8 mL of the respective concentrations mentioned above and were secured with a cable tie on the other end. The outside of the bags were rinsed with Milli-Q® water to ensure the exterior of the bag is clean. The dialysis bags were then placed into the beakers containing the 292 mL of media. Controls that only contained ISO media were run concurrently to determine the presence of background copper. The beakers were then placed on a shaker bed for 96 hr at 17°C ensuring gentle shaking as seen in Figure 2.2.

Aliquots of 5 mL were taken from each beaker at approximately the same depth at 0, 24, 48, 72 and 96 hrs with an Accumax (0.5 – 5 mL) micropipette. These samples were placed in 15 mL falcon tubes and acidified to 1% with nitric acid (HNO_3). The samples were stored in a polystyrene box and placed in a dry cool place until analysed with the graphite furnace atomic absorption spectrometry (GF-AAS).

For GF-AAS, 600 µL of each sample was placed into AAS vials, where 20 µL was injected into the pyrolytic graphite furnace tube for copper measurements. Calibration was performed and a calibration curve with a $R^2 = 0.9998$ was generated.

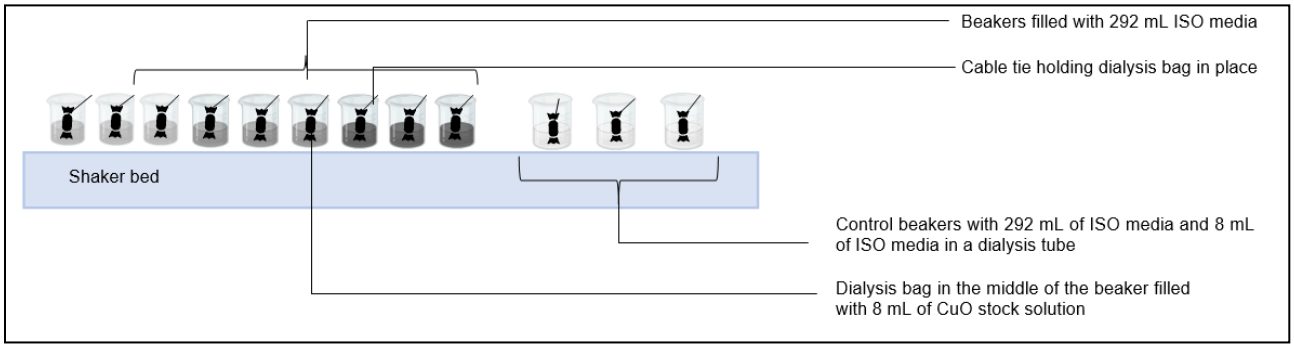

Figure 2.2 Simplified diagram of dissolution exposure.

2.6.3 Dynamic Light Scattering (DLS)

The Malvern Zetasizer (Malvern Zetasizer NanoZS, Malvern Instruments Ltd.) was switched on 30 min prior to running the samples for hydrodynamic size distribution and zeta potential. Diluted stock solutions were made for both NMs: nCuO (0.972 mg/L, 1.944 mg/L and 20 mg/L) and ND-PEG (0.9856 mg/L, 1.9712 mg/L and 20 mg/L).

A 1 mL cuvette was rinsed with MilliQ® water and 1 mL of each sample was pipetted into the cuvette, which was then placed into the Malvern Zetasizer to determine the hydrodynamic size distribution. This is shown by purple arrow in *Figure 2.3* (Botha *et al*., 2016).

A 1 mL folded capillary zeta cell was used to determine the zeta potential of the NMs. The zeta cell was also rinsed with MilliQ® water prior to use, and 1 mL of diluted stock solution for both NMs were injected into the cell for analysis. The formation of bubbles whilst injecting the sample was avoided by filling the cell halfway, rotating it and injecting the rest of the sample in. The cell was closed with stoppers on both sides. This cell was also placed in the Malvern Zetasizer to determine the surface charge/zeta potential of the nanoparticles (shown by orange arrow in *Figure 2.3*) (Botha *et al*., 2016).

After the cuvettes/cells were placed into the Zetasizer instrument, each sample was read in triplicates by default with the Zetasizer Nano software, thus resulting in an average value for each sample.

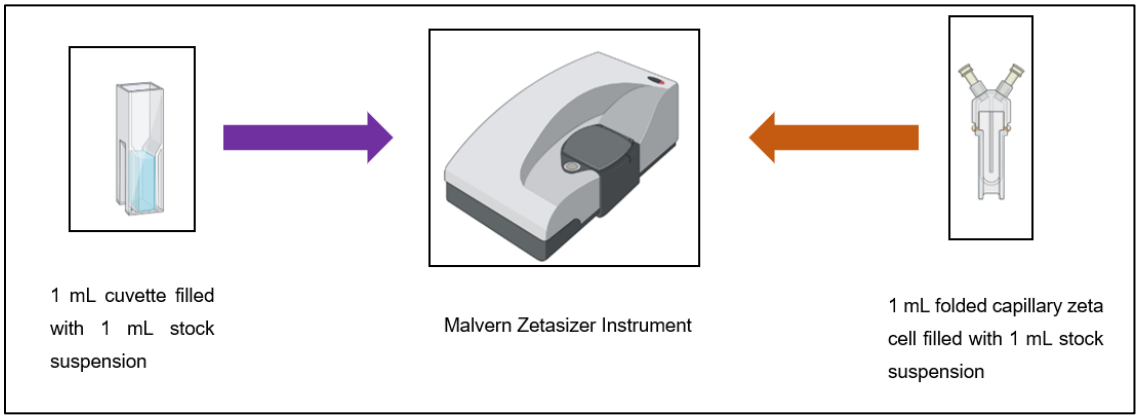

Figure 2.3 Simplified illustration of cuvette and capillary cells used for the Zetasizer instrument for dynamic light scattering characterization.

2.6.4 CytoViva® Hyperspectral Dark Field Imagery

After a 96-hr exposure, shrimp were collected and placed into 1.5 mL Eppendorf tubes and frozen at -20°C until analysis. Whole shrimps and their moults were placed on individual microscope slides, and a paper towel was used on the edges of the organisms to remove any water. The slides were placed on the stage *(*illustrated by orange square in *Figure 2.4)* and held down with stage clips on the CytoViva® 150 unit integrated onto an Olympus BX43 microscope (Botha *et al.*, 2016). The light source came from Fiber-Lite® DC-950 DC Regulated Illuminator to visualize the organism and to determine if and where the nanoparticles adhere to the organisms and their moults. The images were captured with CytoViva® Q imaging and DAGE Exponent Software.

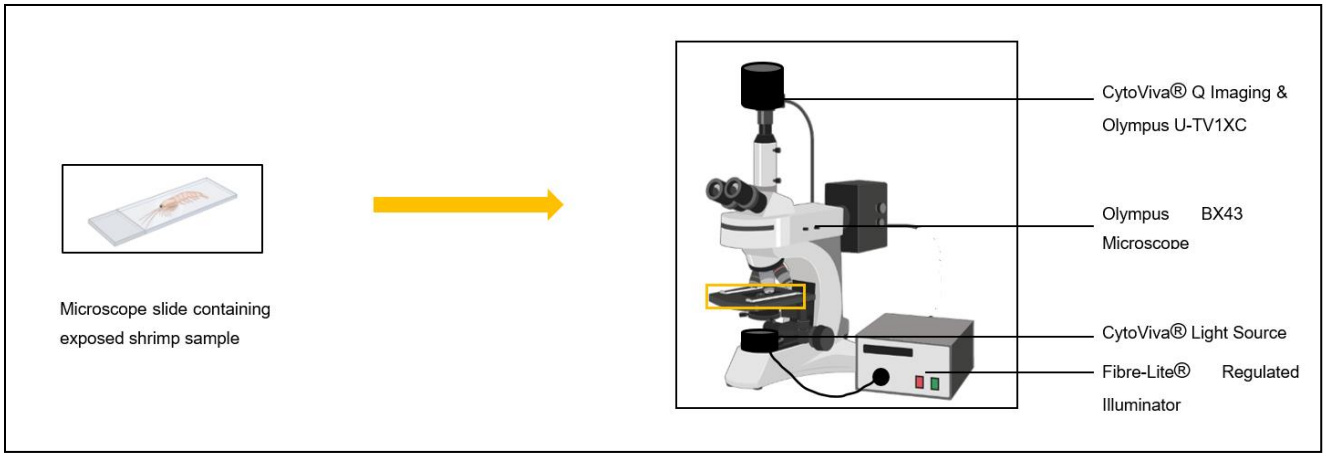

Figure 2.4 Simplified illustration for CytoViva® Hyperspectral Dark Field Imagery integral unit on the Olympus BX43.

2.7 Exposures

2.7.1 Acute Exposures

a) Acute Toxicity Test

The acute toxicity bioassay for the shrimp were adopted and adapted from (OECD, 2004; Mensah *et al.*, 2011).

To determine the 96-hr median lethal concentration (LC_{50}) of ND-PEG, nCuO and $CuCl_2$, the toxicity assay was conducted using the following concentrations:

- ND-PEG: 10 mg/L, 20 mg/L, 40 mg/L, 80 mg/L and 160 mg/L.
- nCuO: 5 mg/L, 10 mg/L, 20 mg/L, 40 mg/L, 60 mg/L, 80 mg/L and 160 mg/L.
- $CuCl_2$: 5 µg/L, 10 µg/L, 20 µg/L, 40 µg/L, 80 µg/L, 160 µg/L and 200 µg/L.

Each concentration contained seven shrimps (1 – 1.5 cm) and was replicated three times (n=21). The beakers contained 300 mL of relevant exposure media, aerated using airline tubing – 4 mm with Hirschmann® glass pipettes on the ends, which were fastened to the side of the beakers (see *Figure 2.5 and 2.6*). This acute toxicity bioassay was conducted in a temperature-controlled room at 23°C, a 12 : 12 light : dark cycle, in ISO media. Shrimp were not fed for the duration of

this exposure. The physico-chemical water parameters, such as the electrical conductivity (EC), total dissolved solids (TDS), pH and temperature, were measured daily, starting at 0 hrs.

Dead shrimps and their moults were recorded twice daily and removed from the beakers with a plastic pipette (Mensah *et al*., 2011). The cumulative number of mortalities were recorded after the 96 hrs and was used to calculate the LC_{50} using Daphnia Acute Immobilization Test worksheet on ToxRat® Professional software.

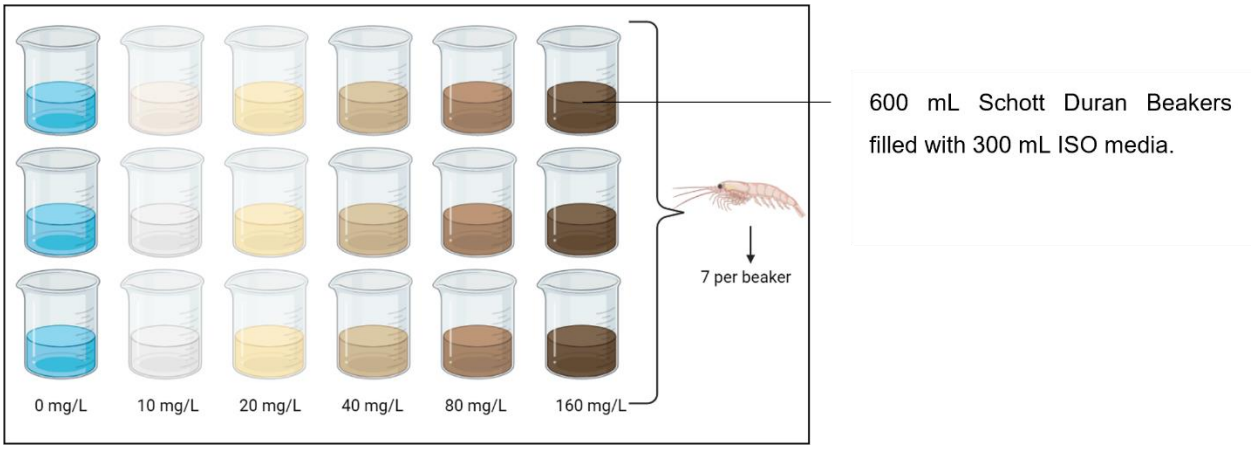

Figure 2.5 Experimental setup for ND-PEG acute toxicity bioassay. The same layout was followed for nano copper oxide and copper chloride.

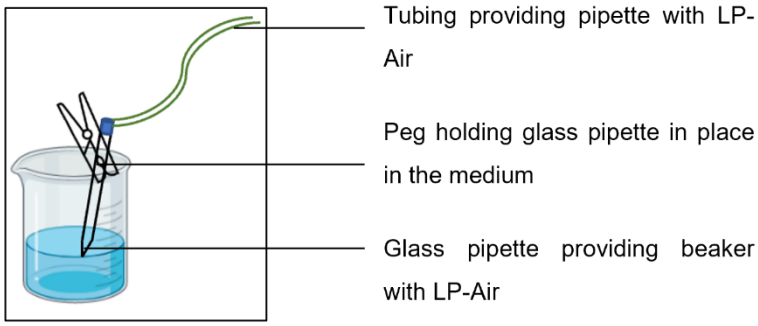

Figure 2.6 Extension of experimental setup for acute toxicity bioassay with LP-Air gas aerating the medium through the fastened glass pipette.

b) Bioaccumulation

Shrimps that were exposed and survived the acute toxicity bioassay were used for bioaccumulation. Only the metal-based exposures were used for bioaccumulation due to the nature of quantification.

Surviving shrimp were removed from the nCuO and $CuCl_2$ exposure beakers and placed into new beakers containing clean ISO media to allow them to depurate for approximately 4 hrs (Gillis *et al.*, 2005). After 4 hrs, the shrimp were rinsed with reverse osmosis (RO) water then removed with plastic pipette (cut at the tip to ensure the shrimp were not damaged during transfer). Individual shrimps were placed into Eppendorf 1.5 mL microcentrifuge tubes, and excess media was pipetted out and the shrimps were snap frozen using liquid nitrogen, then stored at -80°C until further processing.

Once the microcentrifuge tubes were removed from the freezer and samples were weighed using a Radwag balance(AS 220/C2) to determine the wet weight. After weighing, the shrimp were freeze dried using Labcono FreeZone Freeze Drier at -54°C, below 15 Pa for 48 hrs. After 48 hrs, individual shrimp samples were then weighed again to determine the dry weight.

For digestion, methods described by (Wolmarans & Van Aardt, 1985 and Böhme *et al*., 2017) were adopted and adapted. After final weighing, individual, dried shrimps were added into the cells of a 13.5 cm X 13.5 cm 3.5 cm Teflon® digestion block, where they were then crushed/homogenized using the squeeze bulb part of Pasteur pipettes. Three cells were used for the certified reference material (CRM), which was represented by certified mussel tissue powder - ERM-CE278K. Three blanks comprised of a dilutant matrix (HNO_3 and HCl) were added for every 20 samples.

750 µL of nitric acid (HNO_3) and 250 µL of hydrochloric acid (HCl) was added to each well. The wells were then covered with caps and a metal block was placed on top of the heat block and was sealed in place with screws and nuts. This was to avoid any sample loss. The heat block was then placed into an oven at 60°C for 24 hrs to allow digestion of the whole organism to occur. After 24 hrs, the heat block was removed and allowed to cool for 3 hrs at room temperature. The supernatants were pipetted out into 15 mL falcon tubes, and diluted with 1% HNO_3 to a volume of 5 mL. The falcon tubes were then close sealed and wrapped with foil and stored upright at room temperature until further analysis.

Copper concentrations were quantified by GF-AAS. Samples were diluted 2X, 4X and 10X where necessary with 1% HNO_3. 600 µL of each sample was placed into AAS vials, where 20 µL was injected into the pyrolytic graphite furnace tube for copper measurements. Calibration was performed and a calibration curve with a $R^2 = 0.9997$ was generated. GraphPad Prism 8.0.2.263 was used for statistical analysis.

c) Respiration

The exposure set up consisted of seven replicates per treatment group with four shrimp being placed in each beaker, resulting in 28 shrimp per treatment group (*Figure 2.7*). The physico-chemical water parameters, such as the EC, TDS, pH and temperature were measured daily, with the first reading starting at 0 hrs. Shrimp were fed with Shrimp King™ complete, that was ground to a fine powder and mixed with 15 mL of ISO media in a 15 mL falcon tube. The falcon tube was shaken each time, in which 200 µL was pipetted for feeding the shrimp daily until the end of exposure period. The tube was then stored in the refrigerator at 4°C.

After 96 hrs, one exposed shrimp per beaker per treatment were used for each set of data acquisition (n=7 per endpoint) (1 shrimp/beaker/treatment (s/b/t) for respiration, 1 s/b/t for behaviour, 1 s/b/t for heart rate).

Figure 2.7 Exposure set up for sublethal exposures.

After 96-hrs, seven shrimp per treatment group were used for the respiration assay. A 24-well Loligo Systems microplate respirometer chamber (Loligo Systems, Denmark) was rinsed with clean media and each well was filled with 80 µL of ISO media. Individual shrimp were placed per well containing new exposure media to ensure consistency in oxygen consumption as shown in *Figure 2.8*. The arrow shows what each well contained.

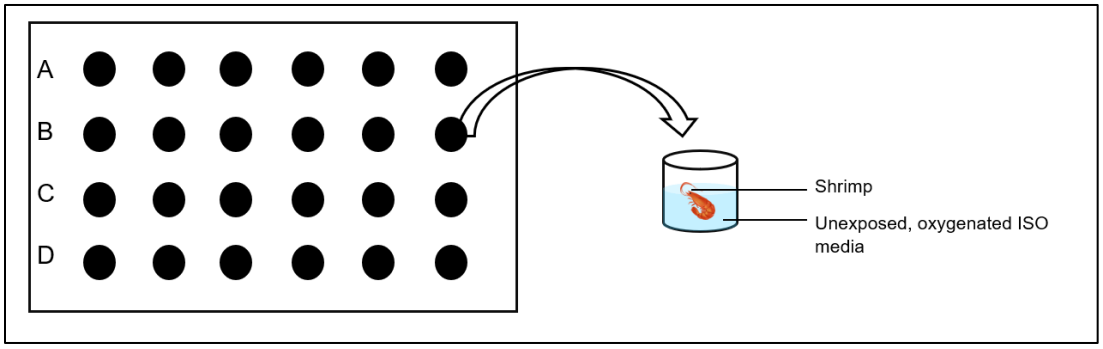

Figure 2.8 Simplified illustration of the respirometer chamber.

Once the shrimp were added, the respiration plate was sealed with a Loligo Systems® sealing film and a compression block was placed on top of the plate to ensure no air leakage. The microplate was placed on SDR® SensorDish and the oxygen measurements within the wells were recorded with PreSens SDR version 38. The test was run for one hr at 20°C, with readings taken as mg/L oxygen consumption, occurring every 15 s. The data was then exported to Microsoft Excel for further data evaluation. Upon completion, individual shrimp were placed into 1.5 mL Eppendorf tubes and were snap frozen in liquid nitrogen and stored at -80°C for metabolomic analysis.

A linear regression graph was initially created with the readings to determine the slope of the graph. The equation used to determine the oxygen consumption is shown below:

$$mx \times 4 \times \frac{1}{average\ shrimp\ weight}$$

The slope (mx) was multiplied by 4 seconds (to get the readings per min) , which was multiplied by one divided by the average weight of the organism. The final data is expressed in mg O_2/mg/min and statistical analysis was conducted in GraphPad Prism.

d) Heart Rate

After the shrimp were exposed for 96 hrs, seven shrimp per treatment group were used – the same setup outlined in the respiration section. Individual shrimps were transferred to petri dishes containing 5 mL of their respective exposed mediums. A Zeiss compound microscope was connected to a personal computer loaded with the Zeiss Labscope 3.4.3 application for Windows. Each petri dish was placed under the microscope, the excess media was pipetted out and shrimps were placed on their side to allow for easier viewing of the heart.

Video recordings were taken with a Axiocam 506 camera for 15 seconds and the videos were analysed on Windows Media Player by playing back the video at -16 X speed. The heartbeat was counted manually using a pen and paper to tap with the beats for 10 seconds (Greene *et al.*, 2017). This value was multiplied by six to get the number of beats per minute (bpm). The data is expressed as frequency and statistical analysis was conducted on GraphPad Prism. The shrimp were placed individuals into 1.5 mL Eppendorf tubes and snapped frozen in liquid nitrogen and stored at -80°C for metabolomic analysis. The heart of the shrimp is located under the carapace in the yellow square as shown in *Figure 2.9.*

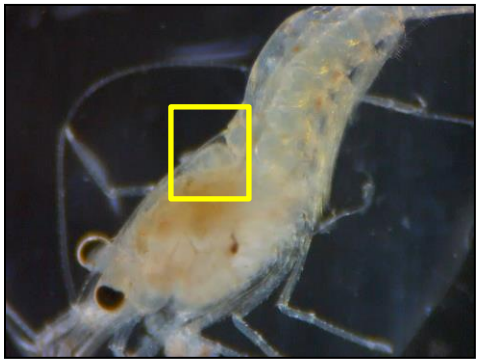

(Scan QR code to see video)
https://drive.google.com/drive/folders/1J2r3s2cXXTdQixYdolDQVGZgdOr1dX2K.

Figure 2.9 Location of the heart in shrimp.

e) Behaviour

The shrimps used for the behaviour study is outlined under the respiration section. Behavioural data acquisition occurred in the designated behaviour room (20°C) in the NABF situated at North-West University, Potchefstroom.

Methods described by Egan *et al.* (2023) were adopted and adapted. Here, seven shrimp/treatment group were used for this analysis, and individual shrimps were placed into a 12-well microplate - as seen in Figure 2.11 - using a Pasteur pipette. Three mL of exposure medium was added to their respective wells. The microplate was placed into the Noldus DanioVision observation chamber and the data was acquired with EthoVision X14 (Noldus Information Technology). The plates were calibrated digitally by measuring from the one side of the microplate to the other side and the arena settings were set (*Figure 2.10 and 2.11*).

A Basler monochrome GigE video camera was used for video recordings, and data acquisition occurred for a minimum of 20 minutes with a white light routine, in which there were two dark and two light phases of five min each. Video analysis was completed on EthoVision X17 (Noldus Information Technology), and the quantitative end points of total distance, average swimming speed, frequency of movement and non-movement, inner and outer zone and mobility were analysed. The raw data was exported into an Excel file and statistical analysis was completed on GraphPad Prism.

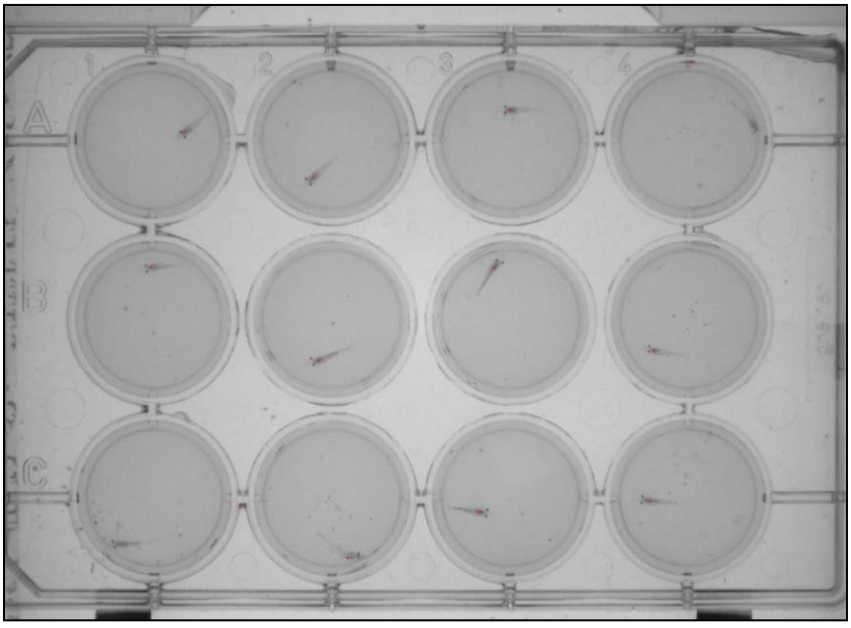

Figure 2.10 Microplate containing test organisms.

Figure 2.11 Arena settings for behavioural analysis for test organisms.

f) Metabolomics

The shrimp that was snap frozen from the respiration, heart rate and behaviour exposure were used for metabolomics. Five replicates per treatment group, each contained a pool of shrimp - two to three – and were used for metabolomic analysis. After being snap frozen with liquid nitrogen in 1.5 mL microcentrifuge tubes, and stored at -80°C, the pooled shrimp were weighed on a Radwag micro balance (AS 220/C2) to determine their wet weight, and they were inserted into new 1.5 mL microcentrifuge tubes, parafilmed and a needle-sized hole was poked through the lid of the tube. The samples were then freeze-dried at -54°C, < 15 Pa and for 72 hrs to ensure complete dryness. After freeze drying, the samples were weighed - to determine their dry weight – and re-parafilmed to be stored at room temperature until metabolomic analysis.

Metabolomic extraction and analysis was done by Centre for Human Metabolomics, North-West University. The protocol for the whole metabolome extraction from the whole crustacean is a single-phase extraction method described by (Beukes *et al.*, 2019) and was applied to all experimental samples of each treatment group. In short, the 1.5 mL Eppendorf tube contained the weights of each sample, 50 µL of the internal standard – 3-Phenylbutyric acid 100 ppm, and 1 mL extraction solution made up of chloroform, methanol and water at a ratio of 1:3:1. A 3 mm

tungsten carbide bead was added to each tube and the sample mixtures were placed in a vibration mill where they were shaken at 30 Hz for 10 minutes. After this, they were centrifuged at 12 000 rpm for 10 minutes at 4°C.

After centrifugation, 800 µL of the supernatant was transferred to a GC vial and were dried under a stream of nitrogen at 40°C for 20 – 30 minutes. 50 µL of methoxyamine HCl – 150 mg in 10 mL pyridine – was added then incubated at 50°C for 90 minutes for derivatization purposes. Hereafter, 40 µL of BSTFA + 1 % TMCS (N,O-Bis(trimethylsilyl)trifluoroacetamide with trimethylchlorosilane – Sigma Aldrich) was added to the sample and the extract was incubated again at 50°C for 60 minutes. After incubation, the extracts were transferred to a 250 µL insert in a sample vial and was capped before the GCxGC-TOF-MS analysis. The GCxGC-TOF-MS is a Pegasus 4D (Leco Corporation, St. Joesph, MI, USA), utilizes Agilent 7890A GC (Agilent, Atlanta, GA) coupled to a time-of-flight mass spectrometer (TOFMS) (Leco Corporation) and is equipped with a Gerstel Multi-Purpose Sampler (GMS) (Gerstel GmbH & co.).

The data were first processed using peak identification, where Leco Corporation ChromaTOF software (version 4.50) was used to find the peaks and mass spectral deconvolution at an S/N ratio of 300 with a minimum of 3 apexing peaks. Mass fragmentation patterns and their GC retention times were used to identify these peaks by comparing it to the commercially available NIST spectral libraries – mainlib, replib – with a similarity of 80% needed for a name to be assigned to a peak. The data was adjusted according to the sample weight.

The raw data were then exported to MS Excel and compounds with the same name and unique mass were consolidated. The data was then organized and filtered on Excel by removing variables that did not show up in 50% or more in a group, as these variables will not be of use when modelling the data. The Excel sheets were saved as a .csv file and uploaded to MetaboAnalyst for analysis where the data was normalized by the median and auto-scaled. Pathway analysis was done using the *Danio rerio* pathway with compound names on MetaboAnalyst.

2.8 Chronic Exposures

a) Lethality/Mortality

Mortality was the endpoint in the chronic exposure. The setup used for the chronic exposure can be seen in see *Figure 2.7*, except there were eight replicates containing three shrimp each per treatment group. Additional features to the exposure system *(Figure 2.12)*, where the tubing (*shown in green)* was connected to a larger pipe that was connected to the LP-Air source. The glass pipette was connected to the green tubing and was placed into the beaker for controlled air flow into the exposure beakers for the shrimps. Beakers were cling wrapped to prevent quick evaporation of the exposure medium (Muller *et al.*, 2011). Mesh netting of 15 cm X 5 cm was cut and placed into the beaker (ensuring the netting doesn't touch the bottom of the beaker), this net was pegged to the side of the beaker and was used as a substrate for the shrimp. The exposure occurred at 23°C in a 12 : 12 light : dark cycle (Muller *et al.*, 2011).

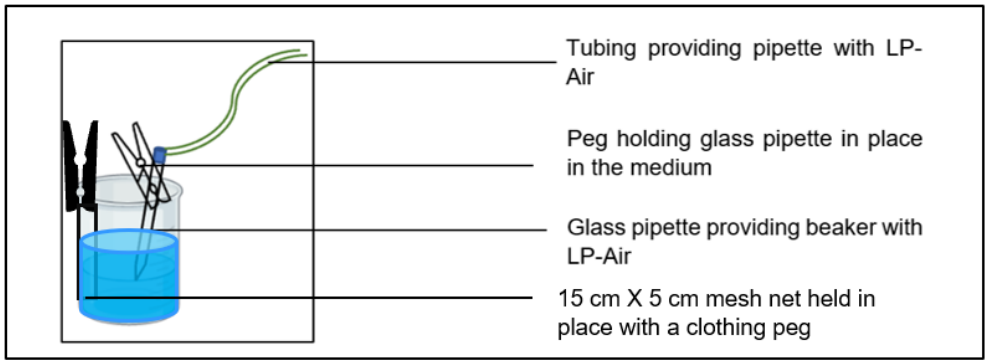

Figure 2.12 Additional features on every beaker during exposure.

This exposure ran for 25 days, allowing for a media change and re-spiking of toxicants every fifth day. Survival was measured by counting and recording the dead organisms in all the groups and removing them daily from the experimental vessel (Muller *et al.*, 2011).

From this, the cumulative mortality rate was determined per replicate in each treatment group. A threshold value was determined where increased mortality occurs. The means of the mortality response categorized by the different toxicants/treatments over the exposure period of four weeks

was completed for all replicates. This data was then plotted as percentage over 25 days (Muller *et al.*, 2011).

2.9 Statistical Analysis

i) Acute Toxicity Test: A built-in Probit analysis of the ToxRat software was applied and makes use of a linear maximum likelihood regression to calculate the LC_{50}.

ii) For bioaccumulation, respiration, heart rate, behaviour, and mortality, the data sets were checked for normality using Kolmogorov-Smirnov test. If the data was normally distributed, an analysis of variance – one way ANOVA, was used, and Tukey's multi-comparison test was used for the differences among the test groups. For data that did not meet the normal distribution assumption, a non-parametric Kruskal-Wallis test followed by a Mann-Whitney test was applied with a significant $p< 0.05$.

iii) Metabolomics: The metabolomic data was filtered to keep the variables the were present more than 80 % within a group. A cut-off coefficient variation of 50 % or more was utilized for any compounds that were not reliably measured. The data sheet was then uploaded to MetaboAnalyst, where the data was log-transformed, centred around the mean and auto-scaled. The data was then subjected to univariate (T-test) and multivariate analysis (Principal Component Analysis (PCA)) and Partial Least Squares – Discriminant Analysis (PLS-DA). Groups were compared with one another with the PCA 2D scores plot to check for any variances within the groups. A one-way analysis of variance (ANOVA), which is a univariate analysis, a post-hoc Tukey's test and a t-test was conducted to determine significant compounds between the various groups. The compounds were said to be significant if their $p \leq 0.05$ and their effect size ($d > 0.8$), which was determined with the post-hoc Tukey and t-test.

CHAPTER 3 RESULTS

3.1 Verification of indicator species

The evolutionary history of the taxa under study is assumed to be represented by the bootstrap consensus tree generated from 1000 replicates. Branches that are associated with partitions that were reproduced in fewer than 50% of bootstrap replicates, were collapsed. The branches are accompanied with the percentage of duplicate trees in which the linked taxa are grouped during the bootstrap test (1000 replicates). By automatically applying the Neighbor-Join and BioNJ algorithms to a matrix of pairwise distances – calculated using the Maximum Composite Likelihood (MCL) technique - and then choosing the topology with the best log-likelihood tree(s) for the heuristic search were created.

A discrete Gamma distribution was used to model evolutionary rate differences among sites (5 categories (+*G*, parameter = 1.4226)). The rate variation model allowed for some sites to be evolutionarily invariable ([+*I*], 20.09% sites). This analysis involved fifteen nucleotide sequences. There were a total of 565 positions in the final dataset. The evolutionary history was inferred by using the Maximum Likelihood method and General Time Reversible model in MEGA X.
Evolutionary analyses were conducted in MEGA X. The phylogenetic tree in Figure 3.1. shows that *Caridina africana* is the organism being tested, with *Daphnia magna* as the outgroup for comparison.

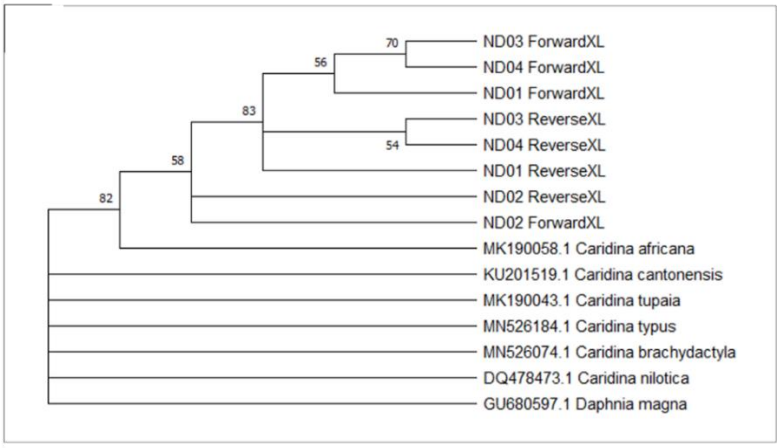

Figure 3.1 Phylogenetic identification and verification of indicator species selected for this project determines that the closest match to the test organism is *Caridina africana.*

3.2 NM characterization

3.2.1 NM Surface Charge & Size

The zeta potential of the two NMs at different concentrations are within the same range between -12 and -15 mV as seen in Table 3.1. There is a trend in the hydrodynamic size distribution between the two NMs, where the size distribution increased with an increase in the exposure concentration, the NDs formed larger agglomerates compared to the nCuO.

Table 3.1 Zeta potential and hydrodynamic size distribution (represented as the mean ± the standard deviation) of different nano copper oxide and nanodiamond exposure concentrations in the ISO media used for exposures.

Nano Copper oxide (nCuO)		
Exposure Concentrations (mg/L)	Zeta Potential (mV)	Hydrodynamic Size Distribution (d.nm)
LC_{10} – 0.97	-15.1 ± 0.9	280.7 ± 48.6
LC_{20} – 1.94	-13.85 ± 0.9	332.5 ± 9.1
20	-14.4 ± 1.3	986.6 ± 458.8
Nanodiamond (NDs)		
LC_{10} - 0.99	-12.4 ± 0.9	479.2 ± 80.3
LC_{20} - 1.97	-15.2 ± 1.1	873.6 ± 92.1
20	-13.5 ± 2.3	1891.0 ± 370.3

3.2.2 Dissolution of copper from nano copper oxide nanomaterial

The dissolution of copper from nCuO was less than 1% throughout all time intervals (*Table 3.2).*

Table 3.2 Dissolution of copper from nano copper oxide (represented as the mean ± the standard deviation) over the exposure duration of 96 hrs, with measurements recorded every 24 hrs in ISO media. *Abbreviations used are nCuO = nano copper oxide.

nCuO					
Exposure Concentrations (mg/L)	Dissolution (%)				
	0 h	24 h	48 h	72 h	96 h
LC_{10} – 0.97	0.05 ± 0.07	0.06 ± 0.04	0.10 ± 0.08	0.09 ± 0.04	0.11 ± 0.04
LC_{20} – 1.94	0	0.05 ± 0.02	0.07 ± 0.04	0.06 ± 0.02	0.07 ± 0.03
20	0	0.02	0.03	0.03 ± 0.01	0.04 ± 0.01

3.2.3 Transmission Electron Microscopy (TEM)

The concentrations used for TEM analysis were 20 mg/L for both NMs. The particle sizes for the nCuO ranges from 19 – 31 nm as seen in Figure 3.2. A – B, whereas for ND-PEG, it ranges from 5.20 – 7.45 nm as seen in Figure 3.2. C – E. It can be deduced from the images in *Figure 3.2* that the primary particle diameter for nCuO is about four times larger than ND-PEG, but large agglomerate could be observed in both groups.

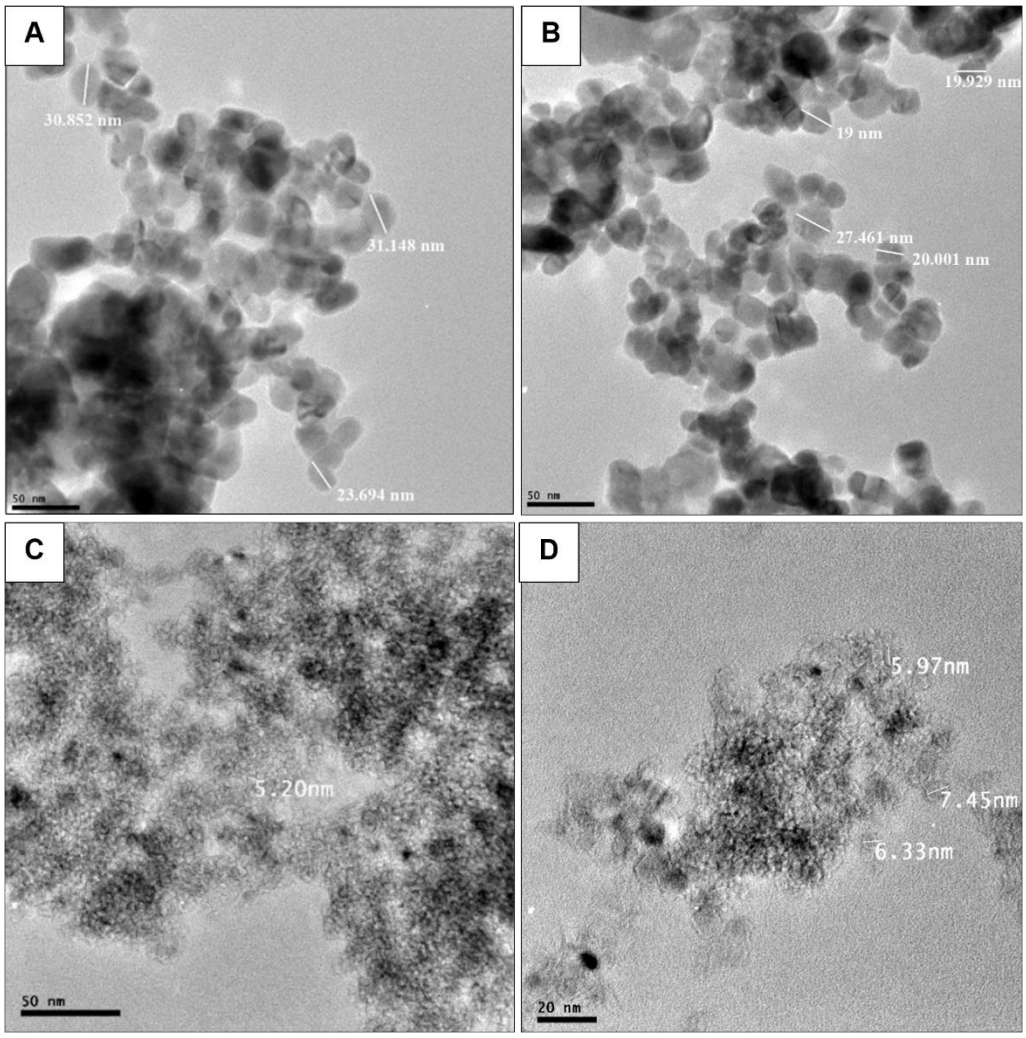

Figure 3.2 Transmission electron microscopy images at 0 hours, visualizing the primary particle size of 20 mg/L stock suspensions of (A – B) nano copper oxide, and (C – E) nanodiamonds in MilliQ® water.

3.3 Toxicity Exposures

3.3.1 Acute Toxicity Test

The $CuCl_2$ concentration effect curve (*Figure 3.3 A*) shows that this toxicant exhibits more of a dose-dependent response when compared to nCuO (*Figure 3.3 B)* and ND-PEG (*Figure 3.3 C*). As the concentration of $CuCl_2$ increases, the percentage immobility increases, except at 40 µg/L, where approximately 67% of the shrimps died. At the highest concentration of 200 µg/L, only 52%

of the shrimps died. For the two NMs, the percentage mobility does not display the same dose-dependency as for $CuCl_2$. There was a bi-modal response with greater mortality at the lowest and the two highest exposure concentrations. For ND-PEG, there was more of a dose-dependent relationship with only the lowest concentration of 10 mg/L showing greater mortality than in the 20 mg/L concentration.

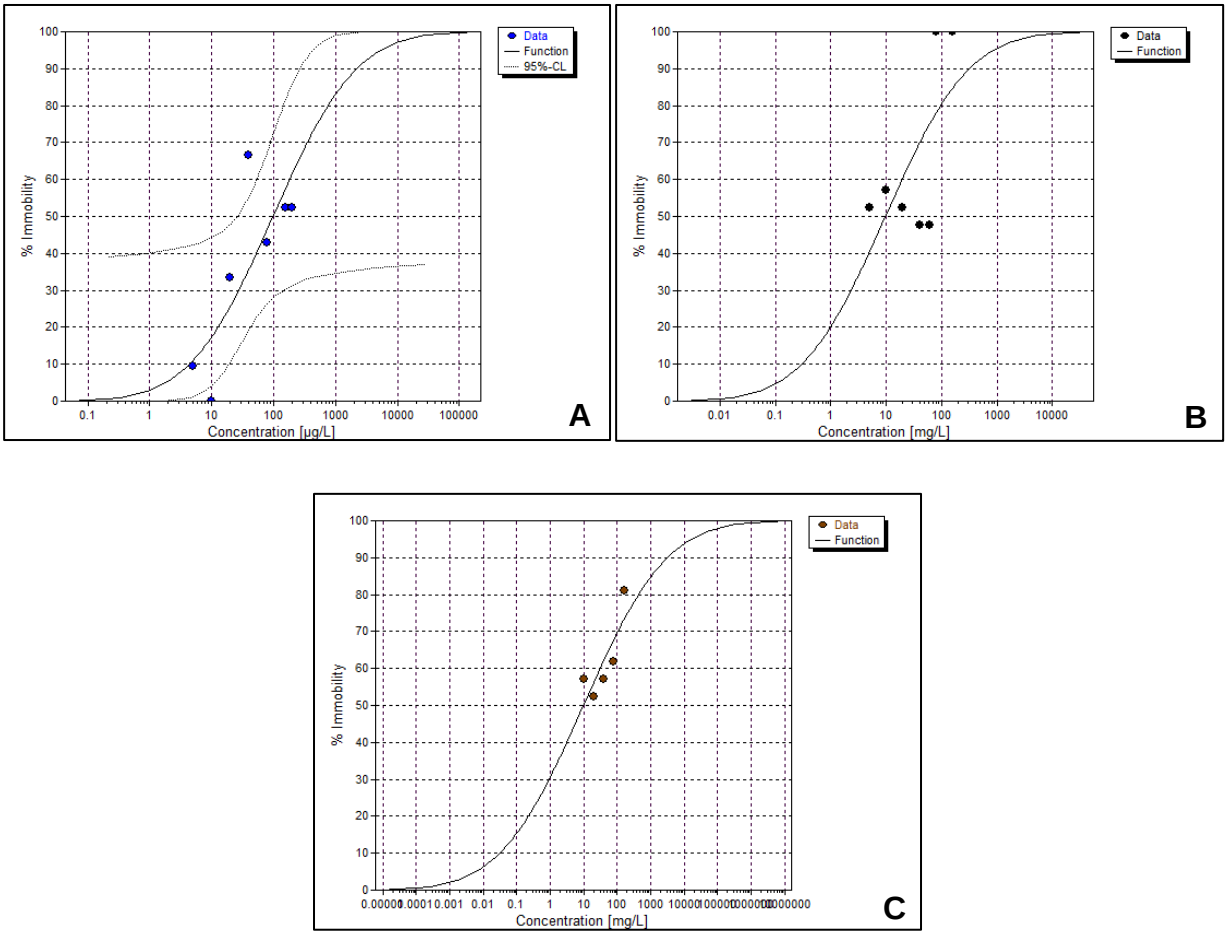

Figure 3.3 Concentration effect curve showing cumulative immobility in *Caridina africana* following exposure to (A) copper chloride (II), (B) nano copper oxide and (C) nanodiamonds after 96 hours.

Less than 10% of the control organisms died (not reported), thus rendering the test valid. The LC_{50}, LC_{10} and LC_{20} values for $CuCl_2$ were calculated using the Probit function in ToxRat. The $CuCl_2$ was deemed more toxic, followed by nCuO and ND-PEG to be the least toxic.

It was not possible to derive the LC_{10} and LC_{20} based on the response data for nCuO and ND-PEG (Table 3.3). Thus, for the purposes of selecting the sublethal exposure concentrations, the LC_{50} value was multiplied by 0.1 (10%) or 0.2 (20%). Therefore, the 10% and 20% of the LC_{50} (henceforth referred as the LC_{10} and LC_{20} for the purposes of this study), was 0.97 mg/L and 1.94 mg/L for nCuO, and 0.99 mg/L and 1.97 mg/L for ND-PEG, respectively.

Table 3.3 Summary of the LC_x values from ToxRat for the mortality of *Caridina africana* after 96 hours, for $CuCl_2$, nCuO and ND-PEG using the OECD202 *Daphnia magna* acute toxicity test worksheet. The lower and upper 95% confidence limits (CL) for the LC_x values are shown. *nd is where values could not be calculated. *Abbreviations used are $CuCl_2$ = copper chloride, nCuO = nano copper oxide, NDs = nanodiamonds.

$CuCl_2$			
	Concentration	**Lower CL**	**Upper CL**
LC_{10}	4.35 µg/L	n.d.	19.21
LC_{20}	12.69 µg/L	n.d.	42.59
LC_{50}	98.37 µg/L	25.89	n.d.
nCuO			
LC_{10}	n.d.	n.d.	n.d.
LC_{20}	n.d.	n.d.	n.d.
LC_{50}	9.720 mg/L	n.d.	n.d.
NDs			
LC_{10}	n.d.	n.d.	n.d.
LC_{20}	n.d.	n.d.	n.d.
LC_{50}	9.856 mg/L	n.d.	n.d.

3.3.2 Chronic toxicity test

a) *Chronic effects (moulting)*

Following long-term exposure to the respective LC_{10} exposure, all treatments exhibited decreased moulting compared to the control. The ND-PEG treatment group exhibited the highest cumulative moults compared to the other treatments within the first five days of exposure and until the end of exposure (*Figure 3.4 A*). The second treatment group that had the highest cumulative moults, was ionic Cu, with nCuO being the lowest in the first five days. However, both Cu-based exposures had the same cumulative moults at the end of the chronic exposure.

The LC_{20} ND-PEG treatment had more cumulative moults than the control, as well as compared to the other two treatments, and the Cu-based exposures had lesser cumulative moults than the control (*Figure 3.4 B*). The ionic copper exposure groups had the highest cumulative moult within the first five days and till the end of exposure when compared to nCuO. When comparing the two exposure concentrations, ND-PEG moulted the most when compared to Cu-based exposures. Out of the Cu-based exposures, the ionic copper group moulted more, followed by nCuO, however, these changes were not statistically different.

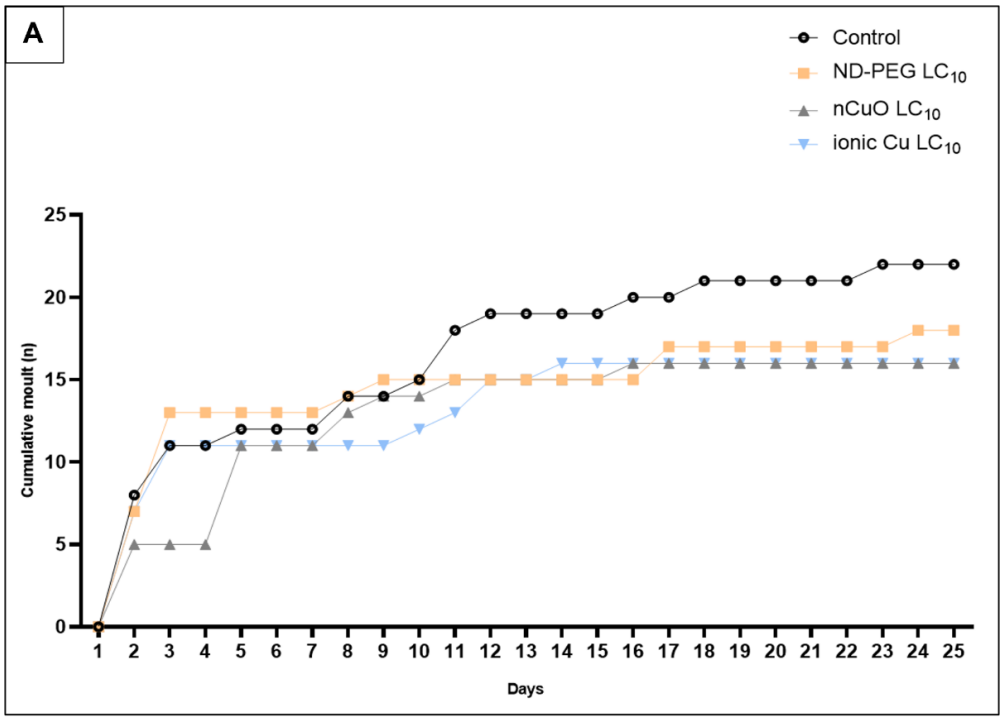

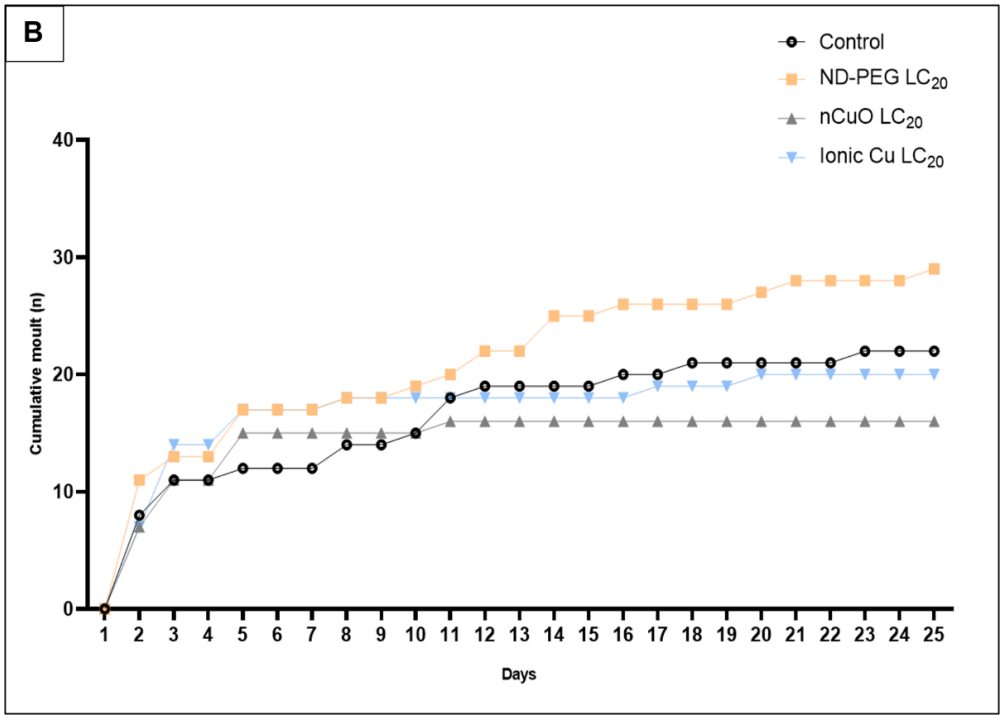

Figure 3.4 Cumulative moults (n) of *Caridina africana* following 25 days exposure to (A) LC_{10} (B) LC_{20} concentrations for nanodiamonds, nano copper oxide and ionic copper.

b) *Chronic time to mortality response*

Following long-term exposure to the respective LC_{10} and LC_{20} concentrations, the ND-PEG treatment reached 50% mortality on day 7, whereas the nCuO reached it on day 14 and the ionic group reached it by day 13 (*Figure 3.5 A*). However, the mortality rate increased more drastically for the two latter groups when compared to ND-PEG, as the mortality rate stayed consistent at 70% at day 12 until the end of exposure, whereby the mortality rate increased for nCuO and the ionic copper group until the end of the exposure period.

The LC_{20} nCuO treatment group reached a 50% mortality on day 7, whereas LC_{20} ND reached it at day 23, and the LC_{20} ionic Cu group reached it on day 12 (*Figure 3.5 B*). The LC_{20} Cu-based groups experienced a higher mortality rate compared to LC_{20} ND over the exposure period.

When comparing the two exposure concentrations, the LC_{10} ND reached a 50% mortality rate quicker than LC_{20} ND and also experienced a higher mortality rate than LC_{20} ND, reaching 70% compared to 50% at the end of the exposure period. With the nCuO groups, a 50% mortality rate was reached much slower in the LC_{10} nCuO than the LC_{20} nCuO. In the LC_{10} nCuO, the group experienced a reduced mortality rate than LC_{20} nCuO, that reached 90% at day 19 compared to 95% at day 14. The LC_{10} and LC_{20} ionic copper treatment groups reached 50% mortality around the same time - at day 13 - and had a similar mortality experience till the end of the exposure period. The control had the lowest mortality in both exposures. It did exhibit an increase in mortality until day 12, where it plateaued until day 23, where it increased slightly within one day and began to plateau till the end of exposure.

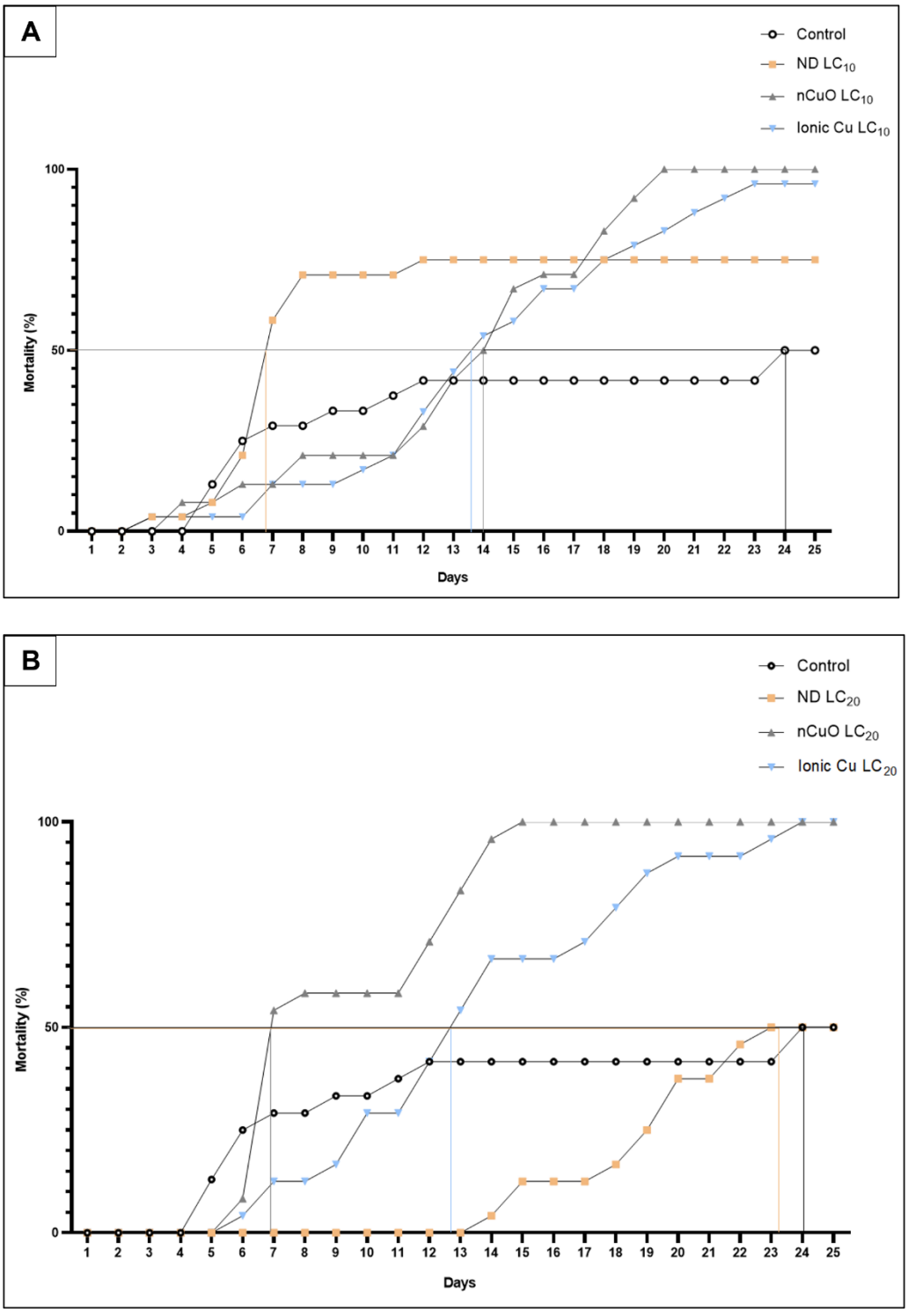

Figure 3.5 Mortality rate (%) of *Caridina africana* over 25 days being exposed to (A) LC_{10} and (B) LC_{20} concentrations for nanodiamonds, nano copper oxide and ionic copper. The lines indicate the lethal median time.

3.4 Sublethal Exposure Assessment

3.4.1 NM Distribution - CytoViva® Hyperspectral Dark Field Imagery

The control group shows the eye, carapace, pleopods, tail base, telson and pereiopods of the shrimp (*Figure 3.6 A – E).* The LC_{10} nCuO exposure group were seen bound to the carapace (*Figure 3.7 A & B*) as well as in the tail base and telson of the shrimp as dark spots/clusters in *Figure 3.7 C & D,* respectively. From the LC_{20} nCuO exposure, nCuO particles were seen via the darkened clusters on the eye, and head as well as the pereiopods, telson moults and near the mouth, as seen in *Figure 3.8 A, B, C & D, E and F*, respectively. Nanodiamond of the LC_{10} exposure can also be visualized as dark spots on the telson of the shrimp in *Figure 3.9 A*. No visible ND-PEG NMs was bound on the eyes of the shrimp in *Figure 3.9 B & C*, but there were visible particles present on the body and telson moult of the shrimp in *Figure 3.9 D & E*, respectively from the LC_{20} ND-PEG exposure.

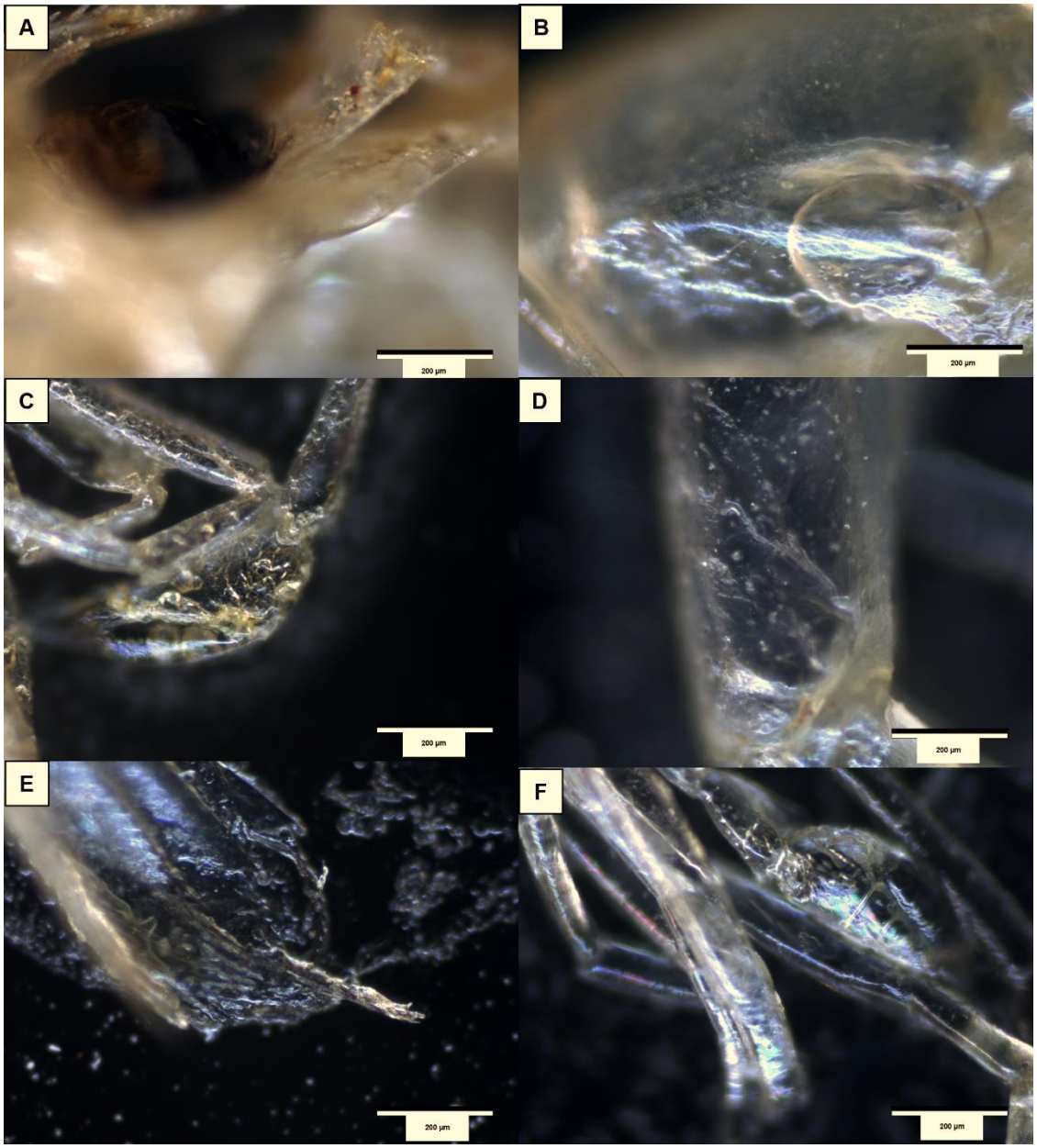

Figure 3.6 CytoViva® imaging of the control group for *Caridina africana* (A) eye (B) carapace (C) pleopods (D) tail base (E) telson (F) pereiopods.

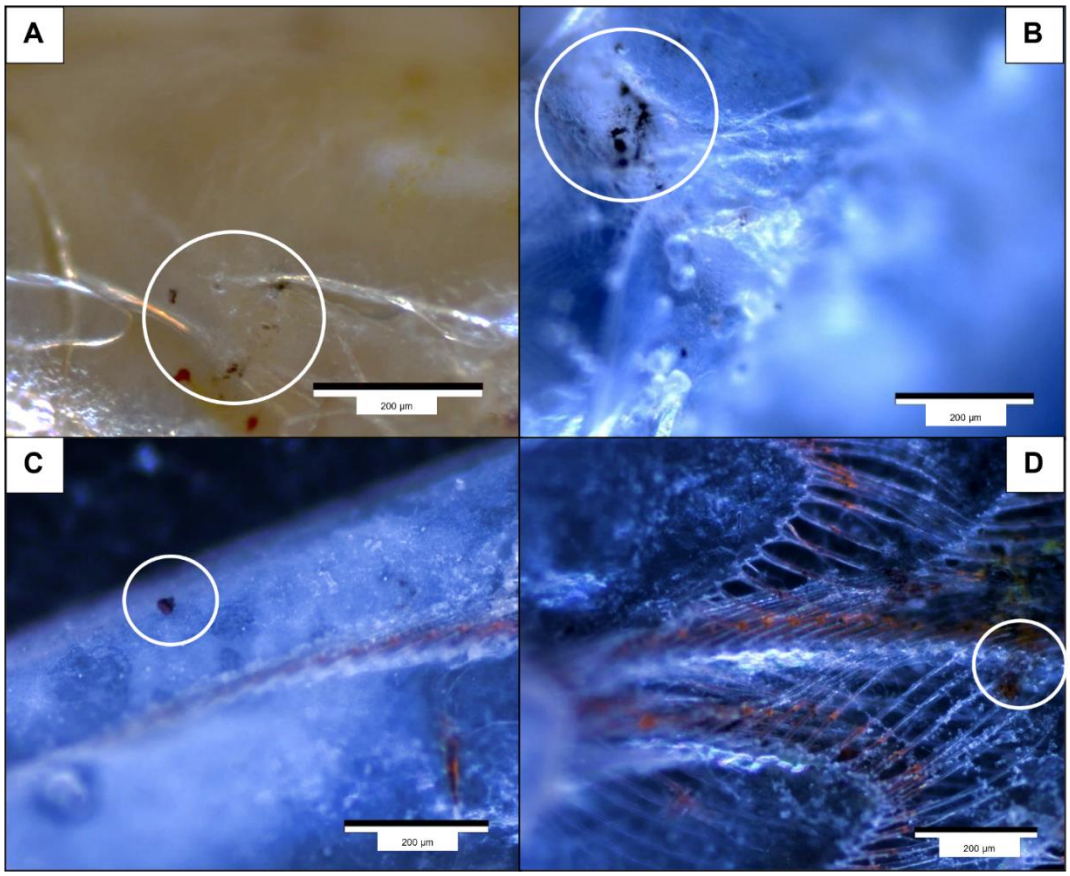

Figure 3.7 CytoViva® imaging of *Caridina africana* and its moults after a 96-hour exposure in LC_{10} nano copper oxide on the (A – B) carapace and (C – D) tail base and telson, respectively.

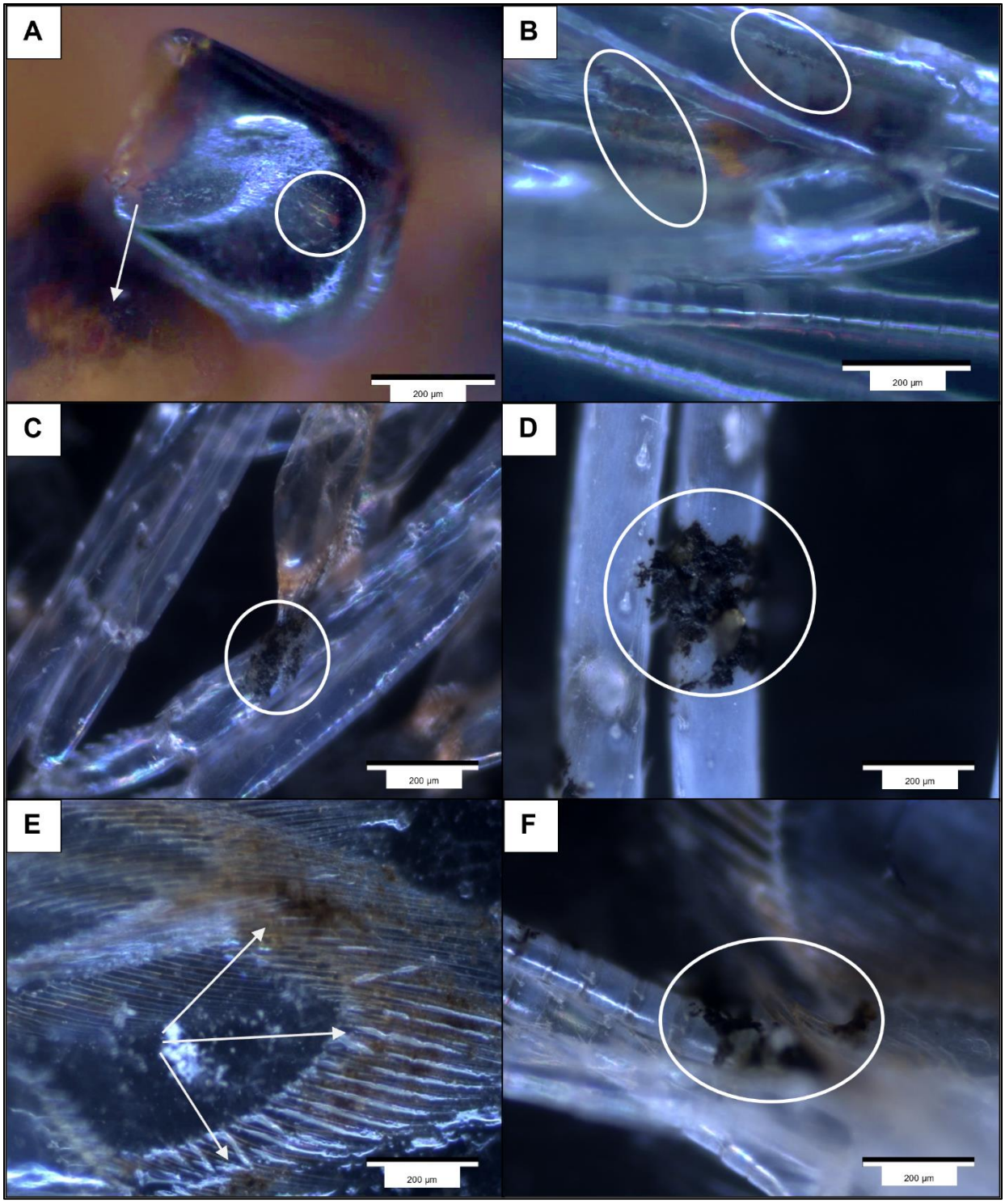

Figure 3.8 CytoViva® imaging of *Caridina africana* and its moults after a 96-hour exposure in LC_{20} nano copper oxide on (A – B) eye and head, (C – D) pereiopods, (E – F) telson moult and near the mouth, respectively.

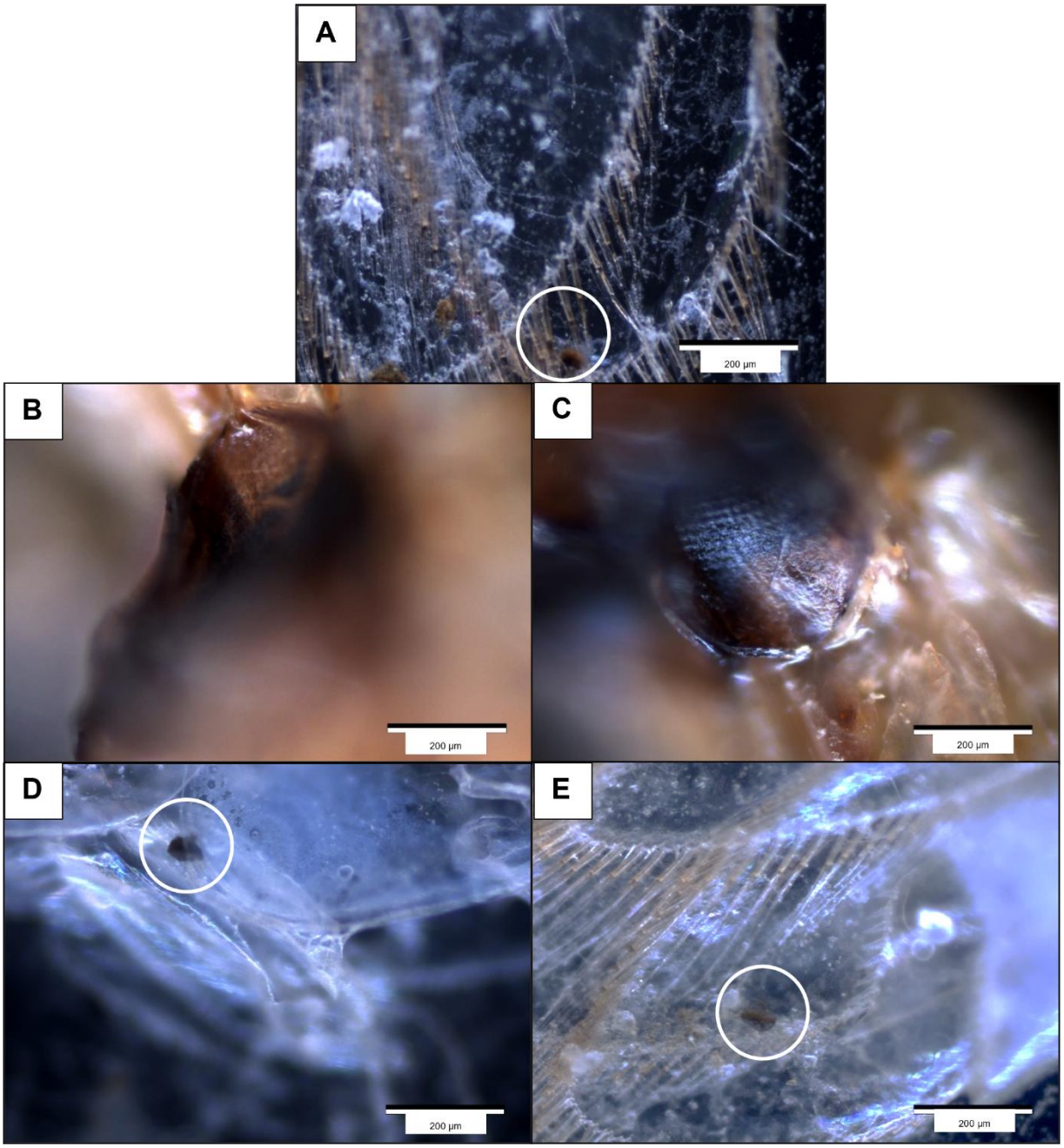

Figure 3.9 CytoViva® imaging of *Caridina africana* and its moults after a 96-hour exposure in (A – C) LC_{10} nanodiamond and (D – E) LC_{20} nanodiamond. (A) telson, (B – C) eye, (D) body moult, (E) telson moult.

3.4.2 Copper Bioaccumulation

The detection and quantification limits for the Cu analysis are reported in *Table 3.4*. Copper within the CRM was determined using GF-AAS and yielded a 73% recovery. It is important to note that even though the recovery rate is below the recommended threshold of 80%. For the purposes of this study, the results were not corrected for under-recovery. The LOD was calculated as three multiplied by the standard deviation of blank/average weight of all shrimp, and the LOQ as nine multiplied by the standard deviation of blank.

Table 3.4 Recovery rate (%), for the certified reference sample (ERM-CE278k), limit of detection (LOD), and limit of quantification (LOQ) for copper. *dw is an abbreviation for dry weight.

	Whole Organism		**ERM-CE278k**
Element	**LOD (µg/g dw*)**	**LOQ (µg/g dw*)**	**Recovery (%)**
Cu	0.2185	0.6555	73 ± 0.17

The shrimps exposed to nCuO, exhibit a higher Cu concentration (µg/g dry weight) in the whole organism when compared to the $CuCl_2$ exposed shrimps. Only the Cu levels in shrimp from the two highest concentrations of (40 and 60 mg/L) nCuO were significantly ($p<0.05$) different from the control (*Figure 3.10*). The Cu concentrations increased in the whole organism as the exposure concentration of $CuCl_2$ increases to a maximum of 325 µg/g at the highest exposure concentration of 200 µg/L.

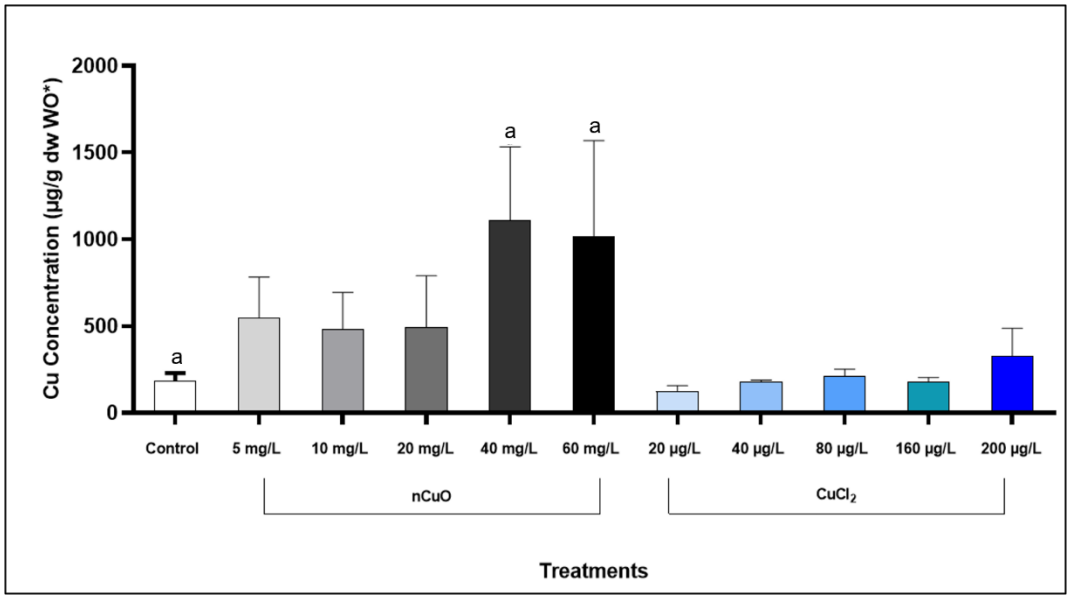

Figure 3.10 Copper concentrations (µg/g DW) in *Caridina africana* after a 96-hour exposure to various nano copper oxide and copper (II) chloride concentrations. The concentrations are represented as the mean ± the standard error of three independent replicates. Alphabetical superscript/s indicate significant differences between treatments relative to the control. Significance was regarded as $p<0.05$. *WO indicates in Whole Organism.

3.5 Sublethal Effects Assessment

3.5.1 Metabolomics

Multivariate analyses were conducted on shrimp exposure groups to determine the metabolomic profiles between the different treatments. All treatment groups along with the control were plotted to obtain a visual representation of their similarities/differences in terms of metabolome analytes (*Figure 3.11 A*). The LC_{10} and LC_{20} treatment groups were then plotted separately with the control to compare toxicants at the same sublethal exposure value to represent their similarities/differences in their metabolome analytes (*Figure 3.11 B and C*, respectively). Finally, ND-PEG/nCuO (nano-based treatments) and nCuO/$CuCl_2$ (Cu-based treatments) were compared to also represent any similarities/differences amongst their metabolome analytes (*Figure 3.12 A and B; C and D,* respectively).

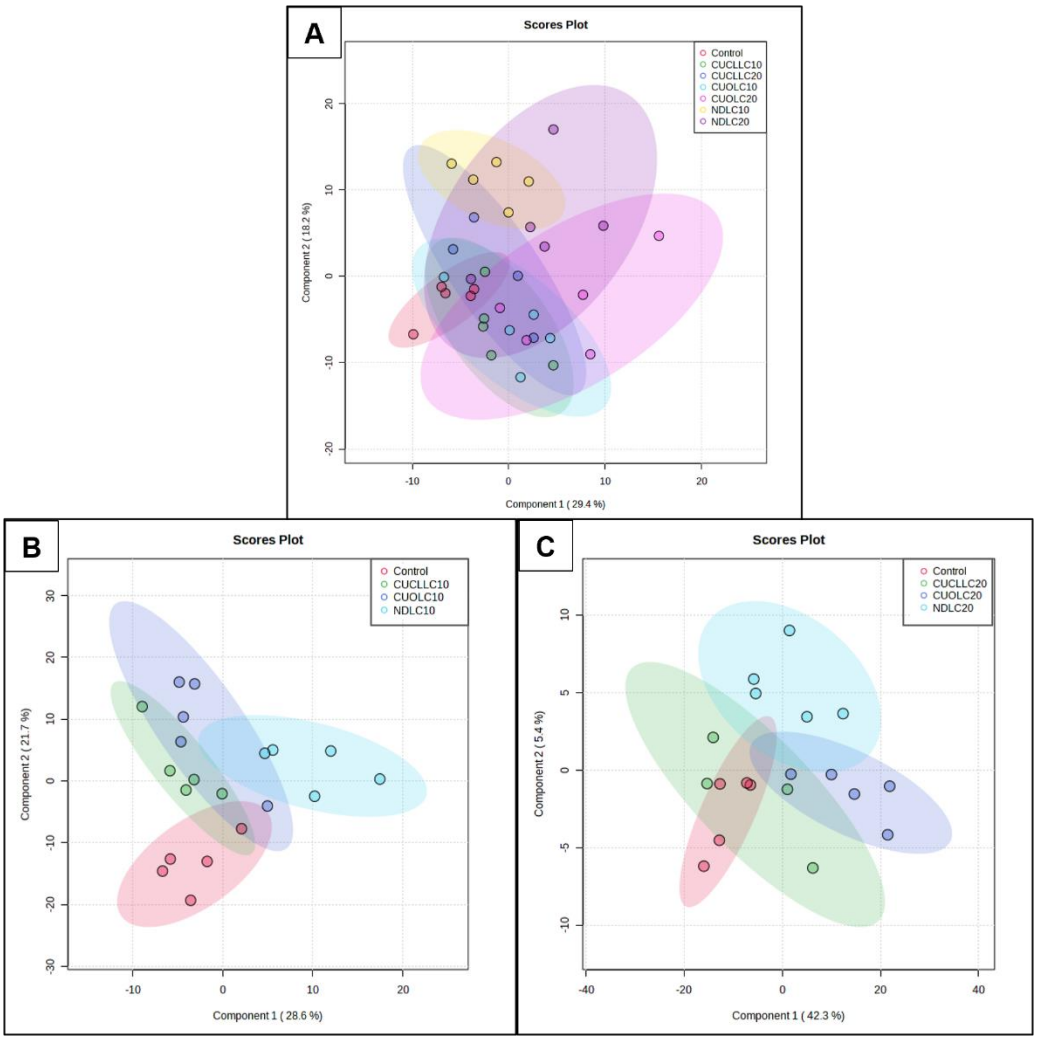

Figure 3.11 Multivariate analysis of partial least squares discriminant analysis for (A) all treatments (B) all LC_{10} treatments (C) all LC_{20} treatments (n=5 per group, except $CuCl_2$ that had 4 per group).

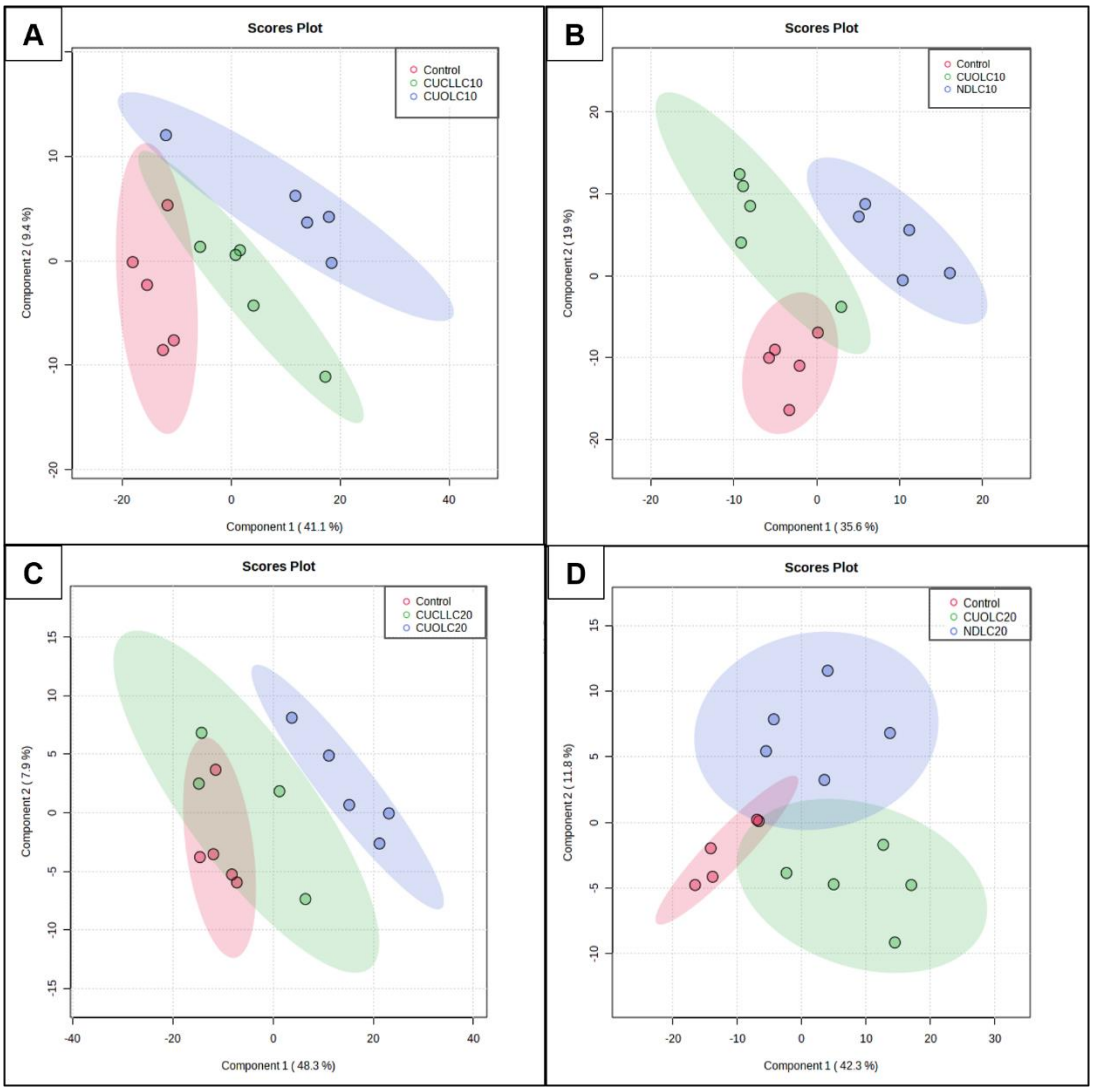

Figure 3.12 Multivariate analysis of partial least squares discriminant analysis for (A) LC_{10} copper chloride (II)/nano copper oxide (B) LC_{10} nano copper oxide/nanodiamonds (C) LC_{20} copper (II) chloride/nano copper oxide (D) LC_{20} nano copper oxide/nanodiamonds (n=5 per group, except $CuCl_2$ that had 4 per group).

PLS-DA Plots

The differences between the treatments and the controls based on the PLS-DA plots were further analyzed using a pairwise t-test, comparing nCuO and $CuCl_2$ (*Table 3.5*) and nCuO and NDs (Table 3.6), respectively. There are 40 significant ($p<0.05$) metabolites that differ between the control and nCuO LC_{20} treatment, while there were 25 and 20 metabolites that differ between the

control and LC_{10} $CuCl_2$ and LC_{10} nCuO treatments, respectively (*Table 3.5*). Only one metabolite was significantly ($p<0.05$) different between the control and LC_{20} $CuCl_2$ treatment. There were only 3 and 8 significant ($p<0.05$) metabolites that differ from the control and ND LC_{10} and ND LC_{20}, respectively (Table 3.6).

Heatmaps

Heatmaps allow for the visualization of patterns in the metabolite concentrations across samples – graphically repesents the information from *Tables 3.5* and *3.6* by using coloured blocks and a scale of either “4 to -4” or “2 to -2”, with either 4/2 showing the metabolites that are highly expressed in a treatment group and the -4/-2 represents metabolites that are least expressed in a treatment group. In *Figure 3.13* shows the heatmap of all the variables of importance (VIPs) within each sample in each treatment group, with “4” on the scale bar corresponding to a stronger correlation / more expression of a metabolite within a sample, with “- 4” on the scale bar illustrating a more negative correlation / less expression of a metabolite within a sample.

There were very clear differences in metabolites differentiated between the two concentrations of the NMs (nCuO and NDs) (*Figure 3.14 A* and *Figure 3.15*) and between the LC_{20} concentrations of the two Cu treatments (nCuO and $CuCl_2$) (*Figure 3.14 B*). There are no heatmaps for LC_{20} $CuCl_2$ and LC_{20} nCuO, as there were too few significant ($p<0.05$ and $d>0.8$) metabolites responsible for differences between the treatments.

Table 3.5 Pairwise comparison of all significant metabolites ($p<0.05$, and $d>0.8$) in *Caridina africana* following exposure to LC_{10} and LC_{20} of copper-based exposures. The grey sections indicate where no comparisons were run/analysed.

	$LC_{10}CuCl_2$	$LC_{20}CuCl_2$	$LC_{10}nCuO$	$LC_{20}nCuO$
Control	2,5-Bis((trimethylsilyl)oxy)pyrazine 2'-Desoxyuridine 4-Aminobutanoic acid 5-Dodecenoic acid 5-Methyluridine 9-Tetradecenoic acid a-D-Glucopyranose a-L-(-) Fucopyranose Cadaverine DL-Phenylalanine D-Lyxose Gluconic acid Glyceric acid L-Methionine l-Prolylglycine L-Serine L-Tryptophan Myristic acid N-Acetyl-D-glucosamine Oleic Acid (UM129) Putrescine Ribitol Serine Stearic acid Uracil	Gluconic acid	2,5-Bis((trimethylsilyl)oxy)pyrazine 2'-Desoxyuridine 5-Ethyl-1-(4-[trimethylsilyloxy]-3-[trimethylsilyloxy]methyltetrahydrofuran-2-yl)pyrimidine-2,4(1H,3H)-dione 5-Methyluridine 9H-Purin-6-ol 9-Tetradecenoic acid a-D-Glucopyranose a-L-(-)-Fucopyranose Cadaverine D-Lyxose d-Mannose Gluconic acid Glucopyranose Glyceric acid L-Lysine Putrescine Serine Stearic acid Uridine	11-Eicosenoic acid 2'-Desoxyuridine 4-Aminobutanoic acid 5-Methyluridine 9,12-Octadecadienoic acid 9H-Purin-6-ol 9-Tetradecenoic acid a-D-Allopyranose a-D-Glucopyranose a-L-(-)-Fucopyranose Arachidonoyl amide Benzenepropanoic acid, a-(methoxyimino)-, trimethylsilyl ester Benzenepropanoic acid, a-(methoxyimino)-4-[trimethylsilyloxy]-, trimethylsilyl ester Cadaverine D-(-)-Ribofuranose D-Arabinose DL-Phenylalanine D-Lyxose d-Mannose Gluconic acid Glucopyranose Heptadecanoic acid L-5-Oxoproline L-Lysine L-Methionine L-Proline l-Prolylglycine L-Rhamnose L-Serine Myristic acid N-Acetyl-D-glucosamine Oleic Acid

				Pentanedioic acid Phosphoric acid Putrescine Ribitol Serine Stearic acid Tyrosine Uracil
$LC_{10}CuCl_2$		11-Eicosenoic acid 5-Methyluridine a-D-Allopyranose DL-Phenylalanine D-Lyxose		
$LC_{20}CuCl_2$				11-Eicosenoic acid 9-Tetradecenoic acid a-D-Allopyranose Glucopyranose DL-Phenylalanine D-Lyxose D-Proline Gluconic acid Glucopyranose L-Glutamic acid L-Proline L-Serine Methyl stearate N-Acetyl-D-glucosamine Stearic acid Tyrosine
$LC_{10}nCuO$				2,5-Bis((trimethylsilyl)oxy)pyrazine Benzenepropanoic acid, a-(methoxyimino)-, trimethylsilyl ester L-Threonine

Table 3.6 Pairwise comparison of all significant metabolites ($p<0.05$, and $d>0.8$) in *Caridina africana* following exposure to LC_{10} and LC_{20} of nanodiamonds and nano copper oxide nanomaterials. The grey sections indicate where no comparisons were run/analysed.

	LC_{10}nCuO	LC_{20}nCuO	LC_{10}ND	LC_{20}ND
Control	See Table 3.5	See Table 3.5	D-(-)-Ribofuranose L-Rhamnose Uridine	4-Aminobutanoic acid 9-Tetradecenoic acid Cadaverine Methyl stearate Myristic acid Phosphoric acid Tridecanoic acid Uracil
LC_{10}nCuO		See Table 3.5	2'-Desoxyuridine 5-Ethyl-1-(4-[(trimethylsilyl)oxy]-3-{[(trimethylsilyl)oxy]methyl}tetrahydrofuran-2-yl)pyrimidine-2,4(1H,3H)-dione 9H-Purin-6-ol 9-Tetradecenoic acid a-D-Glucopyranose a-L-(-)-Fucopyranose Butanedioic acid Cadaverine D-(-)-Ribofuranose Diethylene glycol d-Mannose d-Proline Gluconic acid Glucopyranose Glyceric acid Heptadecanoic acid L-Proline l-Prolylglycine L-Rhamnose L-Serine Palmitelaidic acid Putrescine Serine	

			Stearic acid Tridecanoic acid Tyrosine Uridine	
$LC_{20}nCuO$	See Table 3.5			2'-Desoxyuridine 9-Tetradecenoic acid a-D-Glucopyranose DL-Phenylalanine D-Lyxose d-Proline Gluconic acid Heptadecanoic acid L-5-Oxoproline L-Lysine L-Methionine Myristic acid Palmitic Acid Serine Stearic acid
$LC_{10}ND$				9-Tetradecenoic acid Arachidic acid Cadaverine D-(-)-Ribofuranose Glyceric acid L-Rhamnose L-Serine Methyl stearate Myo-Inositol Palmitelaidic acid Putrescine Thymidine Uracil

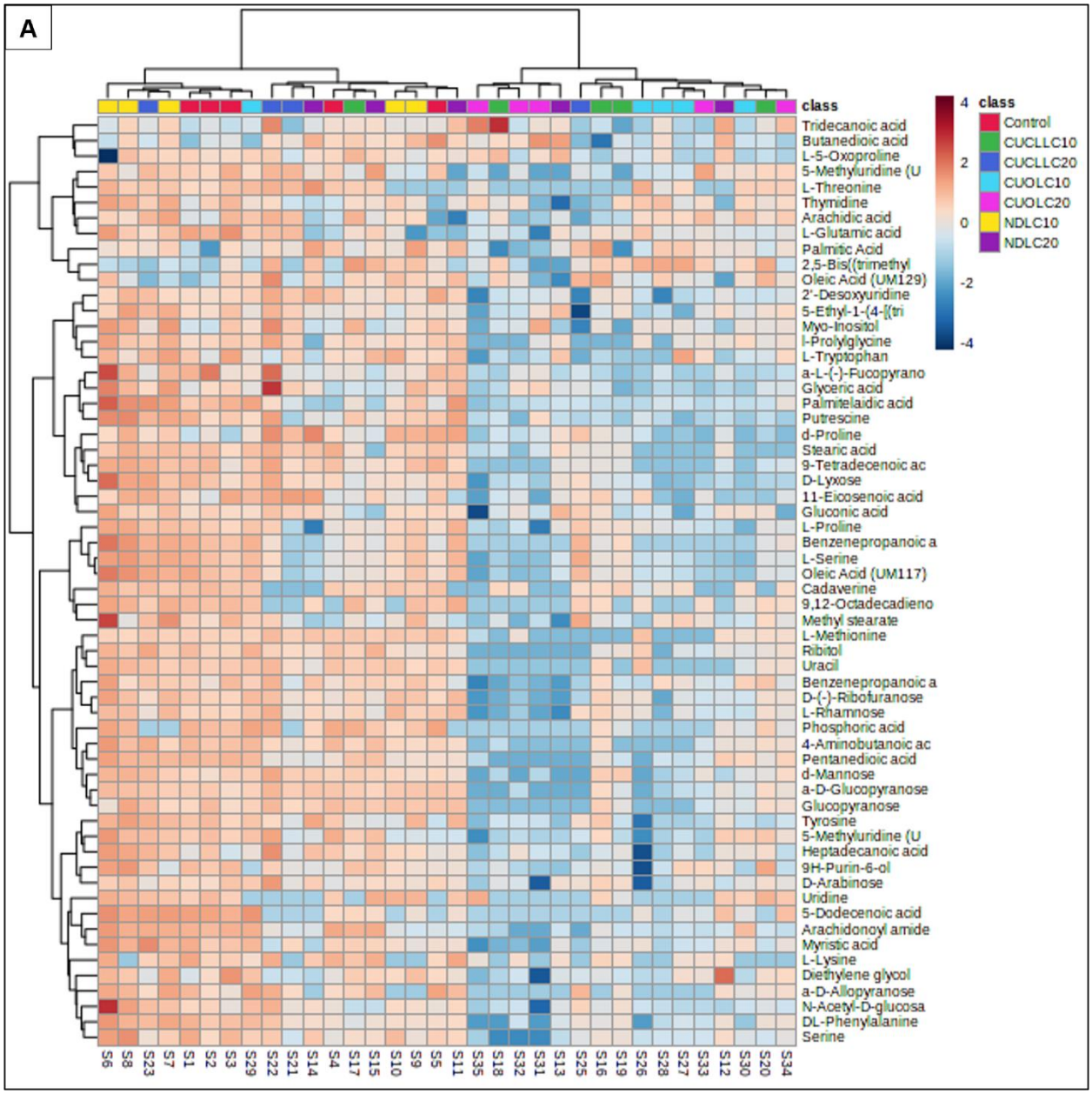

Figure 3.13 Heatmap for all VIP metabolites in all treatment groups.

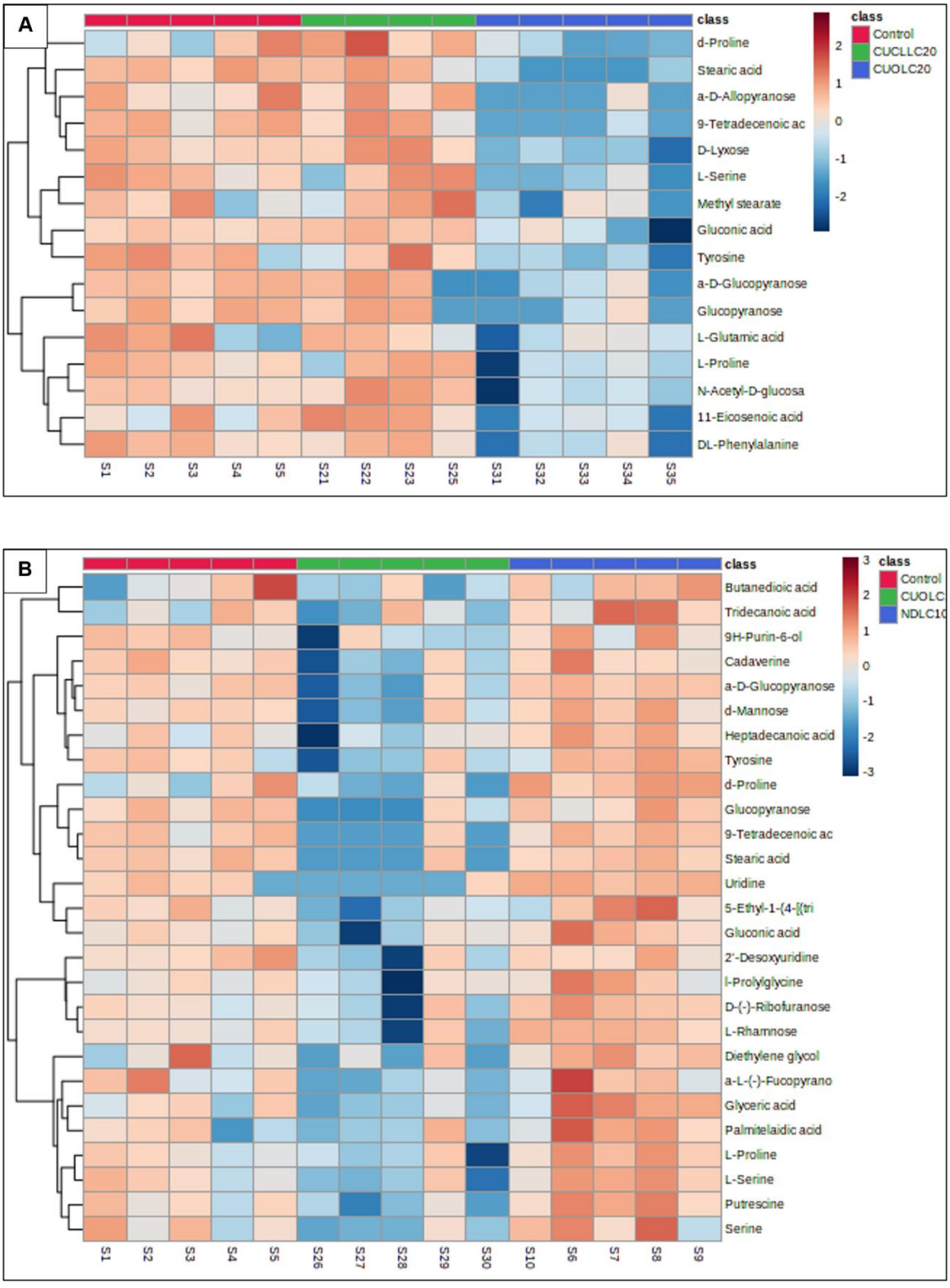

Figure 3.14 Heat maps of VIP metabolites for (A) LC_{20} nano copper oxide and LC_{20} copper chloride (B) LC_{10} nano copper oxide and LC_{10} nanodiamonds. Significance was regarded as $p<0.05$ and $d>0.8$.

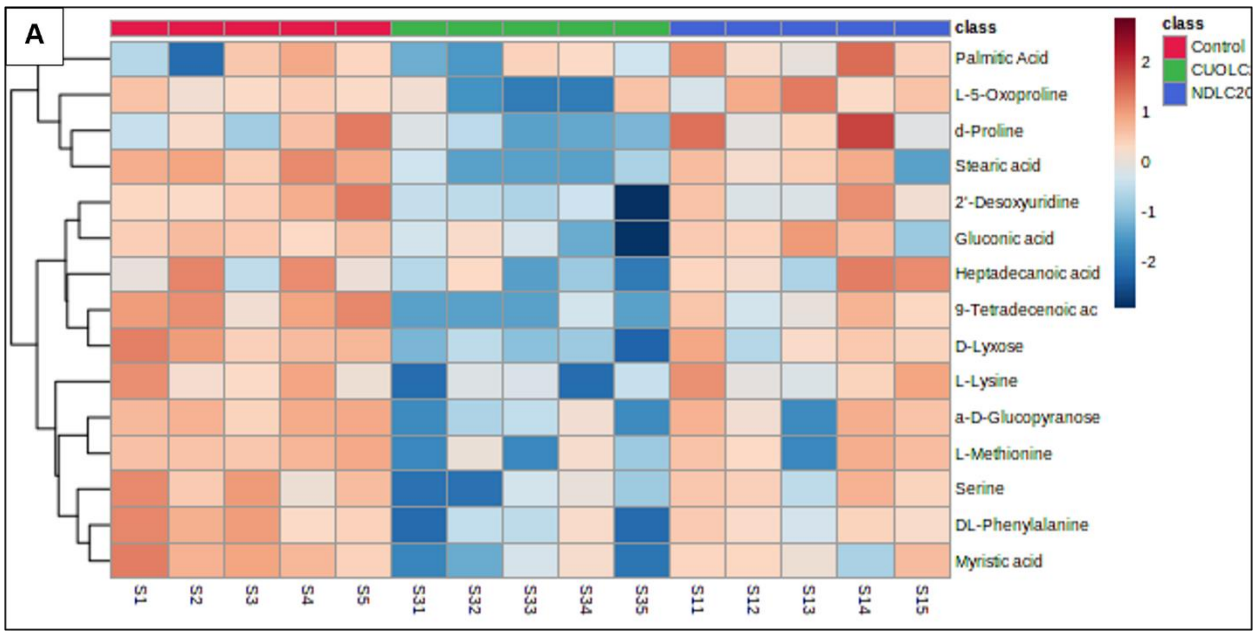

Figure 3.15 Heat map of VIP metabolites for LC_{20} nano copper oxide and LC_{20} nanodiamonds. Significance was regarded as p<0.05 and d>0.8.

Pathway Analysis

The pathway analyses for controls vs treatments and between NM originates from the pairwise comparisons conducted in *Table 3.5* and *3.6*. These analyses are dependent on the number and role a specific metabolite/s play in the pathway. The impact factors (shown on the x axis) range from 0 to 1, with 1 being the highest impact a certain metabolite has on the pathway. Significance was regarded as p<0.5 and d>0.8.

Controls vs treatments

The glycerine, serine and threonine metabolism and the arginine and proline metabolism fall under than amino acid biosynthesis pathway, which is one of the major pathways affected in this group. The pentose phosphate pathway, the glutathione metabolism and pyrimidine metabolism are the other major pathways that were affected in the control vs LC_{10} nCuO (*Figure 3.16 A*, *Table 3.5*).

For control vs LC_{20} nCuO treatment group, the most important pathways affected were the amino acid biosynthesis pathways (i.e. arginine, proline and phenylalanine, tyrosine and tryptophan biosynthesis and cysteine and methionine metabolism) (*Figure 3.16 B, Table 3.5*). Other

pathways also affected were the glutathione metabolism, biosynthesis of unsaturated fatty acids, fatty acid biosynthesis, pyrimidine metabolism as well as aminoacyl-tRNA biosynthesis.

The major pathways affected in the control vs LC_{20} ND treatment group were the amino acid biosynthesis (i.e. arginine, proline and alanine metabolism and aspartate and glutamate metabolism). The pyrimidine metabolism and the butanoate metabolism were amongst affected pathways (*Figure 3.16 C, Table 3.6*).

Amino acid biosynthesis (i.e. arginine, proline, alanine, aspartate and glutamate metabolism, cysteine and methionine metabolism, glycine, serine and threonine metabolism) were affected in the control vs LC_{10} $CuCl_2$ treatment group. Other pathways include: glyoxylate and dicarboxylate metabolism, the glycerolipid metabolism, pyrimidine metabolism and the tryptophan metabolism (*Figure 3.16 D, Table 3.5*).

There are differences within the controls vs the different treatment groups (*Figure 3.16 A, B, C and D).* The most affected pathway is the amino acid biosynthesis and the pyrimidine metabolism. There are a few notable differences, such as the biosynthesis of fatty acids and fatty acid biosynthesis (*Figure 3.16 B*). It is the only major pathways that differs. The glyoxylate, dicarboxylate and the tryptophan metabolism are the only pathways that differ in the control vs LC_{10} $CuCl_2$ treatment group from the rest of the treatment groups (*Figure 3.16 D*). The butanoate metabolism, is the only major pathway that is only present in the control vs LC_{20} ND treatment group that differs from the other treatment groups (*Figure 3.16 C*).

nCuO vs ND

The major pathways in LC_{10} nCuO and LC_{10} ND that were affected based on the significant metabolites, included: the amino acid biosynthesis (i.e. glycerine, serine and threonine, and arginine, proline and phenylalanine, as well as phenylalanine, tyrosine and tryptophan) (*Figure 3.17 A, Table 3.6).* The pentose phosphate pathway and glutathione, glyoxylate and dicarboxylate as well as the aminoacyl-tRNA biosynthesis pathways were also affected.

The amino acid biosynthesis, pyrimidine metabolism as well as the galactose metabolism in the LC_{20} nCuO vs LC_{20} ND were affected (*Figure 3.17 B, Table 3.6*). The most common metabolism affected was the amino acid biosynthesis. The galactose and pyrimidine metabolism are affected in the LC_{20} nCuO vs LC_{20} ND, whereas they're not mentioned in the LC_{10} treatment groups.

Nanomaterial vs ionic

In LC_{20} nCuO vs LC_{20} $CuCl_2$, the glyoxylate, dicarboxylate and amino acid biosynthesis is one of the major pathways affected (*Figure 3.17 C, Table 3.5*).

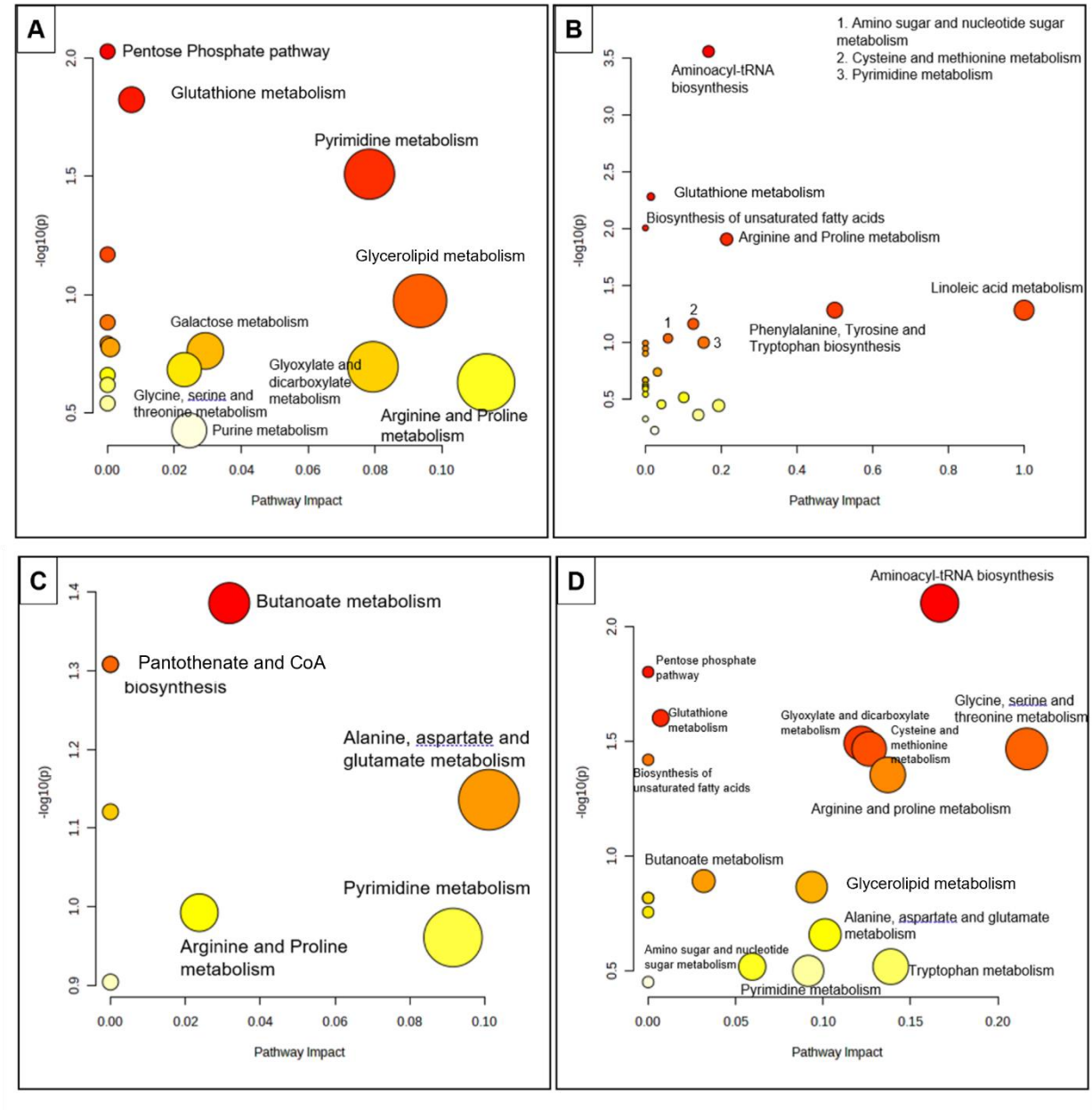

Figure 3.16 Pathway analysis for (A) control and LC_{10} nano copper oxide (B) control vs LC_{20} nano copper oxide (C) control vs LC_{20} nanodiamond (D) control vs LC_{10} copper chloride. The size of the pathway's circles are determined by the relationship between the significance and impact factor.

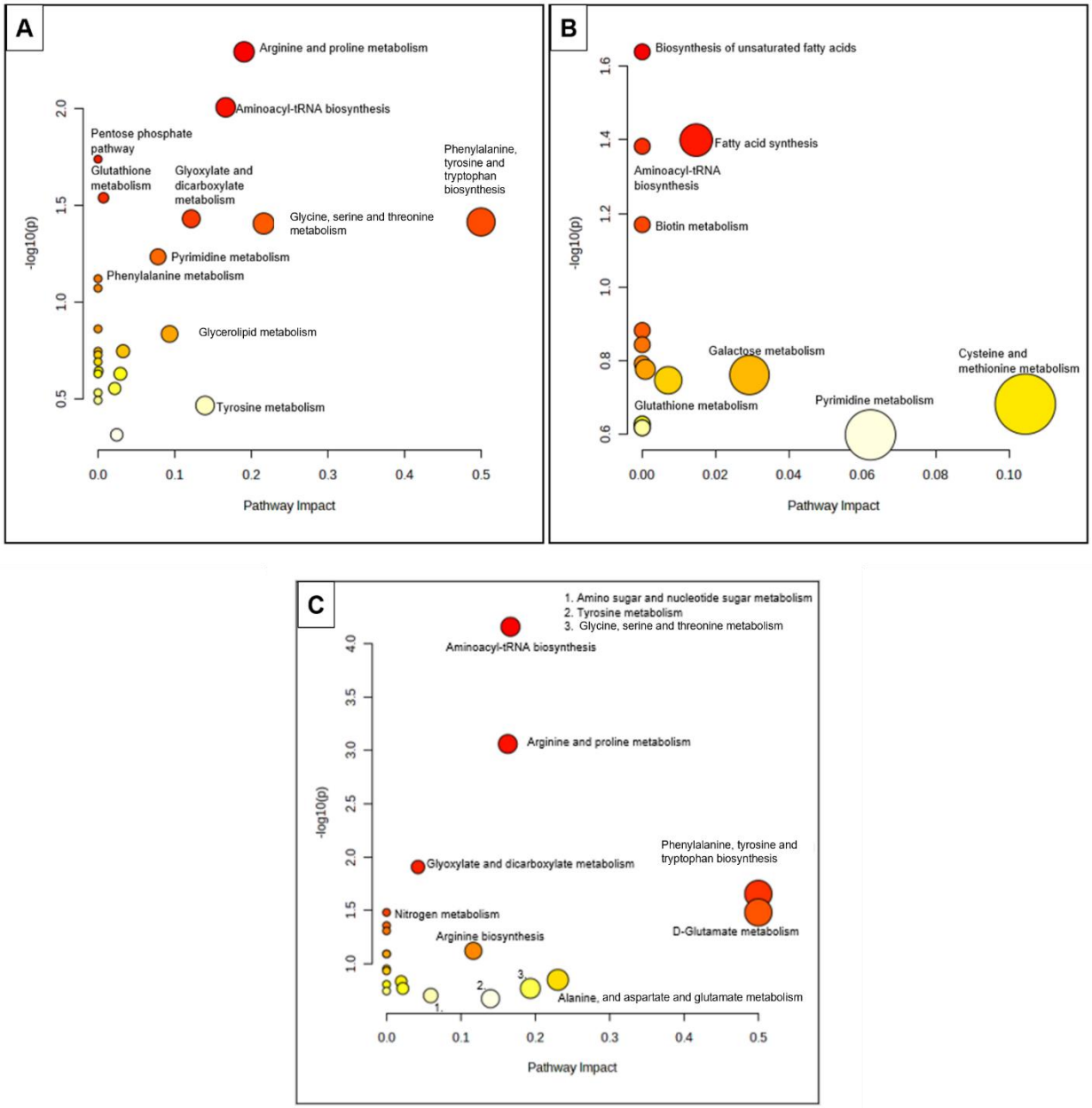

Figure 3.17 Pathway analysis for (A) LC_{10} nano copper oxide and LC_{10} nanodiamonds (B) LC_{20} nano copper oxide and LC_{20} nanodiamonds (C) LC_{20} nano copper oxide and LC_{20} copper chloride. The size of the pathway's circles are determined by the relationship between the significance and impact factor.

The significant metabolites and the major pathways in which they fall under are summarized in *Table 3.7.*

Table 3.7 Significant metabolites based on their p and d value, and their corresponding pathways for various treatments groups.

Group	Significant Metabolite/s	p-value	d-value	Affected Pathway/s
Control vs $nCuO_{10}$	D-Glycerate	0.025	1.575	Pentose Phosphate Pathway
	Cadaverine	0.008	1.785	Glutathione Metabolism
	Deoxyuridine	0.025	1.575	Pyrimidine Metabolism
	Putrescine	0.016	1.901	Glutathione Metabolism
Control vs $nCuO_{20}$	L-Phenylalanine	0.017	1.380	Amino acid biosynthesis
	Serine	0.009	1.611	Amino acid biosynthesis
	Methionine	0.000	3.151	Amino acid biosynthesis
	Lysine	0.014	1.520	Amino acid biosynthesis
	Tyrosine	0.006	1.693	Amino acid biosynthesis
	Proline	0.004	1.863	Amino acid biosynthesis
	Cadaverine	0.000	2.934	Glutathione metabolism
	Putrescine	0.011	2.072	Glutathione metabolism
	Oxoproline	0.049	1.056	Glutathione metabolism
	Deoxyuridine	0.006	1.737	Pyrimidine metabolism
	Uracil	0.000	4.861	Pyrimidine metabolism
Control vs $CuCl_{10}$	Gluconic acid	0.012	1.714	Pentose Phosphate Pathway
	Serine	0.038	1.213	Amino acid biosynthesis
	Methionine	0.035	1.274	Amino acid biosynthesis
	L-Phenylalanine	0.028	1.224	Amino acid biosynthesis
	Deoxyuridine	0.035	1.239	Pyrimidine metabolism
	Uracil	0.015	1.438	Pyrimidine metabolism/DNA synthesis
	Cadaverine	0.013	1.599	Glutathione metabolism
	Putrescine	0.044	1.406	Glutathione metabolism
$nCuO_{10}$ vs ND_{10}	D-Proline	0.001	3.227	Amino acid biosynthesis
	L-Proline	0.017	1.533	Amino acid biosynthesis
	Putrescine	0.002	2.375	Glutathione metabolism
	Serine	0.031	1.217	Amino acid biosynthesis/Glyoxylate & dicarboxylate metabolism
	Tyrosine	0.021	1.521	Amino acid biosynthesis
	Gluconic acid	0.019	1.526	Pentose phosphate pathway
	Cadaverine	0.025	1.623	Glutathione metabolism
	Deoxyuridine	0.025	1.650	Pyrimidine metabolism
	Uridine	0.000	4.452	Pyrimidine metabolism
$nCuO_{20}$ vs ND_{20}	Phenylalanine	0.023	1.712	Amino acid biosynthesis
	Methionine	0.045	1.146	Amino acid biosynthesis
	Lysine	0.026	1.307	Amino acid biosynthesis
	Palmitic acid	0.050	1.317	Biosynthesis of unsaturated fatty acids
	Tetradecenoic acid	0.016	1.382	Fatty acid biosynthesis
$nCuO_{20}$ vs $CuCl_{20}$	Phenylalanine	0.026	1.282	Amino acid biosynthesis
	Serine	0.040	1.114	Amino acid biosynthesis
	Tyrosine	0.040	1.115	Amino acid biosynthesis
	D-Proline	0.006	1.783	Amino acid biosynthesis
	L-Proline	0.018	1.373	Amino acid biosynthesis
	Glutamate	0.026	1.586	Amino acid biosynthesis
	Glucosamine	0.003	2.147	Energy metabolism
	Glucose	0.039	1.126	Energy metabolism

(p and d values for all group metabolites are present in appendix C).

3.5.2 Respiration

All exposure treatments caused an increase in oxygen consumption rates when compared to the control. The nCuO exposure groups (*Figure 3.18 A and 3.18 B*) exhibit significantly higher oxygen consumption rates when compared to the rest of the exposure treatments. The ND treatments resulted in the second highest oxygen consumption rates, with the lowest increase recorded in the LC_{20} $CuCl_2$ exposure.

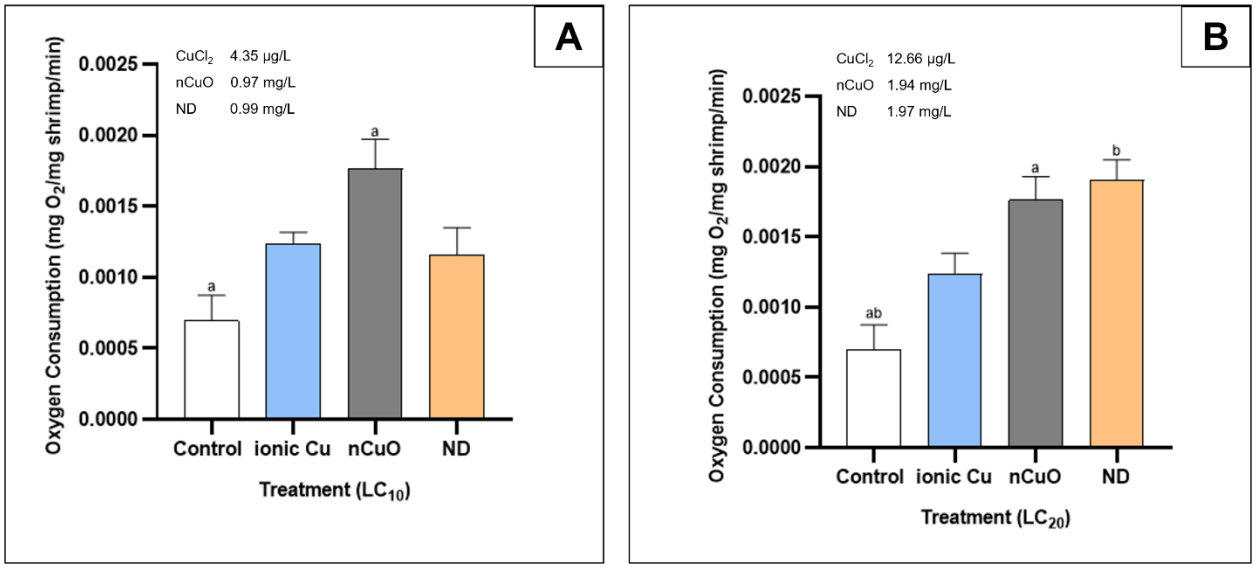

Figure 3.18 The oxygen consumption (mg O_2/mg shrimp/min) in *Caridina africana* after a 96-hour exposure to nanodiamonds, nano copper oxide and copper chloride (II) at their respective (A) LC_{10} and (B) LC_{20} concentrations. The oxygen consumption rate is represented as the mean ± the standard error of seven independent replicates. Bars with common alphabetical superscript/s indicate significant differences within their respective treatment groups relative to the control. Significance was regarded as $p<0.05$.

3.5.3 Heart Rate

There are similar trends with the heart rate (*Figure 3.19 A, and 3.19 B*). The heart rate of both LC_{10} and LC_{20} nCuO and ionic Cu, were lower when compared to the control. The LC_{10} and LC_{20} ND exposures resulted in significantly higher ($p<0.05$) heart rates when compared to the control and the Cu-based treatments.

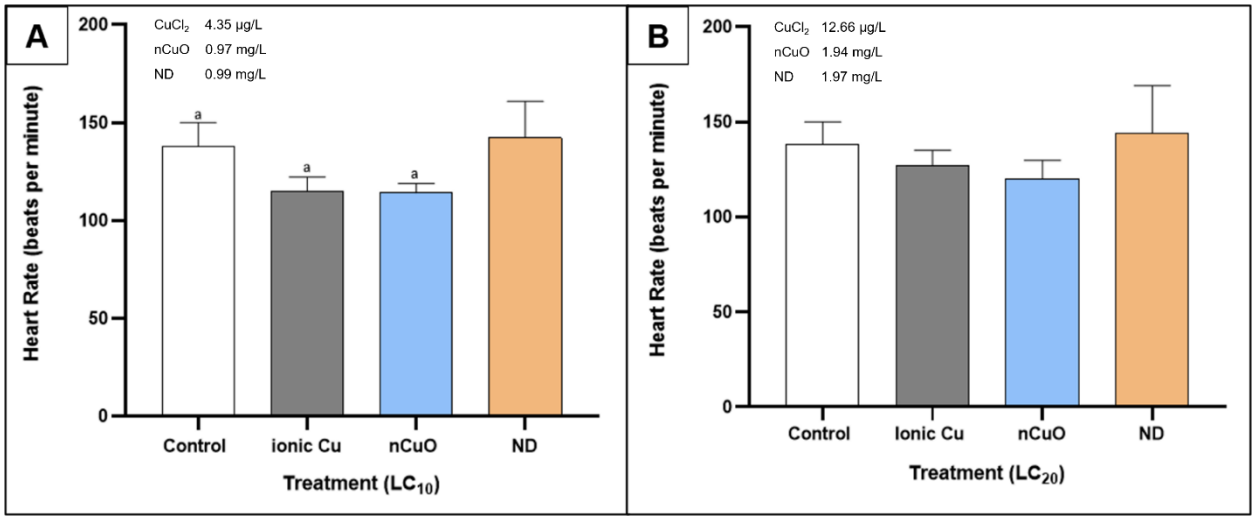

Figure 3.19 The heart beats/minute in *Caridina africana* after a 96-hour exposure to nanodiamonds, nano copper oxide and copper chloride (II) at their respective (A) LC_{10} and (B) LC_{20} concentrations. The heart rate is represented as the mean ± the standard error of seven independent replicates. Bars with common alphabetical superscript/s indicate significant differences within their respective treatment groups relative to the control. Significance was regarded as $p<0.05$.

3.5.4 Behaviour

Total Distance moved (mm)

The total distance travelled in LC_{10} ND and both $CuCl_2$ treatments in both dark and light phases were greater than the control (*Figure 3.20 A*). Both nCuO treatments moved less than the controls during both the light and dark phases. In all instances, the distances moved were not significantly ($p>0.05$) different from the control. However, it was noted there was a large variation between individual replicates.

The total distance travelled in LC_{20} ND exposure group was less than the control group in both the dark and light phases. The nCuO treatments also resulted in less distance travelled compared to the control. Both $CuCl_2$ treatments travelled significantly ($p<0.05$) further than the nCuO treatments. Generally, the differences in the distances travelled were greater during the light phase than the dark phase (*Figure 3.20 B*). When the two exposure concentrations were compared, the differences in distances were more pronounced in the LC_{20} exposure groups.

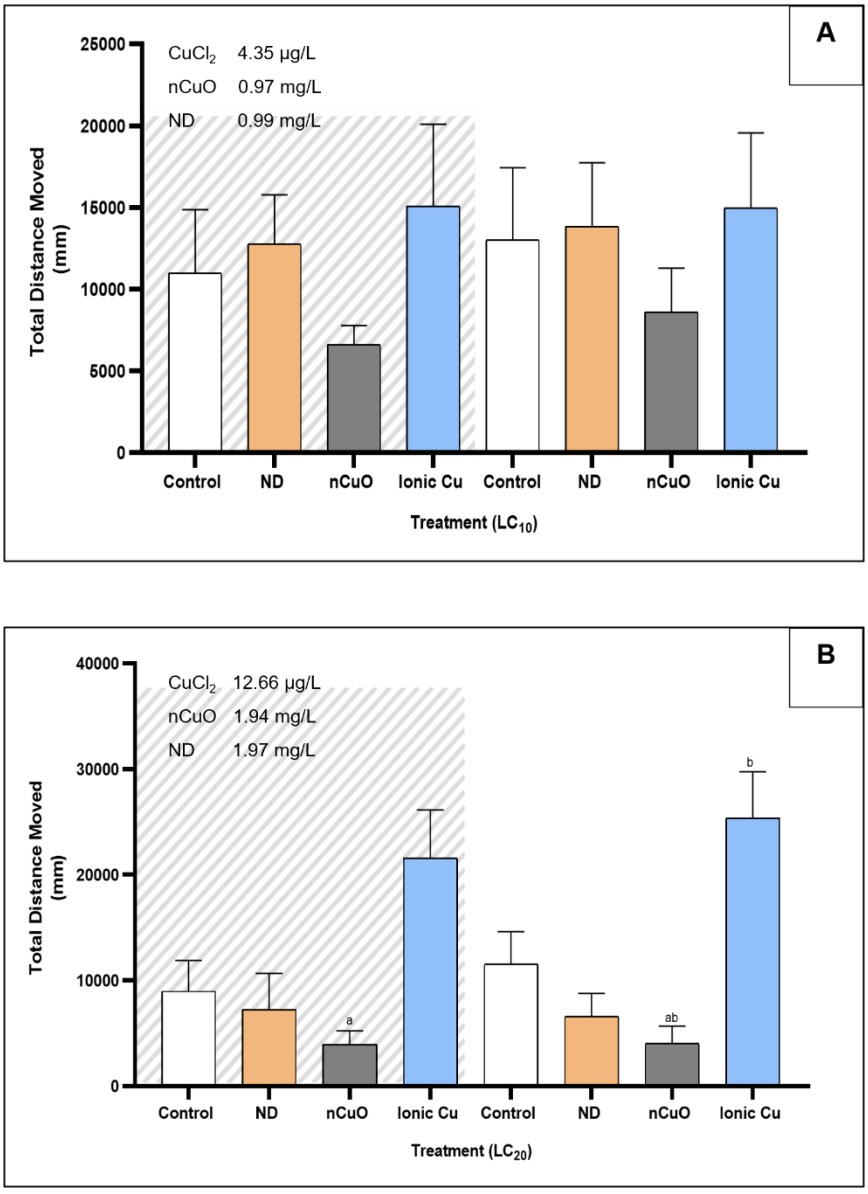

Figure 3.20 Average total distance (mm) travelled by *Caridina africana* after a 96-hour exposure to nanodiamonds, nano copper oxide and copper chloride (II) at their respective (A) LC_{10} and (B) LC_{20} concentrations. These graphs represent the mean ± the standard error between seven individual replicates per treatment. The superscript letters show the significant ($p<0.05$) differences within their respective treatment groups. The shaded area represents the combined dark phase of behavioural data acquisition.

Swimming speed (mm/s)

The average swimming speed of LC_{10} ND and $CuCl_2$ treatments were higher than the control in both the dark and light phases (*Figure 3.21 A*). Both nCuO treatment groups had a lower average swimming speed than the control in both dark and light phases. In all instances, the average swimming speed moved were not significantly ($p>0.05$) different from the control. The average

swimming speed of LC_{20} ND and nCuO were lower than the control in the dark and light phases (*Figure 3.21 B*). Both LC_{20} ionic Cu treatments had a greater average swimming speed than the control in both dark and light phases. In all materials, the average swimming speed moved were not significantly ($p>o=0.05$) different from the control. When the two exposure concentrations were compared, the average swimming speed was more pronounced in the LC_{20} exposure group.

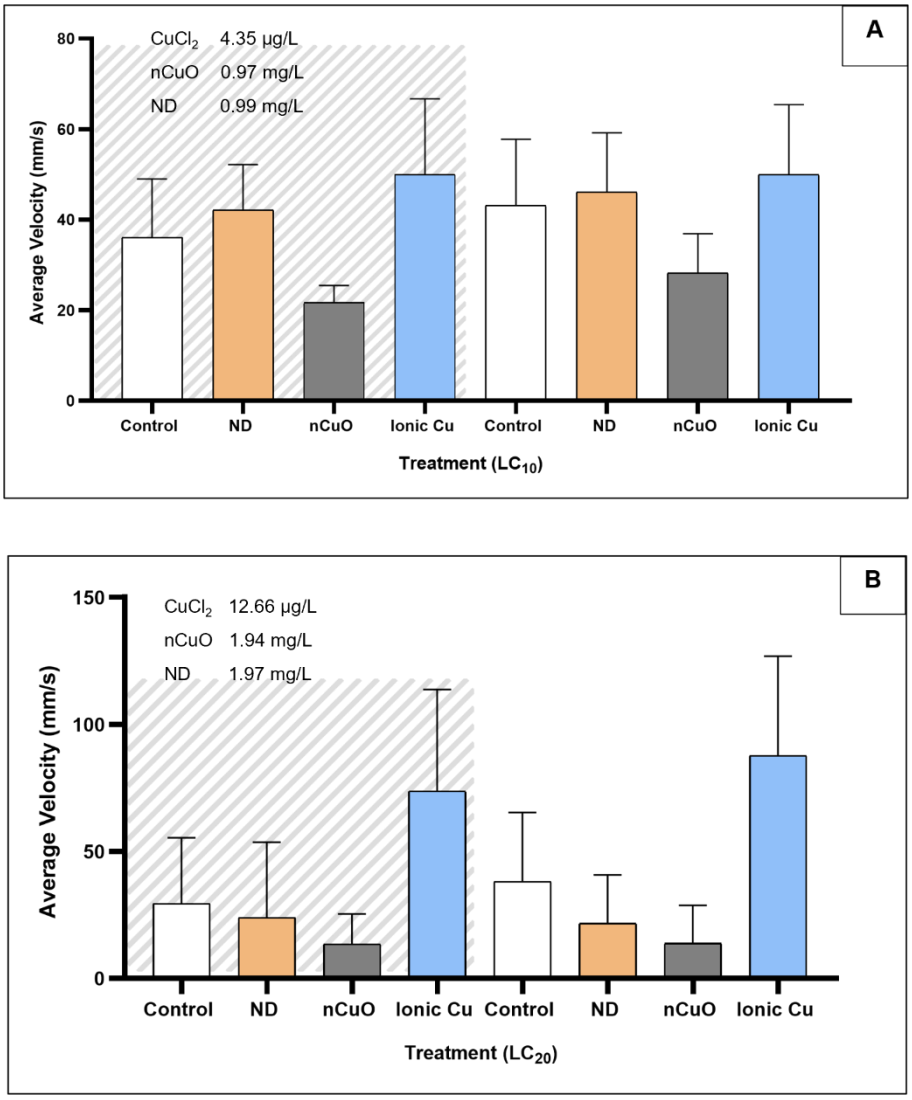

Figure 3.21 Average swimming speed (mm/s) of *Caridina africana* after a 96-hour exposure to nanodiamonds, nano copper oxide and copper chloride (II) at their respective (A) LC_{10} and (B) LC_{20} concentrations. These graphs represent the mean ± the standard error between seven individual replicates per treatment. The shaded area represents the combined dark phase of behavioural data acquisition. Significance was regarded as ($p<0.05$).

Frequency of movement

The LC_{10} ND experienced lesser movement than the control and the other two LC_{10} groups of nCuO and $CuCl_2$ in both the dark and light phases (*Figure 3.22 A*). The LC_{10} ionic Cu exerted more movement than the control, LC_{10} nCuO and ND for both phases.

The LC_{20} nCuO exposure groups experienced lesser movement in both phases than the control and the other two exposure groups. The LC_{20} ND and LC_{20} ionic Cu had more movement than the control. (*Figure 3.21 B*). When the two exposure concentrations were compared, the movement frequency was more pronounced in the LC_{20} treatments. The LC_{20} ionic Cu experienced the most movement frequency.

Average Mobility (%)

The LC_{10} ionic Cu had a higher mobility rate than the control in both phases. The LC_{10} nCuO had a lower mobility rate than the control with LC_{10} ND being the second treatment with the highest mobility rate (*Figure 3.23 A*).

The LC_{20} ionic Cu had a higher mobility rate than the control and the other two LC_{20} treatments. The LC_{20} ND was lower than the control for both phases, with LC_{20} nCuO having experienced the lowest mobility rate out of all treatments (*Figure 3.23 B*). When the two exposure concentrations were compared, the mobility rate was more pronounced in the LC_{20} treatments, with LC_{20} ionic Cu having experienced the highest mobility rate.

Frequency of Mobility

A high mobility frequency was considered above the 60% mobility threshold. The LC_{10} ionic Cu exhibited a higher mobility frequency than control and the LC_{10} nCuO and ND treatments for both dark and light phases (*Figure 3.24 A*). The LC_{10} ND had a higher mobility frequency than the control and the LC_{10} nCuO treatments in both phases. The LC_{10} nCuO was the treatment that had a decreased mobility. The LC_{20} ionic Cu also exhibited a higher mobility frequency than the control and other LC_{20} treatments in both the dark and light phases (*Figure 3.24 B*). However, the LC_{20} ND had experienced a lower mobility frequency than the control and LC_{20} ionic Cu, whereas LC_{20} nCuO was the treatment that had the least mobility.

When the two exposure concentrations were compared, the frequency of high mobility was more pronounced in the LC_{20} treatments. The LC_{20} ionic Cu group experienced the most frequency of high mobility.

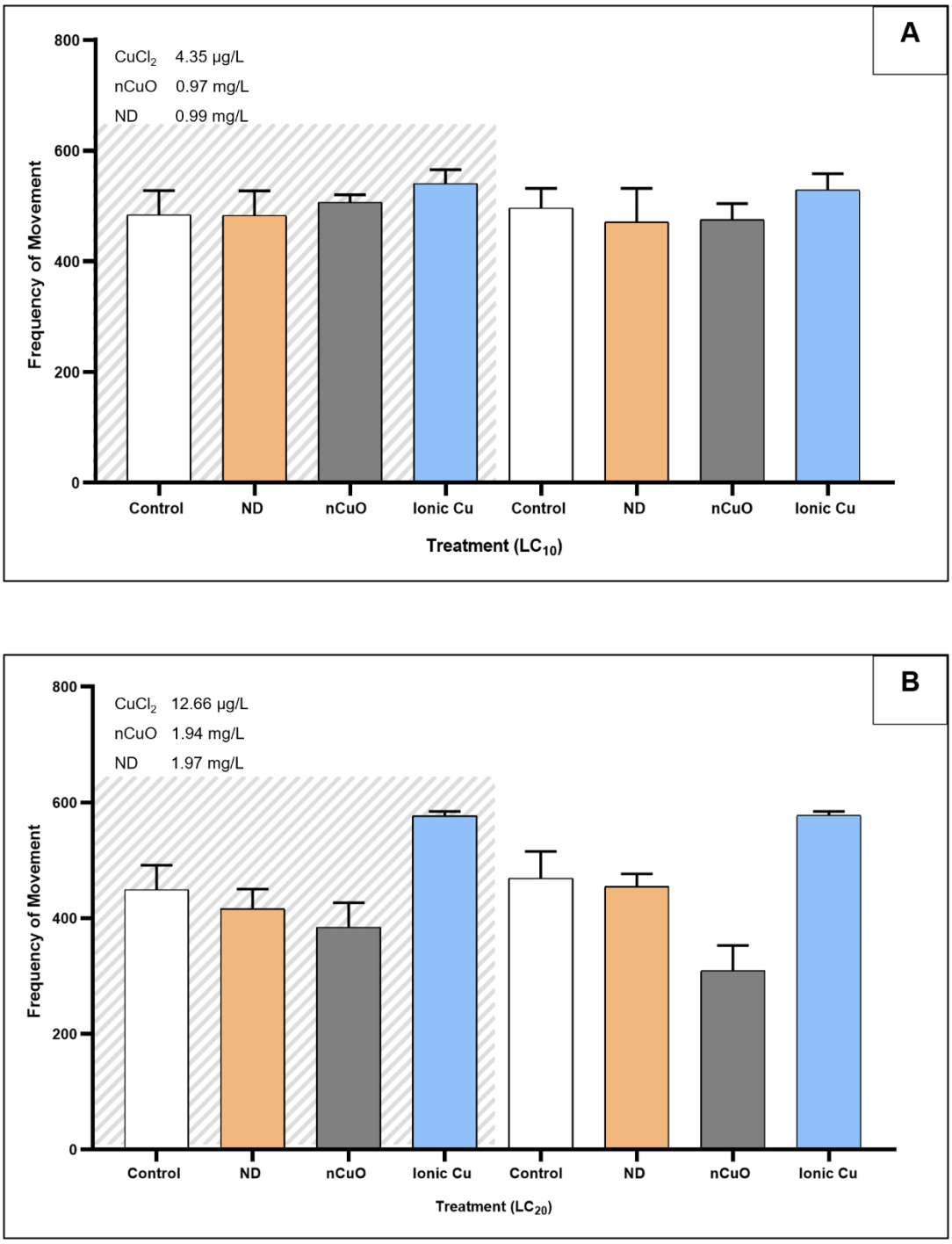

Figure 3.22 Frequency of movement in *Caridina africana* after a 96-hour exposure to nanodiamonds, nano copper oxide and copper chloride (II) at their respective (A) LC_{10} and (B) LC_{20} concentrations. These graphs represent the mean ± the standard error between seven individual replicates per treatment. The shaded area represents the combined dark phase of behavioural data acquisition. Significance was regarded as ($p<0.05$).

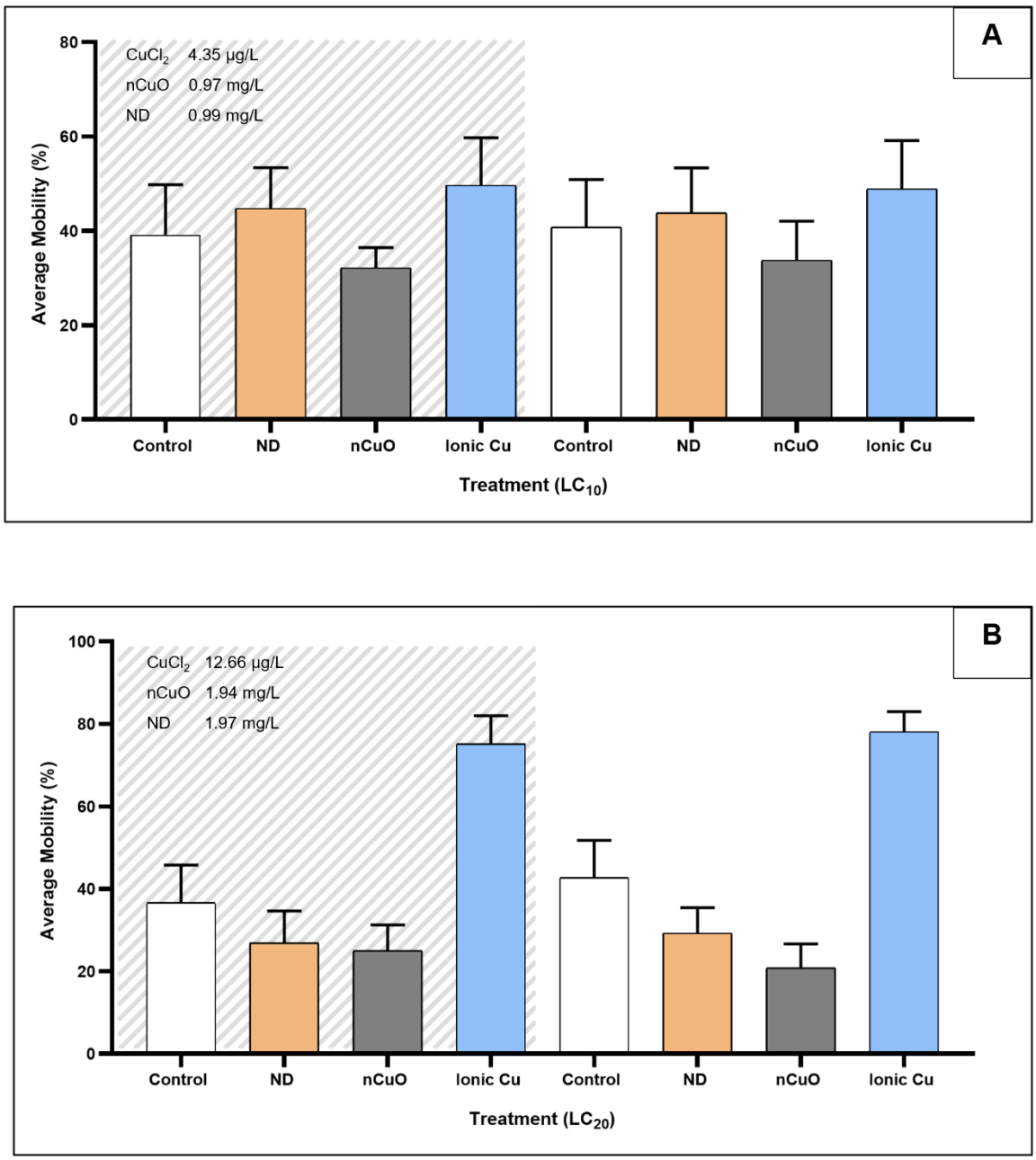

Figure 3.23 Average mobility (%) in *Caridina africana* after a 96-hour exposure to nanodiamonds, nano copper oxide and copper chloride (II) at their respective (A) LC_{10} and (B) LC_{20} concentrations. These graphs represent the mean ± the standard error between seven individual replicates per treatment. The shaded area represents the combined dark phase of behavioural data acquisition. Significance was regarded as ($p<0.05$).

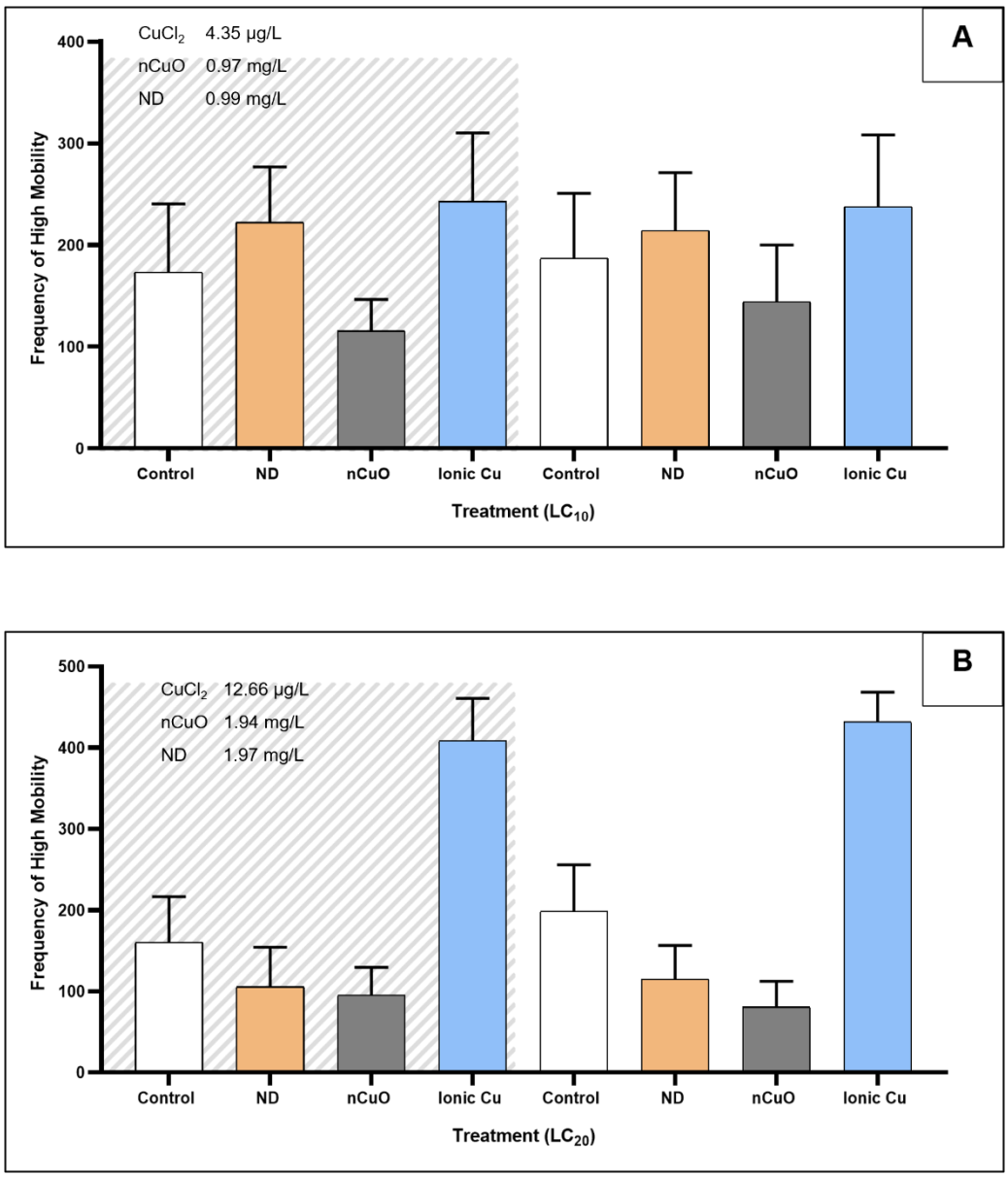

Figure 3.24 Frequency of high mobility (>60%) in *Caridina africana* after a 96-hour exposure to nanodiamonds, nano copper oxide and copper chloride (II) at their respective (A) LC_{10} and (B) LC_{20} concentrations. These graphs represent the mean ± the standard error between seven individual replicates per treatment. The shaded area represents the combined dark phase of behavioural data acquisition. Significance was regarded as ($p<0.05$).

The LC_{10} nCuO exhibited a greater immobility frequency than the control in both the dark and light phases (*Figure 3.25 A*). The LC_{10} ionic Cu had the lowest immobility amongst all groups. The LC_{10} ND treatment group had the second highest immobility frequency amongst all the LC_{10} treatments and had a lesser immobility frequency than the control.

The LC_{20} ionic Cu exhibited a lower mobility frequency than the control and the other LC_{20} treatments (*Figure 3.25 B*). The LC_{20} nCuO had a greater immobility frequency than control and LC_{20} ND. The LC_{20} ND was the second highest immobile treatment group. When comparing the two exposure concentrations, the immobility frequency was more pronounced in the LC_{20} treatments with LC_{20} ionic Cu having exhibited the least immobility.

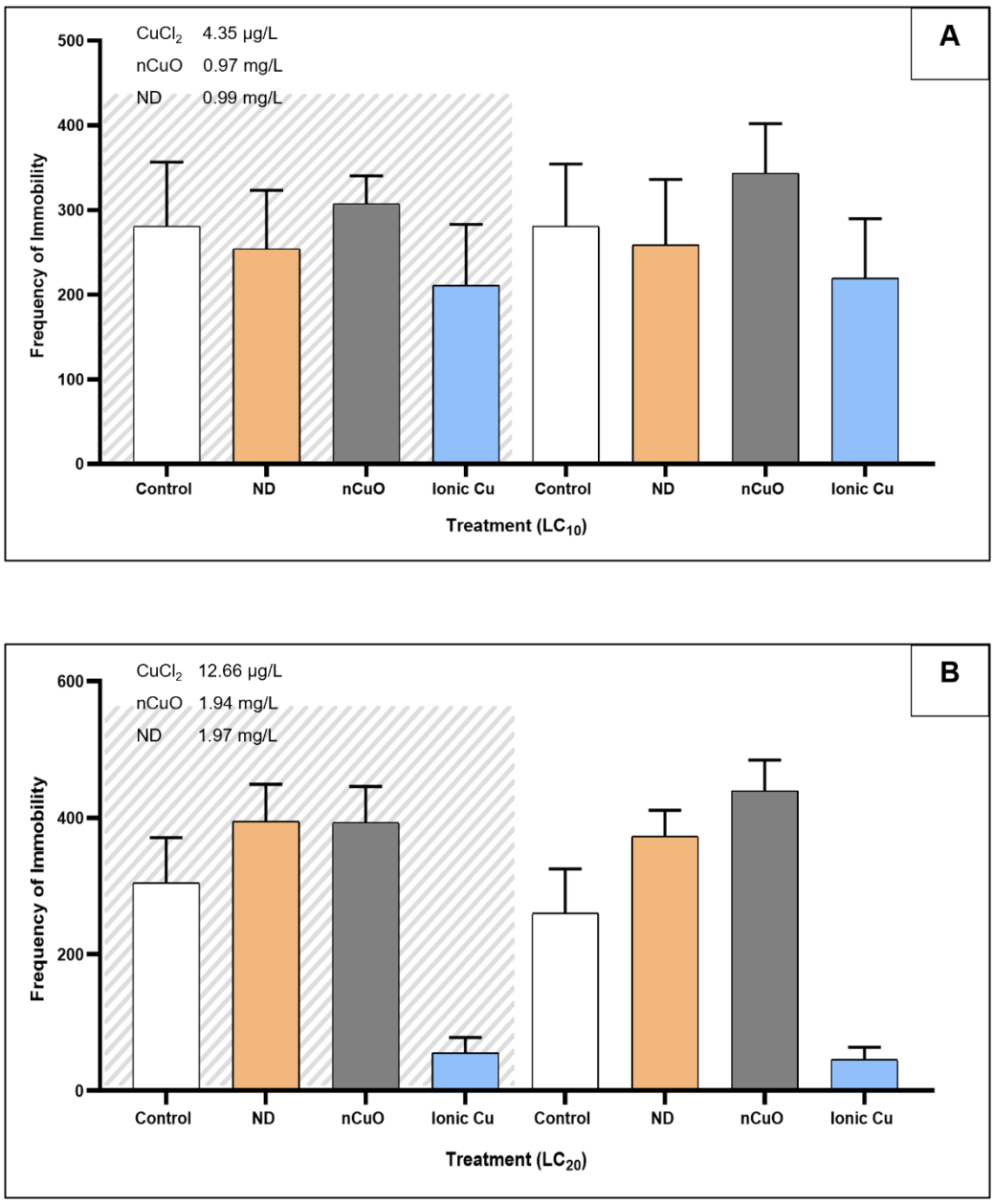

Figure 3.25 Frequency of immobility (<20%) in *Caridina africana* after a 96-hour exposure to nanodiamonds, nano copper oxide and copper chloride (II) at their respective (A) LC_{10} and (B) LC_{20} concentrations. These graphs represent the mean ± the standard error between seven individual replicates per treatment. The shaded area represents the combined dark phase of behavioural data acquisition. Significance was regarded as ($p<0.05$).

CHAPTER 4 DISCUSSION

4.1 Verification of indicator species

The bootstrap values of a phylogenetic tree show how many times – out of 100 – the same branch is shown when the tree generation is repeated (Ojha *et al.*, 2022). For tree construction, bootstrap values below 50 are not considered, whereas a value of 70 and above is the threshold for confidence, indicating support for the branch (Hillis & Bull, 1993; Soltis & Soltis, 2003). The extracted sample sequences and *C. africana* sequences were grouped together in a clade in 82% of the bootstrap replications. When the value is greater than 50, the branch is supported (Ojha *et al.*, 2022). Thus, the species being used in this dissertation is confirmed as *C. africana.*

4.2 Nanomaterial characterization

a) Nanomaterial surface charge and size

The stability of nanomaterials is affected by their surface charge (zeta potential) (Ding *et al.*, 2018). Zeta potential within the range of 30 mV to -30 mV is desired for an electrostatically stable suspension as repulsion forces are greater in this range, ensuring easy re-dispersion. The DLVO theory describes the interaction of particles through balanced repulsive electrostatic potential and attractive van der Waals forces, which leads to this stability (Gumustas *et al*., 2017; Gupta & Trivedi, 2018; Krstić *et al.,* 2018). Particles that have a ZP less than the given range, lead to agglomeration. Zeta potential is often affected by the properties of nanomaterials – size, shape and surface coating, as well as the nature of the media – pH and ionic strength (Niriella & Carnahan, 2006; Salgin *et al.*, 2012; Patra & Baek, 2015; Gumustas *et al.*, 2017; Stepan *et al.*, 2022).

The nano copper oxide showed no direct effect of increased exposure concentrations on ZP. This is in contrast to findings by Rahdar *et al.* (2019), who found that particle concentration can influence ZP, as it is dependent on the valence of ions and their concentration. The pH in this study was between 8 – 8.8, and the ZP of nCuO was within the 30 mV to – 30mV, thus making it a stable suspension. A negative ZP associated with a neutral/elevated pH has been recorded in multiple studies (Sousa & Teixeira, 2013; Khan *et al.,* 2019; Parsai & Jumar, 2019; Çalhan & Gündoğan, 2020).

Anandhavalli *et al.* (2015) explained that the negative ZP was due to the formation of hydroxyl groups (OH^-) on the surface of the particles due to their dispersion in water.

Similar to the nCuO, the ZP of NDs showed no direct relation to the increase in concentration. Gines *et al.* (2017) stated that a negative ZP for NDs was attributed to the functional groups, such as carbonyl or carboxyl, that dissociates from the NM surface. Williams *et al.* (2010) had also explained that untreated powders exerted a negative ZP over the entire pH range, and that the ZP became more negative as the pH increased, which is common for acid cleaned commercial nanodiamond powders. Nanomaterials coated with PEG yielded excellent stability and solubility since according to Ehi-Eromosele (2016), they had more negative ZP than their uncoated equivalents. These authors found that there was an enhanced colloidal stability when ZP was increased, as solubility increased in the aqueous medium from the hydrophilic ethylene glycol repeats present in the PEG coating. The negative ZP of PEG-coated NMs are due to the OH^- groups being ionized, making the charge more negative at elevated pHs (Ehi-Eromosele, 2016; Song *et al.*, 2020).

Other factors that influence the ZP are divalent cations (Mg^{2+} and Ca^{2+}) and anions (SO_4^{2-} and CO_3^{2-}) (Salgin *et al.*, 2012). According to the DLVO theory, when there is an adsorption of protons on the surface of a nanomaterial, these anions could bind with the H^+ that is present on the surface of NMs, thus resulting in the decrease in ZP, reducing the electrostatic repulsion forces (He *et al.*, 2017). Due to the presence of the adsorbed anions and surface coatings of NMs, their ZP can become more negative, resulting in a shift from the isoelectric point to a decreased ZP (Liu *et al.*, 2011). The media used within this study contained four different salts, $MgSO_4$, KCl, $CaCl_2$, and $NaHCO_3$. With these salts, the Mg^{2+} and Ca^{2+} cations and SO_4^{2-} and CO_3^{2-} anions are present in 25 mg/L, 54 mg/L, 99 mg/L and 46 mg/L, respectively. Thus, with such elevated divalent ionic strengths, this could explain the decreased ZP. Salgin *et al.* (2012) continues to explain that this decrease occurs due to the compression of the double layer at elevated ionic strengths, which can cause destabilization of the nanomaterials.

At acidic/decreased pHs, the monovalent cations, K^+ and Na^+ would be more effective at increasing the ZP, but since the pH in this study was alkaline, the divalent cations and anions were more profound in affecting the ZP (Salgin *et al.*, 2012; Wang *et al.,* 2017; Langford *et al*., 2022).

Size and surface charge are just a few of the determining factors for NM toxicity. Others include the surface coating, pH, ionic strength, chemical composition of the media, and the agglomeration potential of NMs (Liu *et al.*, 2011; Patra & Baek, 2015; He *et al.*, 2017; Marciniak *et al.*, 2020).

The size of nCuO showed a correlation between the increase in concentration with the increased in hydrodynamic size distribution. The TEM results revealed that particle sizes aligned with the sizes provided from the manufacturer. The discrepancies between the particle size and hydrodynamic size could be due to the DLS measuring the sizes of the Brownian nanoparticles in colloidal suspensions (Patra & Baek, 2015). A study conducted by Chakraborty & Misra (2019) reported that their particle size of nCuO under TEM was 31 ± 4 nm and a hydrodynamic size of 140 ± 3 nm. They explained that the different salts had an influence on the stability and solubility of the suspension. With NDs, they displayed a similar trend to nCuO, where the hydrodynamic size distribution increased with an increase in exposure concentration. The TEM images indicated that the ND-PEG particles ranged from 5 – 7 nm, which falls within the range stated by the manufacturer. The surface coating on a NM can affect its size (Ehi-Eromosele, 2016). According to Anastasiadis *et al.* (2022), carbon NMs, such as NDs, tend to aggregate in aqueous systems due to the presence of van der Waal's attraction forces and other salts present within the media.

Since the media used in this study contained a variety of salts, this may have affected the stability of the suspension, resulting in agglomeration. He *et al.* (2017) also reported that particles sizes in suspension after sonication is much larger than the initial particle size, indicating that ultrasonic sonication is not that powerful in overcoming the strong van der Waals forces between nanomaterials. Thus, this agglomeration and sedimentation of the materials after sonication resulted in the elevated hydrodynamic size distribution readings on the DLS for nCuO and NDs.

Another reason for the increased hydrodynamic size distributions in nCuO and ND could be attributed to lack of protein corona formation. When a nanoparticle is coated with biomolecules, such as natural organic matter, forming eco-coronas/protein coronas on its surface. The corona formation is influenced by electrostatic interactions, van der Waals forces, steric interactions, hydrogen bonding, hydrophobic interactions and covalent bonding (Xu *et al*., 2020; Wang *et al*., 2022; Tan *et al*., 2023). A high ionic strength can decrease the electrostatic interactions and increase hydrophobic interactions, resulting in steric hindrance (Wang *et al*., 2022). Thus, the formation of eco-corona can influence aggregation kinetics of nanomaterials by modifying its surface charge, increasing steric repulsion and inducing bridging interaction. Barbero *et al.* (2017) explain that protein levels in a medium need to be higher than the NMs to prevent aggregation in a media with high ionic strength. Thus, the possible reason for aggregation in NDs and nCuO is due to a limitation of proteins available in the ISO media. Thus, the steric hindrance is less efficient as the corona formation is not complete, which allows the bridging between the particles, resulting in their aggregation, increasing their hydrodynamic size distribution.

b) Dissolution of copper from nano copper oxide

Toxicity of an NM is attributed to many parameters, such as the size, shape, agglomeration, and dissolution of metals from metal-containing NMs. Nanomaterials are able to induce biological responses based of its ability to generate dissolved species and accumulate metal-ion-inorganic complexes as well as the toxicity of the NM itself (Chakraborty & Misra, 2019). The dissolution of NMs is dependent on various parameters: NM shape, size, surface charge and agglomeration as well as ionic strength (Chakraborty & Misra, 2019; Boyle *et al.*, 2020). The dissolution of Cu from nCuO was below 0.12% for all concentrations at all the time intervals. A decreased dissolution after 96 hrs can be attributed to the nCuO forming aggregates with less surface area available to the aqueous media.

According to Clark *et al.* (2019), dissolution and speciation can be influenced by the chemical composition of the media, i.e. chloride presence. Any form of Cu-based NMs can be dissolved and release cupric/cuprous ions into the surrounding solution (Kent & Vikesland, 2016). Clark *et al.* (2019), found that at a decreased pH, there was an increase in the total dissolved metal when using the rainbow gut-sac methodology to determine NM bioaccumulation. A high ionic strength (e.g. at increased salt concentrations and pH), enhanced agglomeration of NM, which can occur in a short period (Clark *et al.*, 2019). In this study, the pH was around 8 – 8.8, and this very likely meant that agglomeration of the nCuO occurred, reducing its activity via surface area, thus affecting its dissolution through the dialysis membrane, which resulted in its low dissolution rate. A high solute to solvent ratio in the dialysis process led to a lesser degree of freedom of the nCuO to interact with the media, interrupting the dissolved species/ion complexes from diffusing (Chakraborty & Misra, 2019). Due to this, the Cu organic/inorganic complexes get deposited on the inner surface of the dialysis membrane (Chakraborty & Misra, 2019). This deposition could attribute to the underachieved saturation concentration of Cu in this study. The nano copper oxide, agglomerate as large particles and due to their sedimentation potential, Cu is lost from the aqueous media. This had occurred within one hour from the start of experiments in Odzak *et al*. (2014) study, where less than 3% of dissolved Cu was reported at pH 7.7. This rapid agglomeration and sedimentation could explain the low dissolution rate at all time intervals in this study, as it would’ve occurred within the first hour of dosing, thus blocking the dialysis membrane.

4.3 Exposure assessment

a) Bioaccumulation and nanomaterial distribution

When nanomaterials agglomerate, it leads to sedimentation in the aquatic environment. Once sedimentation occurs, the bioavailability of NMs may be impaired for pelagic species, such as fish, as compared to the filtering/benthic species. Fish are then exposed to NMs via oral and dietary exposure (Kuehr *et al.*, 2021b). Delahaut *et al.* (2020) explained that the uptake of copper is facilitated by a transmembrane protein in the common carp, *Cyprinus carpio*, which is insensitive to external Cu concentrations and the apical Na^+ pathway in the branchial epithelial cells, which is sensitive to external Cu concentrations. The Cu accumulation is due to the failure of either the apical Na^+ channel, a divalent cation transported and/or a high affinity copper transporter to regulate the Cu concentrations that are taken up (Delahaut *et al.*, 2020).

Due to the agglomeration potential of NMs, there is only a small mass of NMs that are available for direct uptake from the water column. The remaining agglomerates are deposited into the sediment compartment, resulting in elevated concentrations in benthic-dwelling organisms (Ramskov *et al.*, 2014; Thit *et al.*, 2017). These organisms, such as shrimp collect food via their pereiopods and is passed to their oral parts, starting with the pre-oral cavity that is comprised of the maxillipeds and maxillae. Here, the food is passed to the mandibles that crush the food particles (Parra-Flores *et al*., 2019). Thus, due to the sedimentation potential of nCuO and NDs, the shrimp can access these particles via their pereipods and ingest them. Once ingested, particles can cause lesions or block the gastrointestinal tract, resulting in false satiety as described by Zachariades *et al*. (2017) with microplastics in decapods. The same effect occurs when nanomaterials are ingested in aquatic organisms (Brausch *et al*., 2011; Mendonça *et al*., 2011; Artells *et al*., 2013; Cano *et al*., 2017; Magro *et al*., 2018; Kim *et al*., 2021; Siregar *et al*., 2021). According to Akalin (2021), deposited metal oxides can enter organisms via endocytosis or adhesion to the target cell membrane, negatively impacting their homeostasis.

In this study, the Cu content in *C. africana* exposed to nCuO was higher than those exposed to ionic Cu. However, the Cu bioaccumulation did not increase with an increase in nCuO exposure concentrations as was observed for $CuCl_2$. These findings are supported by Wu *et al.* (2020b), who also found higher Cu uptake in *D magna* after exposure to nCuO when compared to $CuCl_2$. The higher Cu levels in nCuO exposed organisms, may be explained by the adherence (adsorption) of the NMs to the organism as it moves through the exposure medium, and/or if the medium is agitated by the aeration provided during the exposures (Miao *et al.*, 2015). The strong adherence of the NMs to the exoskeleton were clearly shown by the CytoViva images (section

3.4), resulting in elevated Cu levels in the nCuO exposures. Similar findings were reported following exposure of *D. magna* to carbon-based NMs (Cano *et al.*, 2017) and nCuO (Wu *et al.*, 2020b). This adherence can cause the organism to appear “heavy”, as seen with nanogold in *D. magna,* which affects their physiological processes (Botha *et al*., 2016). Botha *et al.* (2016) reported hat as the concentrations increased, the adherence was more persistent. Similar findings can be seen in the CytoViva moult results in this study with the increase of nCuO concentrations. Thus, these organisms need to moult so that their physiological processes aren’t affected.

In this study’s results, the nCuO exhibited a greater copper content than ionic Cu. With the nCuO, it steadily decreased as the concentration increased, but exhibited a greater uptake at the two highest concentrations. With ionic copper, the accumulation steadily increased as the concentration increased, with the highest uptake occurring at the highest concentration. Since the uptake did not correspond linearly with toxicity in the nCuO exposure, there could be other parameters that influenced its toxicity, such as uptake of the particle, rather than just the Cu^{2+} ions, which plays a dominant role in the accumulation process (Akalin, 2021). Another reason for the elevated Cu concentrations from the nCuO exposure, could be the adherence of the nCuO particles to the organism’s exoskeleton, even though the organism was depurated for four hours and rinsed prior to analysis.

4.4 Effects assessment

a) Acute toxicity (mortality)

Nanomaterials can have a variety of negative effects on an aquatic organism, including adherence to the cell’s surfaces, accumulation in tissues and the transformation of the NM into its ionic equivalent. This transformation can result in the disruption of metabolic pathways, upset mitochondrial membrane potential and oxidative stress. In extreme cases, mortality of the organism can occur (Garncarek *et al.*, 2022). Copper is an essential metal required by organism for their optimal functioning, but when introduced at excessive levels, it exerts a toxic effect (Garncarek *et al.*, 2022).

Depending on the type of Cu-NM and the species being exposed, a wide range of toxic concentrations have been reported. For *D. magna*, the LC_{50} values ranged from 0.99 to 6.62 mg/L over a 48-hour period, whereas for *D. rerio,* a LC_{50} of 1.5 mg/L was recorded (Garncarek *et al.*, 2022). Kovrižnych *et al.* (2013), reported LC_{50} values for nCuO (<50 nm) using *D. rerio* as 400 mg/L for adults and 840 mg/L for embryos. However, Khoshnood *et al.* (2016) reported a LC_{50} for *D. magna* at 2.99 mg/L, which is similar to the LC_{50} values obtained for this study. Mansano *et al.*

(2018) recorded a Cu salt LC_{50} of 49.8 µg/L for the tropical fish, *Hyphessobrycon eques,* while the nCuO LC_{50} was 211 µg/L, which also demonstrates that nCuO NPs were less toxic than the Cu salt solution, and that their nCuO LC_{50} was 211.4 ± 57.5 µg/L, demonstrating that nCuO were less toxic than the Cu salt solution. Another study confirmed similar findings where the $LC_{50's}$ were 0.25 – 4.0 mg/L, and 0.01 – 0.8 mg/L in *D. magna* for nCuO and Cu salts, respectively (Sørensen *et al.*, 2016). These studies corroborate the findings of the current study of a higher nCuO NP LC_{50} value as compared to the LC_{50} value for $CuCl_2$.

Nanodiamonds are regarded to be inert NPs. The LC_{50} in rainbow trout was greater than 100 mg/L (Adámas Nanotechnology fluorescent nanodiamond power safety data sheet, 2018). While Malhotra *et al.* (2020) reported that for C60 fullerenes, no median lethal dose could be calculated at concentrations that were less than 10 mg/L for the fish, *Fundulus heteroclitus.* The LC_{50} value for ND-PEG was reported by Brand *et al.* (2020) for zebrafish larvae as 32 mg/L. This differs from this study as zebrafish are not filter feeders and swim within the water column, whereas shrimps are filter feeders and live on the substrate, thus being more exposed to the aggregates/agglomerates of ND-PEG nanoparticles that settle.

b) Metabolomics

Copper plays an important role in aquatic organisms for their biological, physiological and immune responses. The biological processes include embryonic development, mitochondrial respiration as well as neuronal functions. Copper is desirable for the growth, survival and specific/nonspecific immune responses in crustaceans. However, when copper is present in excessive levels, it can suppress the immune, growth and survival responses. In crustaceans, copper is associated with hemocyanin, which is responsible for the oxygen transport system (Muralisankar *et al.*, 2016). This is due to the metal association which can form ROS's, which results in oxidative stress. The use of metabolomics allows biomarkers associated with oxidative stress within an organism to be screened via the concentrations of metabolites, following nanomaterial perturbation (Schnackenberg *et al*., 2012). The use of metabolomics revealed that metabolisms associated with oxidative stress were affected.

As seen from the heatmaps and significant VIP take, the Cu-based exposures can induce oxidative stress. This can be validated through the various sublethal biological responses when shrimp were exposed to two Cu-based exposures. The reoccurrence of significant metabolites associates with oxidative stress gives an indication that generation of ROS occurs and causes the antioxidant metabolite concentrations to be affected (Boyles *et al*., 2015). Some of the metabolites identified were associated with nucleotides and glutathione metabolism. The overall

concentration patterns of these metabolites were revealed by heatmap analysis , and these metabolites can increase/decrease with the concentrations of Cu-based exposures. A perturbation of the glutathione metabolism can induce oxidative stress (Wang *et al*., 2020c).

In this study, the main pathways/metabolisms associated with oxidative stress, includes the pentose phosphate pathway, glutathione metabolism, and amino acid biosynthesis (with specific metabolites). With these results, the pentose phosphate pathway was affected in the control vs nCuO LC_{10}, only. This pathway can also reduce oxidative stress and provides the precursors necessary for amino acid biosynthesis (Stincone *et al.*, 2015). Glucose was affected in the nCuO LC_{20} and $CuCl_2$ LC_{20} energy metabolism, and is responsible for producing energy, in which the final product is pyruvate - needed for amino acid synthesis. In a study conducted by Lauer *et al.* (2012), they reported that Cu from $CuCl_2$, exposure stimulates the pentose phosphate pathway in order to support antioxidant system requirements, as Cu can disrupt that energy balance at the gills of *Neohelice granulate*, an estuarine crab. They specifically looked at the enzymes involved in glycolysis to determine whether there'd be a shunt in the pentose phosphate pathway, as this is responsible for the production of cofactor for glutathione reoxidation, which would counteract oxidative stress. Also, Cu ion exposure was reported to reduce the abundance of metabolites involved with glycolysis in zebrafish embryos (Wang *et al.*, 2021b).

The pathways affected in the control vs Cu-based treatments, was the glutathione metabolism, specifically affecting metabolites cadaverine and putrescine, which are responsible for aversive behaviour in zebrafish. These two metabolites play a key role in the trypanothione pathway, which aids in the defence against oxidative damage (Fairlamb & Cerami, 1992; Ma *et al*., 2017; Yadav *et al*., 2018; Bekebrede *et al*., 2020). A study conducted by Boyles *et al*. (2015), reported that when exposing human lung cell lines nCuO, the metabolites associated with the glutathione metabolism, were the reduced and oxidized form of glutathione, GSH and GSSG, respectively, along with cysteine-glutathione disulfide. They reported that the mode of toxicity for Cu-based NM lies in its delivery and its intracellular dissolution of Cu ions. Amino acid biosynthesis is affected in majority of the treatments. Lysine was a common metabolite affected in the nCuO treatment, indicating the need for more energy by the shrimps. The phenylalanine pathway is also limited to Cu exposure, which is linked to mortality in zebrafish (Ganesan *et al.*, 2021). The main metabolites that have been affected in this pathway by the treatment groups are: phenylalanine, serine, methionine, lysine, proline and glutamate. Phenylalanyl-tRNA has an essential role in developmental angiogenesis in *D. rerio,* which is a potential contributor to cardiovascular diseases (Li *et al.*, 2021). A study conducted by Lari *et al.* (2018), reported that phenylanayl-tRNA

increased mandible rolling in daphnids, which is behavioural trait associated with feeding. Seryl-tRNA plays an important role in translation and regulated the vascular development. Seryl-tRNA is responsible for serylating selenocysteine-specific tRNA, which incorporates selenocysteine. This amino acid is present in all domains of life and affects protein synthesis as well as vascular development, when interrupted via mutations can cause abnormal vasculature and premature death in *D. rerio* (Xu *et al*., 2013). Methionine, which is coded for by N-formylmethionine can promote protein complex formation in the mitochondria and also functions as a degradation signal within bacteria and yeast (Kim & Hwang, 2022). It can also inactivate ROS, and prevent oxidative damage (Huang *et al.*, 2020). It was noted by Strain and Lynch (1990) that the supplementation of methionine can decrease Cu poisoning. Also, shrimp source their methionine through the breakdown of dietary protein or from their body protein, which can improve their growth and is advantageous to intestinal health and improves antioxidative capacity (Ji *et al.*, 2021). Lysine affects protein synthesis and growth in fish and can also induce higher feeding rates when there is inadequate lysine available. When lysine is abundant in an organism, they exhibit increased energy storage as fat and have enhanced muscle growth on *D. rerio* (de Vareilles *et al.*, 2012). Lysine can combine with methionine to form carnitine, which increases lysosomal and catalase in juvenile seabream (Hosseintabar *et al.*, 2015). It can also increase the antioxidant capacity (Ribas *et al.*, 2014). Carnitine is responsible for nutritional metabolism as well as producing energy and reducing amino acid catabolism, which causes a reduction in peroxidation (Huang *et al.*, 2020). Proline is involved in protein synthesis and plays in an important role in collagen synthesis and tissue repair (Huang *et al.*, 2020; Karna *et al.*, 2020). Karna *et al.* (2020) explain that proline metabolism can affect the immune system of shrimp by improving antioxidant capacity in *Penaeus vannamei.* Glutamate can enhance antioxidant capacity (Huang *et al.*, 2020). It is the primary excitatory neurotransmitter in zebrafish (Edwards & Michel, 2002). It is associated with neurodevelopment (Horzmann & Freeman, 2016). It is also responsible for cell membrane stability (Sun *et al.*, 2018). These metabolites play vital roles in organisms, and some of them improve antioxidant activity, which speculates that if they're decreased, it causes a reduction in the ROS defence, allowing its continuous generation which can cause deleterious effects on the cells. A study conducted by Hayat *et al*. (2012) reported that proline plays a beneficial role in plants and plays an antioxidant defence role to bring ROS concentrations to normal ranges. González-García *et al*. (2019) reported that carbon nanomaterials increases the role of glutathione as oxidative enzymes increase. These nanomaterials can induce oxidative stress in plants and cause them to overexpress the genes to decrease the oxidative stress, which improves its defence. In this study, proline was affected in the amino acid biosynthesis in control vs ND LC_{20} heatmap.

Unsaturated fatty acids and fatty acid biosynthesis pathways were only linked to nCuO LC_{20} vs ND LC_{20} exposures. Fatty acid synthesis is essential for organisms, as it plays a vital role in cells from producing triglycerides for lipid storage units to the generation of phospholipids to aid in cell membrane building (Nowinski *et al.*, 2018). These unsaturated fatty acids have an essential role in the development of the brain and cellular signalling (Gonçalves *et al.*, 2017). Fatty acid synthesis also plays a role in regulating the cell wall and is critical for growth and survival as they are metabolized as a main source of energy (Brett & Müller-Navarra, 1997; Gonçalves *et al.*, 2017). Ganesan *et al.*, (2021) reported that carbon nanotubes at 10 mg/L in zebrafish affected pathways associated with energy. Although, not unsaturated fatty acids and fatty acid biosynthesis, it affected phenylalanine, tyrosine and tryptophan biosynthesis, glycolysis/gluconeogenesis and panthothenate as well as glycine, serine and threonine metabolism at 50 mg/L of carbon nanotubes and at elevated concentrations of 100 mg/L, glycolysis metabolism is impacted. Thus, carbon nanomaterials can influence metabolisms associated with energy.

c) Respiration

Copper ions are toxic to aquatic organisms due to the structural damage it exerts on the gills, but within the crustaceans, the physiological effects are not well understood. The gills and hepatopancreas of *Macrobrachium rosenbergii* may be harmed by high Cu concentrations, which could also decrease their natural physical functions (Kaoud & Ahmed, 2013). According to Kaoud & Ahmed (2013) the majority of crustaceans are less sensitive to Cu than freshwater prawns.

The gill filaments of *Charybdis japonica* thickened irregularly and had enlarged gill chambers where the haemolymph cells appeared to have increased following exposure to 2 mg/L Cu (Kaoud & Ahmed, 2013). In *Caridina* spp. elevated Cu concentrations resulted in gill alterations (Ghate & Mulherkar, 1979). When structural damages occur, it can result in lesions, which may affect the respiratory function of the organism, affecting gas exchanges which may decrease the respiratory area of the gills, decreasing the oxygen uptake capacity of the organism (Kaoud & Ahmed, 2013). This could be the reason for the decreased respiration rate observed for the ionic Cu LC_{20} exposure when compared to the other two toxicants. The oxygen consumption for nCuO LC_{10} and LC_{20} was higher than the ionic Cu exposures. This could be attributed to the agglomeration potential of the NMs in the exposure media, resulting in less Cu^{2+} from the NM attaching to the gills of the organism. The ionic Cu was in dissolved form, allowing the gills to be more exposed in the water column, thus damaging the structure of the gills, affecting respiration.

The maxilliped of shrimp plays an important role in feeding and facilitating oxygen consumption. The increased agglomeration observed during the ND-PEG exposures may have reduced the maxilliped movement, due to the adherence of the NMs to their appendages. This could be responsible for the abnormal respiration rates observed, with the ND-PEG treatments exhibiting the lowest oxygen consumption from the three materials. According to Cardeilhac & Whitaker (1988) that toxicity responses are accompanied by an increase in respiration along with other distress signs. Thus, the results from this study indicate that all three toxicants resulted in elevated oxygen consumption when compared to the control, which could be attributed to stress.

d) Heart rate

The use of cardiac activity in toxicological studies is important as it can reveal cardio-toxic effects (De Luca *et al*., 2014). Although the heart rate was significantly lower for Cu in the LC_{10} exposure, there was no clear relationship between the respiration and heart rate, as there usually would be as an increased respiration rate corresponds with increased heart rate, as when the cardiac activity increases, it uses more energy and more oxygen is sent to the body, thus increasing the respiration rate.

These heart beat and gill ventilation changes are only seen at higher exposure concentrations to NMs (Siregar *et al.*, 2021). A study conducted by Fekete-Kertész *et al.* (2020) , reported that there was a inhibition of the heart rate when there was an increase in exposure concentrations of graphene oxide. They also mentioned that the heart rate is decreased due to an increase in oxidative stress. A similar trend can be seen with this study's results regarding the Cu exposures, as the nCuO exhibits the lowest heart rate in both exposures, followed by ionic Cu. It was stated by Naeemi *et al.* (2020) that nCuO decreased the heart rate of the zebrafish embryos. This could be attributed to the combination of Cu^{2+} ions and nCuO particles (Grosell, 2011). As mentioned by Chao *et al.* (2021), the generation of ROS can disrupt cardiovascular functions, which may be the cause of the decreased heart rate observed during the nCuO and ionic Cu exposures.

Nanodiamond-PEG is the toxicant that caused the highest heart rate. Although not significantly different from the control. A similar increase in heart rate was observed by Fekete-Kertész *et al.* (2020) following exposure of *D. magna* to C60 fullerenes. Similar results were reported by Lovern *et al.* (2007) where the heart rate prior to C60 fullerenes exposure was 317 BPM, and after exposure it was 360 BPM, with the control having 309 BPM. The slightly elevated heart rate observed for ND-PEG in this study could be attributed to the adherence of the NMs on the shrimps' appendages, restricting their movement, resulting in a decreased heart rate.

e) Behaviour

Cano *et al.* (2017) exposed *D magna* to C60 and graphene oxide and found a decrease in swimming speed. They attributed this to the aggregation of the NM on the surface of the organism that can restrict their movement. Also, carbon nanotubes were lodged within the intestinal gut of *D magna,* which could have caused a loss in nutrients, providing them with less energy required for survival. In our results, the shrimps exhibited a higher swimming speed than the control during both the dark and light phases in the LC_{10} exposure but exhibited a decrease in swimming speed compared to the control in the LC_{20} exposure. Thus, the rapid aggregation of ND-PEG could have occurred in the LC_{20} exposure treatment, as the hydrodynamic size increases when the concentration increases (as seen with DLS characterisation). Also, the attachment of these particles/aggregates to the exoskeleton is seen in the CytoViva images, which could result in the decreased swimming speed of the shrimp in the higher exposure group. Stanley *et al.* (2016) found that following exposure to C60, the swimming speed in daphnids also decreased. The decreased swimming speed in nCuO exposures could also be attributed to particle adherence, as it negatively affects the mechanical ability of locomotion, adhering to daphnids antennas as reported by Noss *et al.* (2013). Since the shrimp are sediment dwellers, adherence of sedimented nCuO to appendages is easier, thus resulting in this decreased swimming speed. Brand *et al.* (2020) reported that zebrafish larvae exposed to QD-PEG swam longer distances than the control. They also reported that NDs did not cause any significant changes, except the zebrafish larvae exposed to 1 mg/L ND which covered a greater distance. This can also be seen with the results in this current study, as the ND-PEG LC_{10} exposure group was very similar in distance covered as the control. However, with the LC_{20} treatment, the distance covered was reduced compared to the control, but greater than nCuO exposure treatments. This could be because the organisms tried to maintain their swimming capability, but due to the adherence of the ND-PEG to the exoskeleton of the shrimp, their locomotion was restricted in the higher treatment group due to the adsorption of agglomerates. The agglomeration potential in the LC_{10} treatment group was not as high as the LC_{20} group, resulting in less particle adherence, allowing the shrimp to travel greater distances (Artells *et al.*, 2013).

However, the ionic Cu exposures in both treatment groups exhibited the highest swimming speed. da Silva Acosta *et al.* (2016) also reported an increase in swimming speed following exposure of zebrafish to 9µg/L Cu. They explained that assessing locomotor activity can indicate compounds that regulate the neuron firing plate, presenting the potential to affect their swimming speed. Ionic Cu resulted in the most distance moved in both treatment groups and nCuO had the lowest distance moved in both treatments. The ND-PEG LC_{10} displayed an increased distance, whereas

the ND LC_{20} treatment moved less than the control. Thit *et al.* (2017) reported that the distance travelled was impacted by Cu ions at the lower concentrations compared to nCuO exposures. This supports the findings of this study. Griffitt *et al.* (2008) also exposed organisms to metal NPs in which they reported that dissolved metals were more toxic than their NM counterpart. Thit *et al.* (2017) explain that the distance moved was impacted by the addition of Cu, and that the zebrafish displayed an unnatural response to light in both the Cu ions and nCuO exposures. According to these authors, the fry are more active during the dark than the light, but the nCuO increased the activity of the fry during the light cycles. This corroborates the results in this study as there is more distance covered during the light cycles of both the Cu treatment groups. The fry had an unnatural response to light with the Cu ions and nCuO and darkness with just the Cu ions. Also, there was an increase in distance travelled in the LC_{20} light phase as compared to the dark phase. A reduction in distance travelled in nCuO exposure could be due to the loss of coordination (Untersteiner *et al.*, 2003) - as seen from the NM adhering to the surface of the eye under CytoViva. Sun *et al.* (2016) explain that nCuO exposure resulted in reduced movement distances and had a reduced locomotion capacity than the control.

f) Chronic effects (moulting)

Moulting is the replacement of an old exoskeleton with a new one and plays an important role in crustaceans and its main structural component is chitin (Ladchumananandasivam *et al.*, 2012; Lažetić & Fay, 2017). This physiological process starts with hormonal increments within the haemolymph and is a growth-related phenomenon that is energy-demanding and key for survival (Devaraj & Natarajan, 2006; Song *et al.*, 2017; Lemos & Weissman, 2021).

In crabs, moulting is required for their vegetative growth and in *D. magna*, it is also needed for growth, as well as to discard externally accumulated metals and surface adherents (Nasser *et al.*, 2016; Hosamani *et al.*, 2017). Thus, the inability to moult yields the inability to regulate internalized metal concentrations which can impede the ability to survive (Nasser *et al.*, 2016). Physical damage to an organism can also occur when particles adhere to its surfaces as seen by Wang and Liu (2022) with *D. magna.*

Botha *et al.* (2016) noted daphnid moulting when exposed to nanogold. They reported that as the concentration of nanogold increased the more intense the adherence of nanoparticles on the daphnid's moult. Similar trends can be seen in this study as when the concentration of NMs increased, the more the NMs are present on *C. africana* exoskeleton. Botha *et al.* (2016) also reported that the moults had an elevated density of nanogold, which made the organism "heavy", thus affecting their swimming behaviour, but once moulted, swimming reverted to normal. This

explains how adherence of particles to an organism's surface can alter its physiological processes. According to Noss *et al.* (2013), coating of the exoskeleton delays moulting. This explains the reduction in moulting with ND LC_{10} and all nCuO exposure treatments, as nCuO nanoparticles can adhere to the carapaces through direct exposure - waterborne exposure (Wu *et al.*, 2017). These adherences can be seen in the CytoViva images in this study for nCuO. The nCuO particles were present on *C. africana* swimming appendages, eye and carapace, which can further explain the physiological stress they experienced. The NDs also adhered to the shrimp's exoskeleton, resulting in a decreased moulting experience in LC_{10} ND. Jackson *et al.* (2013) reported that the burrowing copepod, *Amphiascus tenuiremis,* had a reduction in moulting after being exposed to SWCNT due to the coating of the exoskeleton. The adherence and binding of particles may increase the load and resistance on animals during swimming (Botha *et al.*, 2016; Wang *et al.*, 2021a). Based on the results in this study, a reduction in moulting, resulted in an increased mortality rate. Thus, when the shrimp are unable to moult, it impedes their growth and thus impaired their ability to survive. However, when moulting was increased, as seen in LC_{20} ND, it exhibited a prolonged survival compared to the other two treatments that experienced a decrease in moulting, as the moulting released the adherence of the NDs from the exoskeleton, but not necessarily alleviated it from the possible accumulation in the gut and gills.

g) Chronic time to mortality response

Nanomaterials adhere to the surfaces of aquatic organisms where they can restrict their movement, as NM usually have hydrophobic properties, so they adhere to negatively charged biological material. Nanomaterials can also cause a physical blockage in the intestinal gut of aquatic organisms. This usually results in starvation and loss of nutrients in the organism which leaves them with minimal energy for survival, thus resulting in death (Brausch *et al.*, 2011; Mendonça *et al.*, 2011; Artells *et al.*, 2013; Cano *et al.*, 2017; Magro *et al.*, 2018; Kim *et al.*, 2021; Siregar *et al.*, 2021).

Gündoğdu (2008) reported that the Cu LT_{50} (time to 50% mortality) in rainbow trout was shorter at higher concentrations. Similar trends were mentioned by Shuhaimi-Othman *et al.* (2011), where an increase in Cu ion concentrations, led to a decreased LT_{50}. With these results, the LT_{50} for ionic Cu LC_{10} treatment was more than 13 d compared to the 12 d for the LC_{20} treatment. The uptake of metals from an aquatic organism from solution is concentration dependent. The more elevated dissolved metal concentrations, the more the uptake until saturation (Gündoğdu, 2008). Thus, at higher Cu concentrations, the ions interact with the organism, affecting its gills and locomotor activity, decreasing the time taken to reach an LT_{50}.

Ramadan *et al.* (2020) recorded the LT_{50} for nCuO in the desert locust to be 10 d and a LT_{90} at 33 d. of exposure. They had noted paralysis and decreased locomotion in the locust, corroborating the effect of NMs on the nervous system of organisms. In this study, nCuO LC_{10} treatment resulted in a LT_{50} of 14 d with half the time (7 d) for the LC_{20} treatment group. The LT_{90} for nCuO LC_{10} was at 19 d and for LC_{20} at 14 d.

In this study, the LT_{50} of ND-PEG for shrimp was at the 7^{th} day for the LC_{10} treatment, and 23 d for the LC_{20} treatment group, showing an adverse result compared to the nCuO treatments. This could be due to the agglomeration of ND-PEG not being reactive with the shrimp at a higher concentration. Multi-walled carbon nanotubes have been reported to accumulate in the gut and on the carapace of daphnids (Stanley *et al.*, 2016). This is probably why the LT_{50} was reached earlier in the LC_{10} treatment group when compared to the LC_{20}, as the particles were more bioavailable for uptake. This could have resulted in the mechanical disruption of feeding appendages and penetration of the gut wall, resulting in immobilization and mortality. Damage to the digestive occurred in *D. magna* following long-term exposure to low concentrations of NDs (Mendonça *et al.*, 2011). At a higher concentrations, ND-PEG aggregates and precipitates, resulting in an increased hydrodynamic size distribution. Thus, the LC_{20} treatment increased in aggregation, resulting in reduced bioavailability.

4.5 Adverse outcome pathways

An AOP is a conceptual framework that organizes existing knowledge pertaining to casual linkages (key event relationships) between measurable/observable biological changes (key events), that progress from an molecular initiating event to an adverse outcome (Ankley *et al.*, 2010; Tollefsen *et al.*, 2014; Villeneuve *et al.*, 2014; Groh *et al.*, 2015; Hu & Palić, 2020; Murugadoss *et al.*, 2021).

Vinken (2013) and Murugadoss *et al.* (2021) explains that the MIE is the first anchor for any AOP. Here, an interaction occurs on a molecular level with a chemical and a biological system, which causes a perturbation of a molecular target. Examples of this interaction includes ligand-receptor, binding to proteins, nucleic acids, tissue alterations, cellular function and signalling pathways (Vinken, 2013; Hu & Palić, 2020). This anchor dictates the nature of the adverse outcome, which is the apical endpoint, that can be located at different biological organization levels (Hu & Palić, 2020). In an AOP, there are multiple key events that can be experimentally measurable and aid towards the generation of the AO . These KEs are responses at either molecular, cellular, or organismal levels (Tollefsen *et al.*, 2014; Groh *et al.*, 2015; Hu & Palić, 2020). Typical examples

of AOs are the impact on survival, reproduction or growth in individuals. Groh *et al.* (2015) reported that behavioural alterations linked to the reduction in food uptake, is locomotion impairment and that concentrations that can affect locomotion is similar to those causing growth impairment in a prolonged period.

In a study conducted by Liu *et al.* (2021), they reported that microplastics influences oxidative stress, energy, protein and lipid metabolism as well as the cuticle and chitin pathways. Microplastics affect the glutathione pathways which plays a role in antioxidant defence. This has an effect on the energy metabolism as nano-plastics can create false satiety. This has a domino effect on the protein and lipid metabolism as well as the cuticle and chitinase pathways (responsible for shedding/moulting). This can have a negative effect on *D. pulex* growth and reproduction. Thus, particle exposure may impact reproduction and growth of the daphnids. In this study, the most affected pathway was the glutathione metabolism, which plays a protective role from the generation of ROS.

AOPs that are specific to nanomaterials are scarce, but one of the few MIEs pertaining to NMs is the generation of ROS (Murugadoss *et al.*, 2021). With NMs, their unique surface characteristics affects the interaction with biomolecules, which results in cellular uptake and internalization (Halappanavar *et al.*, 2021). This is an important MIE in any AOP. Halappanavar *et al.* (2021) indicated that the MIE occurs in response to cellular injury, which induces oxidative stress, causing imbalanced oxidant and antioxidant levels that can modify biomolecules.

Frías-Espericueta *et al.* (2022) explain that when organisms are exposed to sublethal metal concentrations, they experience deleterious effects, as seen in this study's sublethal exposures. Metals have been associated with ROS generation, resulting in oxidative stress, causing negative cellular effects (Wei & Yang, 2015). An increase in oxygen consumption (respiratory bursts), as seen in this study's results, reveal that the shrimp were experiencing oxidative stress. The antioxidant defence system (the glutathione metabolism and other metabolites) protects aerobic organisms from these free radicals that leak from the mitochondria into the cytoplasm, as biomolecule damage can occur (Wei & Yang, 2016). This could explain why the glutathione metabolism was affected at the different exposure concentrations. Jena *et al.* (2022) explains that oxidative stress occurs when ROS generation is higher than the neutralization from the antioxidants. This ROS production can alter many metabolic and physiological functions. This may explain why the shrimps experienced different physiological effects under the same sublethal endpoints.

Nanomaterials negatively affect the growth of organisms, and can damage their DNA and protein, and can also cause oxidative stress (Jena *et al.*, 2022). Nanodiamonds have been reported to also cause cellular damage and increase the activity of oxidative stress biomolecule. Oxidative stress associated with carbon based nanomaterials have been conducted on nanodiamonds (*D. magna*), multiwalled carbon nanotubes (bivalves) and nanotubes, single walled carbon nanotubes and fullerenes (*D. magna)* (Karpeta-Kaczmarek *et al.*, 2016; Domínguez *et al.*, 2018; Bodó *et al.*, 2020).

Within this study, *C. africana* was exposed to three different treatments, NDs, nCuO and $CuCl_2$. The main MIE shared among all three treatments, is the generation of ROS. The heatmaps and significant VIP table were analysed to determine if the antioxidant defence metabolites were influenced. Sublethal endpoints that linked to one another were evaluated as KEs and placed in a proposed AOP, such as respiration, behaviour and moulting (*Figures 4.1, 4.2 and 4.3*). The AO considered in this study was mortality.

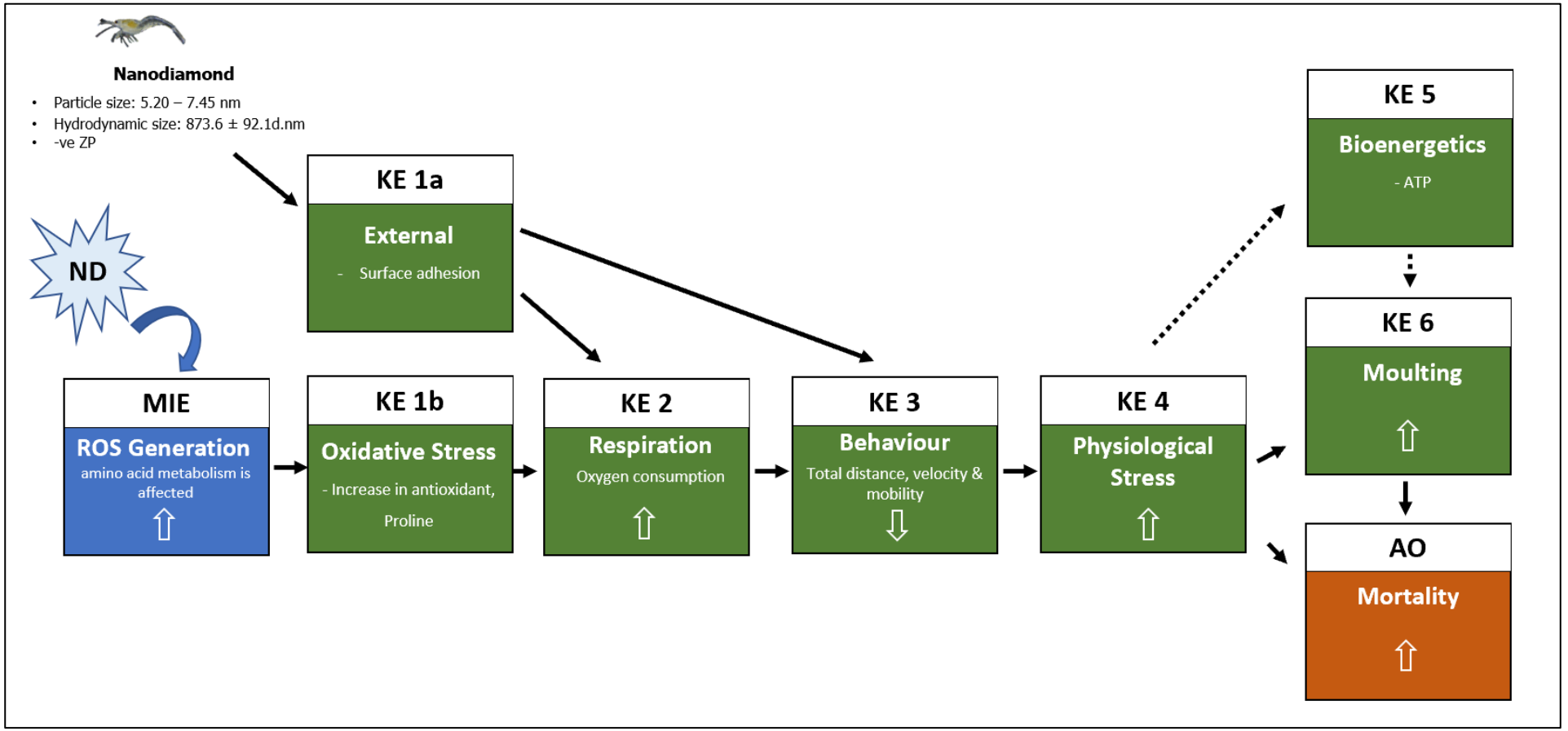

Figure 4.1 Proposed adverse outcome pathway for *Caridina africana* exposed to LC_{20} nanodiamonds.

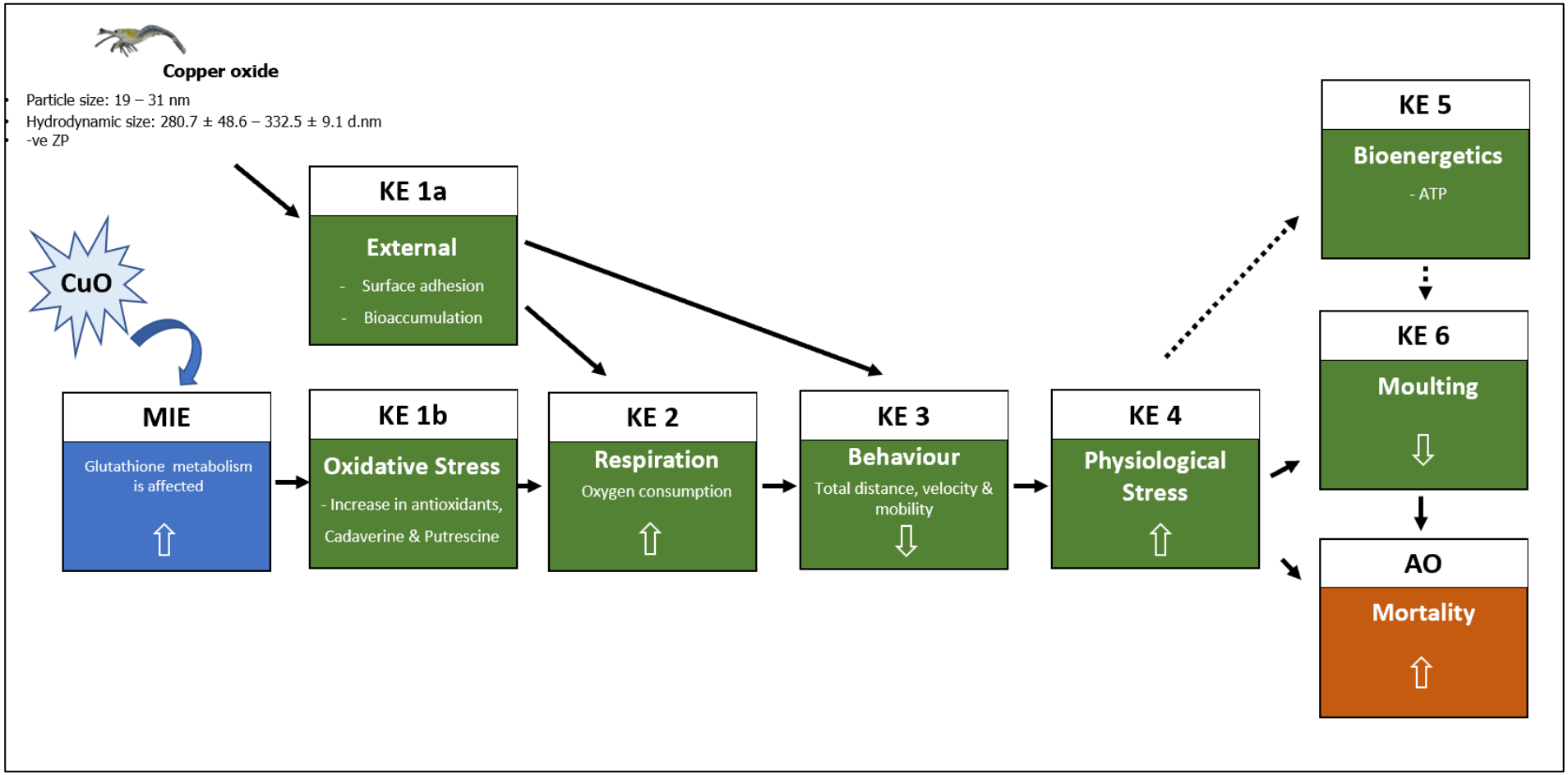

Figure 4.2 Proposed adverse outcome pathway for *Caridina africana* exposed to LC_{20} copper chloride.

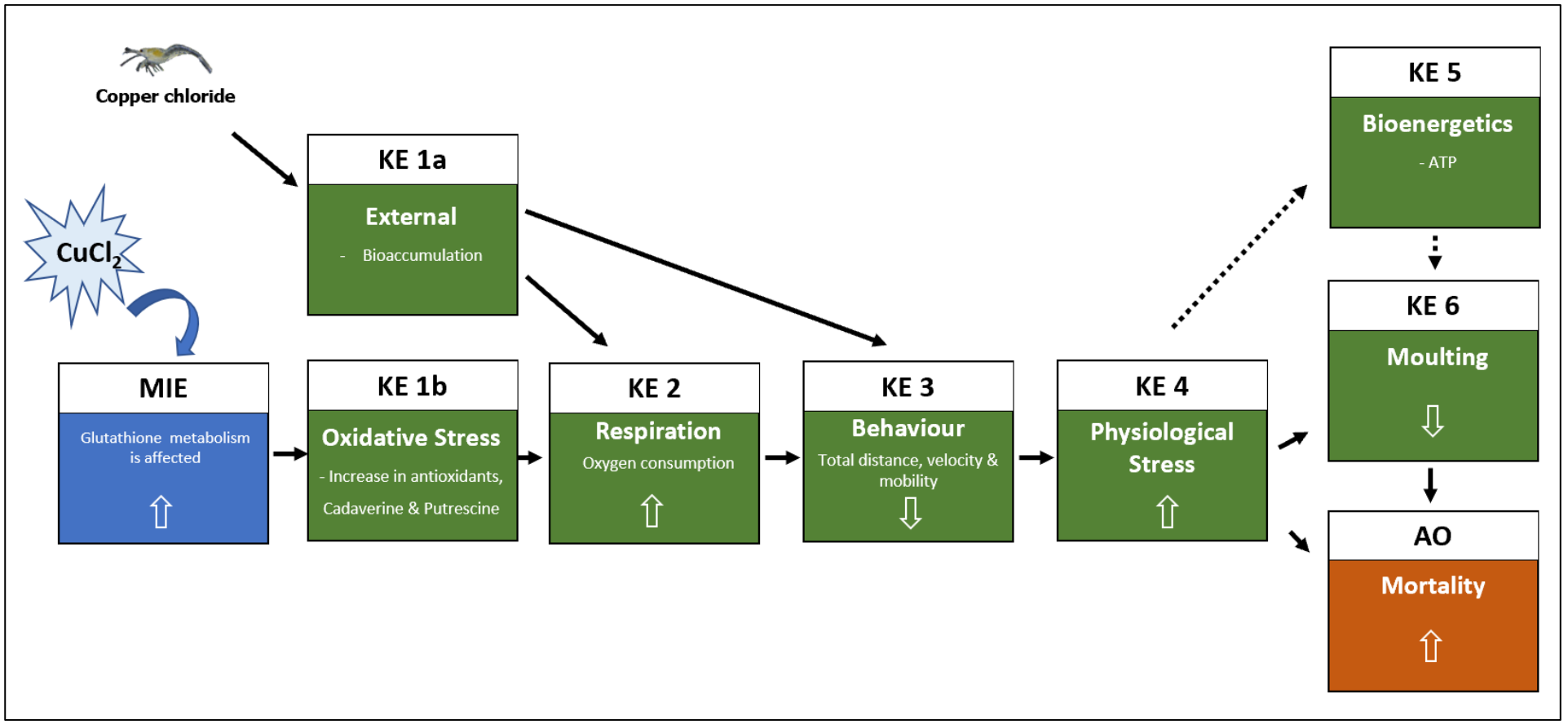

Figure 4.3 Proposed adverse outcome pathway for *Caridina africana* exposed to LC_{10+20} nano copper oxide.

CHAPTER 5 CONCLUSIONS AND RECOMMENDATIONS

5.1 Conclusions

Caridina africana is a relatively sensitive organism that allows it to be utilized as an ecotoxicological model, especially for contaminants that settle as it is a sediment dweller. This study found that exposing *C. africana* to nanomaterials altered its metabolome as well as its physiology at sublethal concentrations.

5.1.1 Characterization and Uptake

There are characteristics that affect the toxicity of nanomaterials. These include the size and surface charge of the nanomaterial itself as well as the influence of external parameters, such as the media's ion concentration, pH and temperature. When concentrations of nanomaterials in the exposure treatments increased, aggregation and sedimentation likely occurred, giving rise to the increase in hydrodynamic size distribution seen in the DLS results. Aggregation potential can be attributed to the media used for exposures as it contained four different salts: $CaCl_2$, $MgSO_4^{2-}$, KCl and $NaHCO_3$. The van der Waal's forces play a major role in attraction and repulsions between ion surfaces, resulting in aggregation of the nanomaterial. Aggregation results in a deviation from the initial particle size stipulated by the manufacturers, which in turn may have affected the organism's physiology as seen in our results.

The ZP and dissolution rates may have impacted nanomaterial toxicity, affecting their stability in suspension. The nCuO had a dissolution rate less than 1% over 96 h. This could be attributed to the pH and salts of the media, allowing for the formation of aggregates, causing the particles to remain relatively stable or become too large to diffuse through the dialysis tube, resulting in low dissolution. The ZP of NDs and nCuO were within the negative range, showing that an increase in concentration and/or aggregation, has no influence on the surface charge. Zeta potential plays an important role in nanomaterial toxicity. The more negative/positive the ZP, the easier the nanomaterial will cross due to the electrostatic interactions on the charged cell membrane increasing cellular uptake. External uptake of nCuO and NDs as agglomerate was confirmed by CytoViva via adherence to the exoskeleton on *C. africana*, which could cause the shrimp to moult due to physiological stress. This adherence confirms that the effects observed in metabolomics, respiration, heart rate and behaviour are due to the interaction with NMs.

The Cu content slightly increased as the concentrations increased in both Cu-based exposures. The increase in the $CuCl_2$ could be due to the release of the Cu^{2+} ions in the media as traditional metal ion exposures have shown dose dependent relationships. The decreased levels of Cu associated with $CuCl_2$ compared with nCuO may indicate Cu regulation at certain concentrations that may be favourable to the shrimp. With nCuO, the uptake did not remain consistent with the increased exposure concentrations, as at 40 mg/L, the Cu concentration was higher than 60 mg/L, which is often seen in NM exposure studies. Since the aggregation potential of nCuO is high, it may have settled out of the water column, being less bioavailable in the water column at 60 mg/L than at 40 mg/L which could change as the exposure duration continues since shrimp are bottom dwellers. Another reason for the nCuO exerting such elevated Cu accumulation could be due to the strong adherence of the nanomaterial to the exoskeleton of the shrimp.

5.1.2 Toxicity Exposures

Based on the acute toxicity tests, the nanomaterials exhibited a bimodal response. From this, it was determined that nCuO was more toxic between the two nanomaterials used in this study, and $CuCl_2$ was more toxic compared to nCuO. The nano copper oxide could be more toxic than NDs, due to the release of the Cu ions, or due to the particle itself being more toxic, since the nCuO particles adhere more to the shrimp's limbs, carapace and eyes (as seen by CytoViva), affecting their movements (as seen in behavioural trials) and thus their functioning. The release of Cu^{2+} ions from the metal salt could attribute to its toxicity, resulting in the various effects it has on its metabolome, physiology and behaviour.

At a cellular level, the PLS-DA results reveal that the shrimp's metabolome was affected by the exposure to the three exposure groups. Due to the lack of overlapping of metabolites between the various treatments, toxicity can be attributed to the release of Cu ions from $CuCl_2$. For nCuO, the toxicity response is more likely due to the nanoparticle than the release of ions from the nCuO due to low ion release. Nanodiamonds do have some effect on the metabolome, and this can also be attributed to the NM itself. The main pathways that are affected by all treatments are the aminoacyl-tRNA (amino acid biosynthesis) and glutathione metabolism, which is usually responsible for growth, protein translation and gene transcription. Other important pathways affected include energy metabolism and pathways associated with development and mortality.

Copper is an essential element for aquatic organisms, but at elevated concentrations, it can have detrimental consequences. Overall, with respiration and behaviour, Cu-based exposures exerted more adverse effects compared to NDs, which is attributed to the nCuO nanoparticle itself and its

dissolution, and the Cu ions from $CuCl_2$. Copper is known to affect the gills of aquatic organisms, and the ensuing effects on respiration are attributed to both the Cu ion as well as the NMs, and their agglomeration potential on the surface of the gill. The alterations caused by the addition of the three exposure groups could also be attributed to a general stress response occurring as the metabolomic data clearly indicate the activation of antioxidant responses in the shrimp.

Usually, there is a correlation between respiration and heart rate, as a decreased heart rate occurs when oxidative stress occurs, but with our results, there was no direct relationship. One theory found in literature (Spicer *et al*., 1995) reports that Cu has the ability to change the haemoglobin O_2 affinity during ontogenic shift. Elevated heart rates could be due to the general stress exerted by the addition of these materials. While aa decreased heart rate in the Cu-based treatments can be attributed to the Cu ions and/or the nanoparticle itself since less contractions cause reduced haemolymph flow and less beats per minute.

At an organismal level, locomotor activity is used as a stress indicator. A decrease in swimming speed can be the result of the nanomaterials adhering to the surface causing movement restriction and can result in the energy metabolism being affected. Adherence of the particles to antennas/pereiopods was confirmed through CytoViva.

The adherence of the nanoparticles to the appendages of the shrimp affects their survival by either altering their locomotion ability, possibly damaging their digestive tracts and/or gills or the generation of reactive oxygen species, either leading to starvation or respiratory issues, resulting in their mortality

All the effects exerted by the nanomaterials are attributed to the same parameters: their size, ZP and exposure media characteristics, which affect their agglomeration potential. These characteristics cause surface adhesion and when not released by moulting, potentially allow NMs to pass through the cell membrane of the shrimp, causing effects seen in their metabolome, heart rate, respiration, and the differences in locomotor activity, all of which affect mortality. The nCuO was more toxic than NDs having a more adverse ultimate mortality rate than nanodiamond.

Potential AOPs can be created based on the effects exerted by the shrimp when exposed to these materials, as the respective metabolome is affected, generating the MIE. The KEs also differ between the exposure group, differentially, affecting respiration, heart rate and behaviour, and mortality rates experienced by exposure to NDs, nCuO and $CuCl_2$.

Adverse outcome pathways are utilized to organize biological events that progress from a MIE to an AO. The AOPs that were constructed for the three different exposure groups and their concentrations revealed that NDs MIE is relatively different to the Cu-based exposures, but ultimately still causes oxidative stress by affecting metabolites responsible for antioxidant defence. Each of these MIE's could be linked to the higher level KE's, which would ultimately lead to the mortality of the shrimp.

Thus, the aim to determine the effects that nanodiamond and nano copper oxide exert on *Caridina africana* using the AOP framework was successfully achieved. The data supports the hypothesis of the adverse outcome pathway is effective in testing the effects of nanodiamond and nano copper oxide on *Caridina africana*.

5.2 Recommendations

Based on this study, the following have been highlighted for future studies:

- During this study, nanomaterial uptake and distribution in whole shrimp were studied using CytoViva. To allow for more effective visualization of the internalized nanomaterials, it is recommended to section the shrimp using microtomy techniques.
- Assess nanomaterials and ionic counterparts to different life cycles of the shrimp, such as exposing gravid shrimp and determining any defects in juveniles and alterations at other ages as well as following the long-term effects.
- To conduct environmentally relevant exposures in the shrimp's field water to determine if the behaviour of NMs may differ due to different concentrations of salts and the presence of natural organic matter.
- To assess the different routes of exposure, since shrimp are a sediment dweller, conducting exposures with sediment to determine if the aggregation potential will differ and in turn, how it affects the shrimps' physiology.
- To conduct an endpoint focused on moulting and run targeted metabolomics on the associated metabolite (hydroxyecdysone) to determine its presence in this shrimp's metabolome.
- To include targeted gene expression by focussing on the moulted related gene, the energy metabolism related genes and genetic expression related genes using qPCR.

REFERENCES

Abid, N., Khan, A.M., Shujait, S., Chaudhary, K., Ikram, M., Imran, M., Haider, J., Khan, M. Khan, Q. & Maqbool, M. 2022. Synthesis of nanomaterials using various top-down and bottom-up approaches, influencing factors, advantages, and disadvantages: A review. *Advances in Colloid and Interface Science*, 300:102597.

Acosta-Tlapalamatl, M., Romo-Gómez, C., Anaya-Hernández, A., Juárez-Santacruz, L., Gaytán-Oyarzún, J.C., Acevedo-Sandoval, O.A. & García-Nieto, E. 2022. Metabolomics: A new approach in the evaluation of effects in human beings and wildlife associated with environmental exposition to POPs. *Toxics*, 10(7):380.

Adámas Nanotechnologies Inc. 2018. *Fluorescent nanodiamond powder safety data sheet*. https://www.adamasnano.com/wp-content/uploads/2019/02/Adamas_MSDS_FND-Powder-SDS_Gen_rev11118.pdf.

Adewuyi, A. & Lau, W.J. 2021. Chapter 3 - Nanomaterial development and its applications for emerging pollutant removal in water. In: Lau, W.J., Faungnawakij, K., Ruktanonchai, U.R. & Iyachomkwan, K., eds. *Handbook of Nanotechnology Applications: Environment, Energy, Agriculture and Medicine*. Netherlands: Elsevier. pp. 67–97.

Agathokleous, E. 2022. The hormetic response of heart rate of fish embryos to contaminants–Implications for research and policy. *Science of The Total Environment*, 815:152911.

Akalin, G.O. 2021. Interaction of copper (II) oxide nanoparticles with aquatic organisms: uptake, accumulation, and toxicity. *Toxicological and Environmental Chemistry*, 103(4):342–381.

Akbarzadeh, A., Samiei, M. & Davaran, S. 2012. Magnetic nanoparticles: preparation physical properties, and applications in biomedicine. *Nanoscale Research Letters*, 7(1):144.

Al Ghais, S., Bhardwaj, V., Kumbhar, P. & Al Shehhi, O. 2019. Effect of copper nanoparticles and organometallic compounds (dibutyltin) on tilapia fish. *The Journal of Basic and Applied Zoology*, 80(1):32.

Al-Bairuty, G.A., Boyle, D., Henry, T.B. & Handy, R.D. 2016. Sublethal effects of copper sulphate compared to copper nanoparticles in rainbow trout (*Oncorhynchus mykiss*) at low pH: physiology and metal accumulation. *Aquatic Toxicology*, 174:188–198.

Anandhavalli, N., Mol, B., Manikandan, S., Anusha, N., Ponnusami, V. & Rajan, K. 2015. Green synthesis of cupric oxide nanoparticles using the water extract of *Murrya koenigi* and its photocatalytic activity. *Asian Journal of Chemistry*, 27(7):2523–2526.

Anastasiadis, S.H., Chrissopoulou, K., Stratakis, E., Kavatzikidou, P., Kaklamani, G. & Ranella, A. 2022. How the physicochemical properties of manufactured nanomaterials affect their performance in dispersion and their applications in biomedicine: A review. *Nanomaterials*, 12(3):552.

Anık, Ü., Timur, S. & Dursun, Z. 2019. Recent pros and cons of nanomaterials in drug delivery systems. *International Journal of Polymeric Materials and Polymeric Biomaterials*, 69(17):1090–1100.

Ankley, G.T., Bennett, R.S., Erickson, R.J., Hoff, D.J., Hornung, M.W., Johnson, R.D., Mount, D.R., Nichols, J.W., Russom, C.L. & Schmieder, P.K. 2010. Adverse outcome pathways: A conceptual framework to support ecotoxicology research and risk assessment. *Environmental Toxicology & Chemistry*, 29(3):730–741.

Arnott, S.A., Neil, D.M. & Ansell, A.D. 1998. Tail-flip mechanism and size-dependent kinematics of escape swimming in the brown shrimp *Crangon crangon*. *The Journal of Experimental Biology*, 201(11):1771–1784.

Arole, V.M. & Munde, S.V. 2014. Fabrication of nanomaterials by top-down and bottom-up approaches – an overview. *Journal of Applied Agricultural Science and Technology: Material Science*, 1(2):89–93.

Arome, D. & Chinedu, E. 2013. The importance of toxicity testing. *Journal of Pharmaceutical and BioSciences*, 4:146–148.

Arosio, P. 2021. Applications and Properties of Magnetic Nanoparticles. *Nanomaterials*, 11(5):1297.

Artells, E., Issartel, J., Auffan, M., Borschneck, D., Thill, A., Tella, M., Brousset, L., Rose, J., Bottero, J.Y. & Thiery, A. 2013. Exposure to cerium dioxide nanoparticles differently affect swimming performance and survival in two daphnid species. *Public Library of Science One*, 8(8):71260.

Auffan, M., Santaella, C., Thiéry, A., Pailles, C., Rose, J., Achouak, W., Thill, A., Masion, A., Wiesner, M. & Bottero, J. 2012. Ecotoxicity of inorganic nanoparticles: From unicellular organisms to invertebrates. In: Bhushan, B., ed. *Encyclopedia of Nanotechnology*. Dordrecht: Springer. pp. 623–636.

Augustine, R. & Hasan, A. 2020. Cellular response to nanobiomaterials. In: Mozafari, M., ed. *Handbook of Biomaterials Biocompatibility*. United Kingdom: Woodhead Publishing. pp. 473–504.

Avramescu, M.L., Chénier, M., Palaniyandi, S. & Rasmussen, P.E. 2020. Dissolution behavior of metal oxide nanomaterials in cell culture medium versus distilled water. *Journal of Nanoparticle Research*, 22:222.

Badireddy, A.R., Wiesner, M.R. & Liu, J. 2012. Detection, characterization, and abundance of engineered nanoparticles in complex waters by hyperspectral imagery with enhanced darkfield microscopy. *Environmental Science & Technology*, 46(18):10081–10088.

Barbero, F., Russo, L., Vitali, M., Piella, J., Salvo, I., Borrajo, M.L.,Busquets-Fité, M., Grandori, R., Bastú, N.G., Casals, E. & Puntes, V. 2017. Formation of the protein corona: The interface between nanoparticles and the immune system. *Seminars in Immunology*, 34:52–60.

Barhoum, A., García-Betancourt, M.L., Jeevanandam, J., Hussien, E.A., Mekkawy, S.A., Mostafa, M., Omran, M.M., Abdalla, M.S. & Bechelany, M. 2022. Review on natural, incidental, bioinspired, and engineered nanomaterials: history, definitions, classifications, synthesis, properties, market, toxicities, risks, and regulations. *Nanomaterials*, 12(2):177.

Basso, L., Cazzanelli, M., Orlandi, M. & Miotello, A. 2020. Nanodiamonds: Synthesis and application in sensing, catalysis, and the possible connection with some processes occurring in space. *Applied Sciences*, 10(12):4094.

Batley, G.E., Kirby, J.K. & McLaughlin, M.J. 2012. Fate and risks of nanomaterials in aquatic and terrestrial environments. *Accounts of Chemical Research*, 46(3):854–862.

Bauer, R.T. 1981. Decapod crustacean grooming: functional morphology, adaptive value, and phylogenetic significance. *Functional Morphology of Feeding and Grooming in Crustacea*, 1(2):153–174.

Baun, A., Hartmann, N.B., Grieger, K. & Kusk, K.O. 2008. Ecotoxicity of engineered nanoparticles to aquatic invertebrates: a brief review and recommendations for future toxicity testing. *Ecotoxicology*, 17:387–395.

Bayda, S., Adeel, M., Tuccinardi, T., Cordani, M. & Rizzolio, F. 2019. The history of nanoscience and nanotechnology: From chemical–physical applications to nanomedicine. *Molecules*, 25(1):112.

Bekebrede, A.F., Keijer, J., Gerrits, W.J. & Boer, V.C.D. 2020. The molecular and physiological effects of protein-derived polyamines in the intestine. *Nutrients*, 12(1):197.

Bertolacci, L., Valentini, P. & Pompa, P.P. 2020. A nanocomposite hydrogel with catalytic properties for trace-element detection in real-world samples. *Scientific Reports*, 10(1):18340.

Beukes, D., du Preez, I. & Loots, D.T. 2019. Total metabolome extraction from mycobacterial cells for GC-MS metabolomics analysis. In: Baidoo, E., *ed. Microbial Metabolomics: Methods and Protocols*. New York: Humana Press. pp. 121–131.

Bhagyaraj, S.M. & Oluwafemi, O.S. 2018. Nanotechnology: The Science of the Invisible. In: Bhagyaraj, S.M., Oluwafemi, O.S., Kalarikkal, N. & Thomas, S., eds. *Synthesis of Inorganic Nanomaterials: Advances and Key Technologies*. United Kingdom: Woodhead Publishing. pp. 1–18.

Bierbower, S.M. & Cooper, R.L. 2009. Measures of heart and ventilatory rates in freely moving crayfish. *Journal of Visualized Experiments,* (32):1594.

Blaise, C., Gagné, F., Ferard, J. & Eullaffroy, P. 2008. Ecotoxicity of selected nano-materials to aquatic organisms. *Environmental Toxicology,* 23(5):591–598.

Boddolla, S. & Thodeti, S. 2018. A review on characterization techniques of nanomaterials. *International Journal of Engineering, Science and Mathematics*, 7(1):169–175.

Bodó, K., Baranzini, N., Girardello, R., Kokhanyuk, B., Németh, P., Hayashi, Y., Grimaldi, A. & Engelmann, P. 2020. Nanomaterials and annelid immunity: A comparative survey to reveal the common stress and defense responses of two sentinel species to nanomaterials in the environment. *Biology*, 9(10):307.

Böhme, S., Baccaro, M., Schmidt, M., Potthoff, A., Stärk, H.J., Reemtsma, T. & Kühnel, D. 2017. Metal uptake and distribution in the zebrafish (*Danio rerio*) embryo: differences between nanoparticles and metal ions. *Environmental Science: Nano*, 4:1005–1015.

Boisseau, P. & Loubaton, B. 2011. Nanomedicine, nanotechnology in medicine. *Comptes Rendus Physique*, 12(7):620–636.

Borm, P., Klaessig, F.C., Landry, T.D., Moudgil, B., Pauluhn, J., Thomas, K., Trottier, R. & Wood, S. 2006. Research strategies for safety evaluation of nanomaterials, Part V: Role of dissolution in biological fate and effects of nanoscale particles. *Toxicological Sciences*, 90(1):23–32.

Botha, T.L., Boodhia, K. & Wepener, V. 2016. Adsorption, uptake and distribution of gold nanoparticles in *Daphnia magna* following long term exposure. *Aquatic Toxicology*, 170:104–111.

Botha, T.L., James, T.E. & Wepener, V. 2015. Comparative aquatic toxicity of gold nanoparticles and ionic gold using a species sensitivity distribution approach. *Journal of Nanomaterials*, 2015:986902.

Boyle, D., Clark, N.J., Botha, T.L. & Handy, R.D. 2020. Comparison of the dietary bioavailability of copper sulphate and copper oxide nanomaterials in ex vivo gut sacs of rainbow trout: effects of low pH and amino acids in the lumen. *Environmental Science: Nano*, 7(7):1967–1979.

Boyles, M.S., Ranninger, C., Reischl, R., Rurik, M., Tessadri, R., Kohlbacher, O., Duschl, A. & Huber, C.G. 2015. Copper oxide nanoparticle toxicity profiling using untargeted metabolomics. *Particle and Fibre Toxicology*, 13(1):e.49.

Brand, S.J., Botha, T.L. & Wepener, V. 2020. Behavioural response as a reliable measure of acute nanomaterial toxicity in zebrafish larvae exposed to a carbon-based versus a metal-based nanomaterial. *African Zoology*, 55(1):57–66.

Brausch, K.A., Anderson, T.A., Smith, P.N. & Maul, J.D. 2011. The effect of fullerenes and functionalized fullerenes on *Daphnia magna* phototaxis and swimming behavior. *Environmental Toxicology & Chemistry*, 30(4):878–884.

Brett, M. & Müller-Navarra, D. 1997. The role of highly unsaturated fatty acids in aquatic foodweb processes. *Freshwater Biology*, 38(3):483–499.

Bruinink, A., Wang, J. & Wick, P. 2015. Effect of particle agglomeration in nanotoxicology. *Archives of Toxicology*, 89(5):659–675.

Bundschuh, M., Seitz, F., Rosenfeldt, R.R. & Schulz, R. 2016. Effects of nanoparticles in fresh waters: risks, mechanisms and interactions. *Freshwater Biology*, 61(12):2185–2196.

Çalhan, S.D. & Gündoğan, M. 2020. Copper oxide nanoparticles: synthesis, characterization, antimicrobial activities and catalytic reduction of methylene blue. *Journal of the Turkish Chemical Society Section A: Chemistry*, 7(2):561–570.

Canesi, L. & Corsi, I. 2016. Effects of nanomaterials on marine invertebrates. *Science of the Total Environment*, 565:933–940.

Cano, A.M., Maul, J.D., Saed, M., Shah, S.A., Green, M.J. & Cañas-Carrell, J.E. 2017. Bioaccumulation, stress, and swimming impairment in *Daphnia magna* exposed to multiwalled carbon nanotubes, graphene, and graphene oxide. *Environmental Toxicology & Chemistry*, 36(8):2199–2204.

Cardeilhac, P.T. & Whitaker, B.R. 1988. Copper treatments: uses and precautions. *Veterinary Clinics of North America: Small Animal Practice*, 18(2):435–448.

Carmen, B. 2022. Metabolomics in environmental toxicology: Applications and challenges. *Trends in Environmental Analytical Chemistry*, 34:00161.

Carusi, A., Davies, M.R., De Grandis, G., Escher, B.I., Hodges, G., Leung, K.M., Whelan, M., Willett, C. & Ankley, G.T. 2018. Harvesting the promise of AOPs: An assessment and recommendations. *Science of the Total Environment*, 628:1542–1556.

Cha, C., Shin, S.R., Annabi, N., Dokmeci, M.R. & Khademhosseini, A. 2013. Carbon-based nanomaterials: multifunctional materials for biomedical engineering. *American Chemical Society Nano*, 7(4):2891–2897.

Chakraborty, S. & Misra, S.K. 2019. A comparative analysis of dialysis based separation methods for assessing copper oxide nanoparticle solubility. *Environmental Nanotechnology, Monitoring and Management*, 12:100258.

Chang, E.S. 1995. Physiological and biochemical changes during the moult cycle in decapod crustaceans: an overview. *Journal of Experimental Marine Biology and Ecology*, 193(1-2):1–14.

Chao, S.J., Huang, C., Lam, C.C., Hua, L.C., Chang, S.H. & Huang, C. 2021. Transformation of copper oxide nanoparticles as affected by ionic strength and its effects on the toxicity and bioaccumulation of copper in zebrafish embryo. *Ecotoxicology & Environmental Safety*, 225:112759.

Chattopadhyay, I. 2020. Application of nanoparticles in drug delivery. In: Siddhardha, B., Dyavaiah, M. & Kasinathan, K., *eds*. *Model Organisms to Study Biological Activities and Toxicity of Nanoparticles*. Singapore: Springer. pp. 35–57.

Chaumot, A., Ferrari, B., Geffard, O. & Garric, J. 2014. Ecotoxicology, aquatic invertebrates. In: Wexler, P., ed. *Encyclopedia of Toxicology*. London: Elsevier. pp. 284–288.

Chaurasia, N. 2017. Nanotechnology and nanomaterials in everyday life. *International Journal of Science and Research*, 6(4):1560–1562.

Chen, P.Z., Pollit, L., Jones, L. & Gu, F.X. 2018b. Functional two- and three-dimensional architectures of immobilized metal nanoparticles. *Chem*, 4(10):2301–2328.

Chen, Y., Fan, Z., Zhang, Z., Niu, W., Li, C., Yang, N Chen, B. & Zhang, H. 2018a. Two-dimensional metal nanomaterials: synthesis, properties, and applications. *Chemical Reviews*, 118(13):6409–6455.

Chowdhury, M.M.H., Kubra, K., Kanwar, R.K. & Kanwar, J.R. 2019. Nanoparticles advancing cancer immunotherapy. In: Nurunnabi, M. & McCarthy, J.R., eds. *Biomedical Applications of Graphene and 2D Nanomaterials: Micro and Nano Technologies*. Elsevier. pp. 283–304.

Cid, A., Picado, A., Correia, J.B., Chaves, R., Silva, H., Caldeira, J., de Matos, A.P.A & Diniz, M.S. 2015. Oxidative stress and histological changes following exposure to diamond nanoparticles in the freshwater Asian clam *Corbicula fluminea* (Müller, 1774). *Journal of Hazardous Materials*, 284:27–34.

Clark, N.J., Boyle, D. & Handy, R.D. 2019. An assessment of the dietary bioavailability of silver nanomaterials in rainbow trout using an ex vivo gut sac technique. *Environmental Science: Nano*, 6(2):646–660.

Coady, K., Browne, P., Embry, M., Hill, T., Leinala, E., Steeger, T., Maślankiewicz, L. & Hutchinson, T. 2019. When are adverse outcome pathways and associated assays “fit for

purpose" for regulatory decision-making and management of chemicals?. *Integrated Environmental Assessment and Management*, 15(4):633–647.

Coetzee, D., Venkataraman, M., Militky, J. & Petru, M. 2020. Influence of nanoparticles on thermal and electrical conductivity of composites. *Polymers*, 12(4):742.

Croteau, M.-N.l., Misra, S.K., Luoma, S.N. & Valsami-Jones, E. 2014. Bioaccumulation and toxicity of CuO nanoparticles by a freshwater invertebrate after waterborne and dietborne exposures. *Environmental Science & Technology*, 48(18):10929–10937.

da Silva Acosta, D., Danielle, N.M., Altenhofen, S., Luzardo, M.D., Costa, P.G., Bianchini, A., Bonan, C.D., da Silva, R.S. & Dafre, A.L. 2016. Copper at low levels impairs memory of adult zebrafish (*Danio rerio*) and affects swimming performance of larvae. *Comparative Biochemistry and Physiology Part C: Toxicology & Pharmacology*, 185:122–130.

Dallas, H. & Ross-Gillespie, V. 2015. Sublethal effects of temperature on freshwater organisms, with special reference to aquatic insects. *Water SA*, 41(5):712–726.

Darbyshire, A.K., Oliver, K.H., Dupont, W.D., Plummer, W.D., Jones, C.P. & Boyd, K.L. 2019. Anesthesia and euthanasia of brine shrimp (*Artemia franciscana*). *Journal of the American Association for Laboratory Animal Science,* 58(1):58–63.

Davis, J., Ekman, D., Skelton, D., LaLone, C., Ankley, G., Cavallin, J., Villeneuve, D. & Collette, T. 2017. Metabolomics for informing adverse outcome pathways: androgen receptor activation and the pharmaceutical spironolactone. *Aquatic Toxicology*, 184:103–115.

Davis, J.M., Ekman, D.R., Teng, Q., Ankley, G.T., Berninger, J.P., Cavallin, J.E., Jensen, K.M., Kahl, M.D., Schroeder, A.L. & Villeneuve, D.L. 2016. Linking field-based metabolomics and chemical analyses to prioritize contaminants of emerging concern in the Great Lakes basin. *Environmental Toxicology & Chemistry*, 35(10):2493–2502.

De Luca, E., Zaccaria, G.M., Hadhoud, M., Rizzo, G., Ponzini, R., Morbiducci, U. & Santoro, M.M. 2014. ZebraBeat: a flexible platform for the analysis of the cardiac rate in zebrafish embryos. *Scientific Reports*, 4(1):e.4898.

de Oliveira Eiras, M.I., Costa, L.S. da & Barbieri, E. 2022. Copper II oxide nanoparticles (CuONPs) alter metabolic markers and swimming activity in zebra-fish (*Danio rerio*). *Comparative Biochemistry and Physiology Part C: Toxicology & Pharmacology*, 257:109343.

de Vareilles, M., Conceição, L.E., Gómez-Requeni, P., Kousoulaki, K., Richard, N., Rodrigues, P.M., Fladmark, K.E. & Rønnestad, I. 2012. Dietary lysine imbalance affects muscle proteome in zebrafish (*Danio rerio*): a comparative 2D-DIGE study. *Marine Biotechnology*, 14:643–654.

Delahaut, V., Rašković, B., Salvado, M.S., Bervoets, L., Blust, R. & De Boeck, G. 2020. Toxicity and bioaccumulation of Cadmium, Copper and Zinc in a direct comparison at equitoxic concentrations in common carp (*Cyprinus carpio*) juveniles. *Public Library of Science One*, 15(4):0220485.

Devaraj, H. & Natarajan, A. 2006. Molecular mechanisms regulating molting in a crustacean. *The Federation of European Biochemical Societies Journal*, 273(4):839–846.

Dhas, N.L., Raval, N.J., Kudarha, R.R., Acharya, N.S. & Acharya, S.R. 2018. Core–shell nanoparticles as a drug delivery platform for tumor targeting. In: Grumezescu, A.M., ed. *Inorganic Frameworks as Smart Nanomedicines*. William Andrew Publishing. pp. 387–448.

Din, S.H., Shah, M.A.,Sheikh, N.A. & Butt, M.M. 2020. Nano-Composites and their Applications: A review. *Characterization and Application of Nanomaterials*, 3(1):40–48.

Ding, Z., Jiang, Y. & Liu, X. 2018. Nanoemulsions-based drug delivery for brain tumors. In: Kesharwani, P. & Gupta, U., *eds*. *Nanotechnology-Based Targeted Drug Delivery Systems for Brain Tumors*. Elsevier. pp. 327–358.

Do, V.N. & Pham, T.H. 2010. Graphene and its one-dimensional patterns: from basic properties towards applications. *Advances in Natural Sciences: Nanoscience and Nanotechnology*, 1(3):033001.

Dolez, P.I. 2015. Nanomaterials definitions, classifications, and applications. In: Dolez, P.I., ed. *Nanoengineering Global Approaches to Health and Safety Issues*. Elsevier. pp. 3–40.

Domínguez, G.A., Torelli, M.D., Buchman, J.T., Haynes, C.L., Hamers, R.J. & Klaper, R.D. 2018. Size dependent oxidative stress response of the gut of *Daphnia magna* to functionalized nanodiamond particles. *Environmental Research*, 167:267–275.

Ebina, A., Hossain, S., Horihata, H., Ozaki, S., Kato, S., Kawawaki, T. & Negishi Y. 2020. One-, two-, and three-dimensional self-assembly of atomically precise metal nanoclusters. *Nanomaterials*, 10(6):1105.

Edokpayi, J.N., Odiyo, J.O. & Durowoju, O.S. 2017. Impact of wastewater on surface water quality in developing countries: a case study of South Africa. In: Tutu, H., *ed. Water Quality*. Rijeka: InTech. pp. 401–416.

Edwards, J.G. & Michel, W.C. 2002. Odor-stimulated glutamatergic neurotransmission in the zebrafish olfactory bulb. *Journal of Comparative Neurology*, 454(3):294–309.

Effiong, D., Uwah, T., Jumbo, E. & Akpabio, A. 2020. Nanotechnology in cosmetics: basics, current trends and safety concerns—a review. *Advances in Nanoparticles*, 9(1):1–22.

Egan, N., Stinson, S.A., Deng, X., Lawler, S.P. & Connon, R.E. 2023. Swimming Behavior of *Daphnia magna* Is Altered by Pesticides of Concern, as Components of Agricultural Surface Water and in Acute Exposures. *Biology*, 12(3):425.

Egbuna, C., Parmar, V.K., Jeevanandam, J., Ezzat, S.M., Patrick-Iwuanyanwu, K.C., Adetunji, C.O., Khan, J., Onyeike, E.N., Uche, C.Z., Akram, M. & Ibrahim, M.S. 2021. Toxicity of nanoparticles in biomedical application: nanotoxicology. *Journal of Toxicology*, 2021:9954443.

Ehi-Eromosele, C. 2016. The effect of polyethylene glycol (PEG) coating on the magneto-structural properties and colloidal stability of CO0. 8Mg0. 2Fe2O4 nanoparticles for potential biomedical applications. *Digest Journal of Nanomaterials and Biostructures*, 11(1):7–14.

Eisermann, S., Kronenberger, A., Laufer, A., Bieber, J., Haas, G., Lautenschläger, S., Homm, G., Klar, P.J. & Meyer, B.K. 2011. Copper oxide thin films by chemical vapor deposition: Synthesis, characterization and electrical properties. *Physica Status Solidi,* 209(3):531–536.

El Alfy, K., Elwazir, M. & Medhat Shalaby, A. 2021. Adaptive technologies of nano-architecture for the next generation of sustainable building applications. *Mansoura Engineering Journal*, 46(1):122–133.

El-Atti, M.A., Desouky, M.M.A., Mohamadien, A. & Said, R.M. 2019. Impact of copper oxide nanoparticles on freshwater crayfish, *Procambarus clarkia*. A combined histopathological, biochemical and genotoxicological study. *Journal of Egyptian Academic Society for Environmental Development*, 20(1):1–18.

Etefagh, R., Azhir, E. & Shahtahmasebi, N. 2013. Synthesis of CuO nanoparticles and fabrication of nanostructural layer biosensors for detecting *Aspergillus niger* fungi. *Scientia Iranica*, 20(3):1055–1058.

European Commission. 2022. *Commission Recommendation of 10.6.2022 on the definition of nanomaterial (text with EEA relevance) (2022/C229/01)*. Brussels: Official Journal of the European Union. https://eur-lex.europa.eu/legal-content/EN/TXT/?uri=CELEX:32022H0614(01)#document1.

Exbrayat, J.M., Moudilou, E.N. & Lapied, E. 2015. Harmful effects of nanoparticles on animals. *Journal of Nanotechnology*, 2015:861092.

Fadiji, A.E., Mthiyane, D.M.N., Onwudiwe, D.C. & Babalola, O.O. 2022. Harnessing the known and unknown impact of nanotechnology on enhancing food security and reducing postharvest losses: constraints and future prospects. *Agronomy*, 12(7):1657.

Fairlamb, A.H. & Cerami, A. 1992. Metabolism and functions of trypanothione in the Kinetoplastida. *Annual Review of Microbiology*, 46(1):695–729.

Farzin, A., Etesami, S.A., Quint, J., Memic, A. & Tamayol, A. 2020. Magnetic nanoparticles in cancer therapy and diagnosis. *Advanced Healthcare Materials*, 9(9):1901058.

Fekete-Kertész, I., László, K., Terebesi, C., Gyarmati, B.S., Farah, S., Márton, R. & Molnár, M. 2020. Ecotoxicity assessment of graphene oxide by *Daphnia magna* through a multimarker approach from the molecular to the physiological level including behavioral changes. *Nanomaterials*, 10(10):2048.

Felgenhauer, B.E. 1992. Internal anatomy of the Decapoda: an overview. In: Harrison, F.W. & Humes, F.G., *eds*. *Microscopic anatomy of invertebrates, Decapoda Crustacea*. New York: Wiley-Liss Inc. pp. 45–75.

Floyd, K.A., Eberly, A.R. & Hadjifrangiskou, M. 2017. Adhesion of bacteria to surfaces and biofilm formation on medical devices. In: Deng, Y. & Lv, W., eds. *Biofilms and Implantable Medical Devices: Infection and Control*. Woodhead Publishing. pp. 47–95.

Folmer, O., Black, M., Hoeh, W., Lutz, R. & Vrijenhoek, R. 1994. DNA primers for amplification of mitochondrial cytochrome c oxidase subunit I from diverse metazoan invertebrates. *Molecular Marine Biology and Biotechnology*, 3(5):294–299.

Ford, A.T., Ågerstrand, M., Brooks, B.W., Allen, J., Bertram, M.G., Brodin, T., Dang, Z., Duquesne, S., Sahm, R. & Hoffmann, F. 2021. The role of behavioural ecotoxicology in environmental protection. *Environmental Science & Technology*, 55(9):5620–5628.

Fransen, C. 2014. Shrimps and prawns. In: Carpenter, K.E. & De Angelis, N., eds. *The living marine resources of the Eastern Central Atlantic*. Italy: Food and Agricultural Organization. pp. 38–196.

Frías-Espericueta, M.G., Bautista-Covarrubias, J.C., Osuna-Martínez, C.C., Delgado-Alvarez, C., Bojórquez, C., Aguilar-Juárez, M., Roos-Muñoz, S., Osuna-López, I. & Páez-Osuna, F. 2022. Metals and oxidative stress in aquatic decapod crustaceans: A review with special reference to shrimp and crabs. *Aquatic Toxicology*, 242:106024.

Fusco, L., Avitabile, E., Armuzza, V., Orecchioni, M., Istif, A., Bedognetti, D., Da Ros, T. & Delogu, L.G. 2020. Impact of the surface functionalization on nanodiamond biocompatibility: a comprehensive view on human blood immune cells. *Carbon*, 160:390–404.

Fytianos, G., Rahdar, A. & Kyzas, G.Z. 2020. Nanomaterials in cosmetics: recent updates. *Nanomaterials*. 10(5):979.

Ganesan, R., Vasantha-Srinivasan, P., Sadhasivam, D.R., Subramanian, R., Vimalraj, S. & Suk, K.T. 2021. Carbon nanotubes induce metabolomic profile disturbances in zebrafish: NMR-based metabolomics platform. *Frontiers in Molecular Biosciences*, 8:688827.

Gao, F. & Gu, Z. 2015. Melting Temperature of Metallic Nanoparticles. In: *Handbook of Nanoparticles*. Cham: Springer. pp. 661–690.

Gardner, J. 2015. Nanotechnology in medicine and healthcare: Possibilities, progress and problems. *South African Journal of Bioethics and Law*, 8(2):50.

Garncarek, M., Dziewulska, K. & Kowalska-Góralska, M. 2022. The effect of copper and copper oxide nanoparticles on rainbow trout (*Oncorhynchus mykiss* W.) spermatozoa motility after incubation with contaminants. *International Journal of Environmental Research and Public Health*, 19(14):8486.

Gerloff, K., Landesmann, B., Worth, A., Munn, S., Palosaari, T. & Whelan, M. 2017. The adverse outcome pathway approach in nanotoxicology. *Computational Toxicology*, 1:3–11.

Ghadimi, M., Zangenehtabar, S. & Homaeigohar, S. 2020. An overview of the water remediation potential of nanomaterials and their ecotoxicological impacts. *Water*, 12(4):1150.

Ghassan, A.A., Mijan, N.A. & Taufiq-Yap, Y.H. 2019. Nanomaterials: an overview of nanorods

synthesis and optimization. In: Ghamsari, M.S. & Dhara, S., eds. *Nanorods and Nanocomposites*. London: IntechOpen. pp. 11–34.

Ghate, H. & Mulherkar, L. 1979. Histological changes in the gills of two freshwater prawn species exposed to copper sulphate. *Indian Journal of Experimental Biology*, 17:838–840.

Gillis, P., Chow-Fraser, P., Ranville, J., Ross, P. & Wood, C. 2005. Daphnia need to be gut-cleared too: the effect of exposure to and ingestion of metal-contaminated sediment on the gut-clearance patterns of *D. magna*. *Aquatic Toxicology*, 71(2):143–154.

Gines, L., Mandal, S., Cheng, C.L., Sow, M. & Williams, O.A. 2017. Positive zeta potential of nanodiamonds. *Nanoscale*, 9(34):12549–12555.

Gonçalves, A.M.M., Marques, J.C. & Gonçalves, F. 2017. Fatty acids' profiles of aquatic organisms: revealing the impacts of environmental and anthropogenic stressors. In: Catala, A., ed*. Fatty Acids*. IntechOpen. pp. 89–117.

González-García, L.E., MacGregor, M.N., Visalakshan, R.M., Lazarian, A., Cavallaro, A.A., Morsbach, S., Mierczynska-Vasilev, A., Mailänder, V., Landfester, K. & Vasilev, K. 2022. Nanoparticles surface chemistry influence on protein corona composition and inflammatory responses. *Nanomaterials*, 12(4):682.

González-García, Y., López-Vargas, E.R., Cadenas-Pliego, G., Benavides-Mendoza, A., González-Morales, S., Robledo-Olivo, A., Alpuche-Solís, Á.G. & Juárez-Maldonado, A. 2019. Impact of carbon nanomaterials on the antioxidant system of tomato seedlings. *International Journal of Molecular Sciences*, 20(23):5858.

Goodchild, C.G., Simpson, A.M., Minghetti, M. & DuRant, S.E. 2019. Bioenergetics-adverse outcome pathway: Linking organismal and suborganismal energetic endpoints to adverse outcomes. *Environmental Toxicology & Chemistry*, 38(1):27–45.

Greene, M., Pitts, W. & Dewprashad, B. 2017. Using videography to study the effects of stimulants on *Daphnia magna*. *The American Biology Teacher*, 79(1):35–40.

Griffitt, R.J., Luo, J., Gao, J., Bonzongo, J.C. & Barber, D.S. 2008. Effects of particle composition and species on toxicity of metallic nanomaterials in aquatic organisms. *Environmental Toxicology & Chemistry,* 27(9):1972–1978.

Groh, K.J., Carvalho, R.N., Chipman, J.K., Denslow, N.D., Halder, M., Murphy, C.A., Roelofs, D., Rolaki, A., Schirmer, K. & Watanabe, K.H. 2015. Development and application of the adverse outcome pathway framework for understanding and predicting chronic toxicity: II. A focus on growth impairment in fish. *Chemosphere*, 120:778–792.

Grosell, M. 2011. Copper. In: Wood, C.M., Farrell, A.P. & Brauner, C.J., eds. *Fish physiology – Homeostasis and Toxicology of Essential Metals*. Academic Press. pp. 53–133.

Guadagnoli, J., Tobita, K. & Reiber, C. 2007. Assessment of the pressure–volume relationship of the single ventricle of the grass shrimp, *Palaemonetes pugio*. *Journal of Experimental Biology*, 210(12):2192–2198.

Gumustas, M., Sengel-Turk, C.T., Gumustas, A., Ozkan, S.A. & Uslu, B. 2017. Effect of polymer-based nanoparticles on the assay of antimicrobial drug delivery systems. In: Grumezescu, A.M., ed. *Multifunctional systems for combined delivery, biosensing and diagnostics*. Elsevier. pp. 67–108.

Gündoğdu, A. 2008. Acute toxicity of zinc and copper for rainbow trout (*Onchorhyncus mykiss*). *Journal of Fisheries Sciences*, 2(5):711–720.

Guo, D., Xie, G. & Luo, J. 2013. Mechanical properties of nanoparticles: basics and applications. *Journal of Physics: Applied Physics*, 47(1):013001.

Gupta, V. & Trivedi, P. 2018. *In vitro* and *in vivo* characterization of pharmaceutical topical nanocarriers containing anticancer drugs for skin cancer treatment. In: Grumezescu, A.M., ed. *Lipid nanocarriers for drug targeting.* William Andrew: Applied Science Publishers. pp. 563–627.

Gupta, V., Mohapatra, S., Mishra, H., Farooq, U., Kumar, K., Ansari, M.J., Aldawsari, M.F., Alalaiwe, A.S., Mirza, M.A. & Iqbal, Z. 2022. Nanotechnology in Cosmetics and Cosmeceuticals—A Review of Latest Advancements. *Gels*, 8(3):173.

Habiba, K., Makarov, V., Weiner, B. & Morell, G. 2014. Fabrication of Nanomaterials by Pulsed Laser Synthesis. *Manufacturing Nanostructures*, 10:263–292.

Halappanavar, S., Ede, J.D., Mahapatra, I., Krug, H.F., Kuempel, E.D., Lynch, I., Vandebriel, R.J. & Shatkin, J.A. 2021. A methodology for developing key events to advance nanomaterial-relevant adverse outcome pathways to inform risk assessment. *Nanotoxicology*, 15(3):289–310.

Halappanavar, S., Ede, J.D., Shatkin, J.A. & Krug, H.F. 2019. A systematic process for identifying key events for advancing the development of nanomaterial relevant adverse outcome pathways. *NanoImpact*, 15:100178.

Halappanavar, S., Van Den Brule, S., Nymark, P., Gaté, L., Seidel, C., Valentino, S., Zhernovkov, V., Høgh Danielsen, P., De Vizcaya, A. & Wolff, H. 2020. Adverse outcome pathways as a tool for the design of testing strategies to support the safety assessment of emerging advanced materials at the nanoscale. *Particle and Fibre Toxicology*, 17:e.16.

Handy, R. & Depledge, M. 1999. Physiological responses: their measurement and use as environmental biomarkers in ecotoxicology. *Ecotoxicology*, 8(5):329–349.

Handy, R.D., Eddy, F.B. & Romain, G. 1989. *In vitro* evidence for the ionoregulatory role of rainbow trout mucus in acid, acid/aluminium and zinc toxicity. *Journal of Fish Biology*, 35: 737–747.

Hanna, S.K., Miller, R.J. & Lenihan, H.S. 2014. Accumulation and toxicity of copper oxide engineered nanoparticles in a marine mussel. *Nanomaterials*, 4(3):535–547.

Hart, R.C., Stewart, B.A. & Bickerton, I.B. 2001. Guides to the freshwater invertebrates of southern Africa. Volume 4: Crustacea III. Bathynellacea, Amphipoda, Isopoda, Spelaeogriphacea, Tanaidacea and Decapoda. In: Day, J.A., Stewart, B.A., De Moor, I.J. & Louw, A.E., *eds*. *Guides to the Freshwater Invertebrates of Southern Africa.* Taylor & Francis. pp. 87–109.

Hayat, S., Hayat, Q., Alyemeni, M.N., Wani, A.S., Pichtel, J. & Ahmad, A. 2012. Role of proline under changing environments: a review. *Plant Signaling and Behavior*, 7(11):1456–1466.

He, H., Cheng, Y., Yang, C., Zeng, G., Zhu, C. & Yan, Z. 2017. Influences of anion concentration and valence on dispersion and aggregation of titanium dioxide nanoparticles in aqueous solutions. *Journal of Environmental Sciences*, 54:135–141.

He, X., Deng, H. & Hwang, H. 2019. The current application of nanotechnology in food and agriculture. *Journal of Food and Drug Analysis*, 27(1):1–21.

Heckmann, L. & Connon, R. 2007. Culturing of *Daphnia magna* - Standard Operating Procedure. University of Reading: Daphnia Research Group.(1).

Heera, P. & Shanmugam, S. 2015. Nanoparticle characterization and application: An overview. *International Journal of Current Microbiology and Applied Sciences*, 4(8):379–386.

Heiligtag, F.J. & Niederberger, M. 2013. The fascinating world of nanoparticle research. *Materials Today*, 16(7–8):262–271.

Hillis, D.M. & Bull, J.J. 1993. An empirical test of bootstrapping as a method for assessing confidence in phylogenetic analysis. *Systematic Biology*, 42(2):182–192.

Hobbs, H. & Lodge, D. 2010. Decapoda. In: Thorp, J.H. & Covich, A.P., eds. *Ecology and Classification of North American Freshwater Invertebrates*. Elsevier. pp. 901–967.

Hochella Jr, M.F., Mogk, D.W., Ranville, J., Allen, I.C., Luther, G.W., Marr, L.C., McGrail, B.P., Murayama, M., Qafoku, N.P., Rosso, K.M. & Sahai, N. 2019. Natural, incidental, and engineered nanomaterials and their impacts on the Earth system. *Science*, 363(6434): eaau8299.

Hondow, N., Brown, A. & Brydson, R. 2015. Nanomaterials: Dispersion, Dissolution and Dose. In: Baalousha, M. & Lead, J.R., eds. *Frontiers of Nanoscience*. Elsevier. pp. 183–216.

Horzmann, K.A. & Freeman, J.L. 2016. Zebrafish get connected: investigating neurotransmission targets and alterations in chemical toxicity. *Toxics*, 4(3):19.

Hosamani, N., Reddy, S. and Reddy, R. 2017. Crustacean molting: regulation and effects of environmental toxicants. *Journal of Marine Science: Research and Development,* 7(5):236.

Hosseintabar, B., Dadashbeiki, M., Bouyeh, M., Seidavi, A., van den Hoven, R. & Gamboa, S. 2015. Effect of different levels of L-carnitine and lysine-methionine on broiler blood parameters. *Revista MVZ Córdoba*, 20(3):4698–4708.

Hu, M. & Palić, D. 2020. Micro-and nano-plastics activation of oxidative and inflammatory adverse outcome pathways. *Redox Biology*, 37:101620.

Hu, X., Li, D., Gao, Y., Mu, L. & Zhou, Q. 2016. Knowledge gaps between nanotoxicological research and nanomaterial safety. *Environment International*, 94:8–23.

Huang, Z., Aweya, J.J., Zhu, C., Tran, N.T., Hong, Y., Li, S., Yao, D. & Zhang, Y. 2020. Modulation of crustacean innate immune response by amino acids and their metabolites: inferences from other species. *Frontiers in Immunology*, 11:574721.

Iqbal, P., Preece, J.A. & Mendes, P.M. 2012. Nanotechnology: The “Top-Down” and “Bottom-Up” Approaches. In: Gale, P.A., ed. *Supramolecular Chemistry: From Molecules to Nanomaterials*. John Wiley & Sons.

Ishmukhametov, I. & Fakhrullin, R. 2021. Dark-field hyperspectral microscopy for carbon nanotubes bioimaging. *Applied Sciences,* 11(24):12132.

Ivask, A., Juganson, K., Bondarenko, O., Mortimer, M., Aruoja, V., Kasemets, K., Blinova, I., Heinlaan, M., Slaveykova, V. & Kahru, A. 2014. Mechanisms of toxic action of Ag, ZnO and CuO nanoparticles to selected ecotoxicological test organisms and mammalian cells *in vitro*: a comparative review. *Nanotoxicology*, 8:57–71.

Jackson, P., Jacobsen, N.R., Baun, A., Birkedal, R., Kühnel, D., Jensen, K.A., Vogel, U. & Wallin, H. 2013. Bioaccumulation and ecotoxicity of carbon nanotubes. *Chemistry Central Journal*, 7:e.154.

Jeevanandam, J., Barhoum, A., Chan, Y.S., Dufresne, A. & Danquah, M.K. 2018. Review on Nanoparticles and Nanostructured materials: history, sources, Toxicity and Regulations. *Beilstein Journal of Nanotechnology*, 9(1):1050–1074.

Jena, R.P., Sriyanka, S., Dash, R. & Paital, B. 2022. A mini-review on the effects of (carbon) nanoparticles and oxidative stress in animals. *The Open Biomarkers Journal*, 12(1).

Jennings, V., Goodhead, R. & Tyler, C.R. 2015. Ecotoxicology of nanomaterials in aquatic systems. In: Baalousha, M. & Lead, J., eds. *Frontiers of Nanoscience: Characterization of Nanomaterials in Complex Environmental and Biological Media*. Amsterdam: Elsevier. pp. 3–45.

Ji, R., Wang, Z., He, J., Masagounder, K., Xu, W., Mai, K. & Ai, Q. 2021. Effects of DL-methionyl-DL-methionine supplementation on growth performance, immune and antioxidative responses of white leg shrimp (*Litopenaeus vannamei*) fed low fishmeal diet. *Aquaculture Reports*, 21:100785.

Jose, A. & Krishnankutty, R.E. 2018. Applications of nanomaterials in agriculture and food Industry: applications. In: Ahmed, S. & Hussain, C.M., eds. *Green and Sustainable Advanced Materials*. Wiley. pp. 343–375.

Joshi, R., Khandelwal, A., Shrivastava, M. & Singh, S.D. 2020. Characterization of nanomaterials using different techniques. In: Rakshit, A., Ghosh, S., Chakraborty, S., Philip, V. & Datta, A., eds. *Soil Analysis: Recent Trends and Applications*. Springer. pp. 187–198.

Jung, H.S. & Neuman, K.C. 2021. Surface modification of fluorescent nanodiamonds for biological applications. *Nanomaterials*, 11(1):153.

Kalantar-zadeh, K. & Fry, B. 2008. Characterization techniques for nanomaterials. In: *Nanotechnology-Enabled Sensors*. Boston: Springer. pp. 211–281.

Kandru, A. 2020. Nanotechnology: application in biology and medicine. In. Siddhardha, B., Dyavaiah, M. & Kasinathan, K., eds. *Model Organisms to Study Biological Activities and Toxicity of Nanoparticles*. Singapore: Springer. pp. 1–18.

Kaoud, H. & Ahmed, Q. 2013. Copper intoxication in tropical freshwater prawn, *Macrobrachium rosenbergii*. *International Journal of Engineering and Innovative technology*, 3(5):220–226.

Kareem, S. & Mawllod, S. 2020. Size dependent thermodynamic properties of nanoparticles. *International Journal of Thermodynamics*– 23(4):245–250.

Karna, E., Szoka, L., Huynh, T.Y.L. & Palka, J.A 2020. Proline-dependent regulation of collagen metabolism. *Cellular and Molecular Life Sciences*, 77:1911–1918.

Karpeta-Kaczmarek, J., Dziewięcka, M., Augustyniak, M., Rost-Roszkowska, M. & Pawlyta, M. 2016. Oxidative stress and genotoxic effects of diamond nanoparticles. *Environmental Research*, 148:264–272.

Katz, L.M. 2007. Nanotechnology and applications in cosmetics: general overview. In: Morgan, S.E., Havelka, K.O. & Lochhead, R.Y., eds. *Cosmetic Nanotechnology*. American Chemical Society. pp. 193–200.

Keabadile, O.P., Aremu, A.O., Elugoke, S.E. & Fayemi, O.E. 2020. Green and Traditional Synthesis of Copper Oxide Nanoparticles—Comparative Study. *Nanomaterials,* 10(12):2502.

Kent, R.D. & Vikesland, P.J 2016. Dissolution and persistence of copper-based nanomaterials in undersaturated solutions with respect to cupric solid phases. *Environmental Science & Technology*, 50(13):6772–6781.

Khan, R., Inam, M.A., Zam Zam, S., Akram, M., Shin, S. & Yeom, I.T. 2019. Coagulation and dissolution of CuO nanoparticles in the presence of dissolved organic matter under different pH values. *Sustainability*, 11(10):2825.

Khan, S.A. 2019. Metal Nanoparticles toxicity: role of physicochemical aspects. In: Shah, M.R.,

Imran, M. & Ullah, S., eds. *Metal Nanoparticles for Drug Delivery and Diagnostic Applications*. Elsevier. pp. 1–11.

Khoshnood, R., Jaafarzadeh, N., Jamili, S., Farshchi, P. & Taghavi, L. 2016. Nanoparticles ecotoxicity on *Daphnia magna*. *Transylvanian Review of Systematical and Ecological Research*, 18(2):29–38.

Khosravi-Katuli, K., Prato, E., Lofrano, G., Guida, M., Vale, G. & Libralato, G. 2017. Effects of nanoparticles in species of aquaculture interest. *Environmental Science and Pollution Research*, 24(21):17326–17346.

Kim, D. & Hwang, C. 2022. Where Does N-Formylmethionine Come from? What for? Where Is It Going? *Molecules and Cells*, 45(3):109–111.

Kim, D., Lu, N., Ghaffari, R. & Rogers, J.A. 2012. Inorganic semiconductor nanomaterials for flexible and stretchable bio-integrated electronics. *NPG Asia Materials,* 4(4):e.15.

Kim, K.T., Klaine, S.J., Lin, S., Ke, P.C. & Kim, S.D. 2010. Acute toxicity of a mixture of copper and single-walled carbon nanotubes to *Daphnia magna*. *Environmental Toxicology & Chemistry*, 29(1):122–126.

Kim, Y., Samadi, A., Gwag, E.H., Park, J., Kwak, M., Park, J., Lee, T.G. & Kim, Y.J. 2021. Physiological and behavioral effects of SiO_2 nanoparticle ingestion on *Daphnia magna*. *Micromachines*, 12(9):1105.

Kitching, H., Shiers, M.J., Kenyon, A.J. & Parkin, I.P. 2013. Self-assembly of metallic nanoparticles into one dimensional arrays. *Journal of Materials Chemistry A*, 1(24):6985.

Knapen, D., Angrish, M.M., Fortin, M.C., Katsiadaki, I., Leonard, M., Margiotta-Casaluci, L., Munn, S., O'Brien, J.M., Pollesch, N. & Smith, L.C. 2018. Adverse outcome pathway networks I: development and applications. *Environmental Toxicology & Chemistry*, 37(6):1723–1733.

Kovrižnych, J.A., Sotníková, R., Zeljenková, D., Rollerová, E., Szabová, E. & Wimmerová, S. 2013. Acute toxicity of 31 different nanoparticles to zebrafish (*Danio rerio*) tested in adulthood and in early life stages–comparative study. *Interdisciplinary Toxicology,* 6(2):67–73.

Krstić, M., Medarević, Đ., Đuriš, J. and Ibrić, S. 2018. Self-nanoemulsifying drug delivery systems (SNEDDS) and self-microemulsifying drug delivery systems (SMEDDS) as lipid nanocarriers for

improving dissolution rate and bioavailability of poorly soluble drugs. In: Grumezescu, A.M., ed. *Lipid nanocarriers for drug targeting*. Elsevier. pp. 473–508.

Kuehr, S., Kaegi, R., Maletzki, D. & Schlechtriem, C. 2021a. Testing the bioaccumulation potential of manufactured nanomaterials in the freshwater amphipod *Hyalella azteca. Chemosphere*, 263:127961.

Kuehr, S., Kosfeld, V. & Schlechtriem, C. 2021b. Bioaccumulation assessment of nanomaterials using freshwater invertebrate species. *Environmental Sciences Europe,* 33:e.9.

Kumar, S., Stecher, G., Li, M., Knyaz, C. & Tamura, K. 2018. MEGA X: Molecular Evolutionary Genetics Analysis across Computing Platforms. *Molecular Biology and Evolution*, 35(6):1547–1549.

Ladchumananandasivam, R., da Rocha, B.G., Belarmino, D.D. & Galv, A.O. 2012. The use of exoskeletons of shrimp (*Litopenaeus vanammei)* and crab (*Ucides cordatus*) for the extraction of chitosan and production of nanomembrane. *Materials Sciences and Applications,* 3(7):21160.

Lai, H., Stenzel, M.H. & Xiao, P. 2019. Surface engineering and applications of nanodiamonds in cancer treatment and imaging. *International Materials Reviews*, 65(4):189–225.

Langford, A., Bruchsaler, M. & Gupta, M. 2022. Suspension properties and characterization of aluminum-adjuvanted vaccines. In: Kolhe, P. & Ohtake, S., eds. *Practical Aspects of Vaccine Development*. London: Elsevier. pp. 225–266.

Lari, E., Steinkey, D., Steinkey, R.J. & Pyle, G.G. 2018. *Daphnia magna* increase feeding activity in the presence of four amino acids. *Journal of Plankton Research*, 40(5):537–543.

Lauer, M.M., de Oliveira, C.B., Yano, N.L.I. & Bianchini, A. 2012. Copper effects on key metabolic enzymes and mitochondrial membrane potential in gills of the estuarine crab *Neohelice granulata* at different salinities. *Comparative Biochemistry and Physiology Part C: Toxicology & Pharmacology*, 156(3–4):140–147.

Lažetić, V. & Fay, D.S. 2017. Molting in *C. elegans. Worm*, 6(1):1330246.

Lee, J.W., Won, E.J., Raisuddin, S. & Lee, J.S. 2015. Significance of adverse outcome pathways in biomarker-based environmental risk assessment in aquatic organisms. *Journal of Environmental Sciences*, 35:115–127.

Lemos, D. & Weissman, D. 2021. Moulting in the grow-out of farmed shrimp: a review. *Reviews in Aquaculture*, 13(1):5–17.

Lespes, G., Faucher, S. & Slaveykova, V.I. 2020. Natural Nanoparticles, Anthropogenic Nanoparticles, Where Is the Frontier? *Frontiers in Environmental Science*, 8:71.

Leuven, R.S.E.W., van den Brink, F.W.B. & van der Velde, G. 2008. Biometrics and Fecundity of the Freshwater Shrimp, *Caridina nilotica* (P. Roux, 1833) (Decapoda, Caridea, Atyidae) in the Lower Nile River (Egypt). *Crustaceana,* 81(2):227–239.

Li, B., Chen, K., Liu, F., Zhang, J., Chen, X., Chen, T., Chen, Q., Yao, Y., Hu, W. & Wang, L. 2021. Developmental angiogenesis requires the mitochondrial phenylalanyl-trna synthetase. *Frontiers in Cardiovascular Medicine*, 8:724846.

Li, J., Li, W., Zhang, X. & He, P. 2018a. Physiological and behavioural responses of different modes of locomotion in the whiteleg shrimp *Litopenaeus vannamei* (Boone, 1931)(Caridea: Penaeidae). *Journal of Crustacean Biology*, 38(1):79–90.

Li, Y., Wang, J., Zhao, F., Bai, B., Nie, G., Nel, A.E. & Zhao, Y. 2018b. Nanomaterial libraries and model organisms for rapid high-content analysis of nanosafety. *National Science Review*, 5(3):365–388.

Lim, J., Yeap, S.P., Che, H.X. & Low, S.C. 2013. Characterization of magnetic nanoparticle by dynamic light scattering. *Nanoscale Research Letters*, 8(1):e.381.

Liu, X., Chen, G. & Su, C. 2011. Effects of material properties on sedimentation and aggregation of titanium dioxide nanoparticles of anatase and rutile in aqueous phase*. Journal of Colloid and Interface Science*, 363(1):84–91.

Liu, Y., Zhu, S., Gu, Z., Chen, C. & Zhao, Y. 2022. Toxicity of manufactured nanomaterials. *Particuology*, 69:31–48.

Liu, Z., Li, Y., Sepúlveda, M.S., Jiang, Q., Jiao, Y., Chen, Q., Huang, Y., Tian, J. & Zhao, Y. 2021. Development of an adverse outcome pathway for nanoplastic toxicity in *Daphnia pulex* using proteomics. *Science of the Total Environment*, 766:144249.

Lovern, S.B., Strickler, J.R. & Klaper, R. 2007. Behavioural and physiological changes in *Daphnia magna* when exposed to nanoparticle suspensions (titanium dioxide, nano-C60, and C60HxC70Hx). *Environmental Science & Technology*, 41(12):4465–4470.

Lu, A.H., Salabas, E. L. & Schüth, F. 2007. Magnetic Nanoparticles: Synthesis, Protection, Functionalization, and Application. *Angewandte Chemie International Edition*, 46(8):1222–1244.

Ma, W., Chen, K., Li, Y., Hao, N., Wang, X. & Ouyang, P. 2017. Advances in cadaverine bacterial production and its applications. *Engineering*, 3(3):308–317.

Ma, Y.B., Lu, C.J., Junaid, M., Jia, P.P., Yang, L., Zhang, J.H. & Pei, D.S. 2018. Potential adverse outcome pathway (AOP) of silver nanoparticles mediated reproductive toxicity in zebrafish. *Chemosphere*, 207:320–328.

Magro, M., De Liguoro, M., Franzago, E., Baratella, D. & Vianello, F. 2018. The surface reactivity of iron oxide nanoparticles as a potential hazard for aquatic environments: A study on *Daphnia magna* adults and embryos. *Scientific reports*, 8(1):13017.

Malakar, A., Kanel, S.R., Ray, C., Snow, D.D. & Nadagouda, M.N. 2021. Nanomaterials in the environment, human exposure pathway, and health effects: A review. *Science of The Total Environment*, 759:143470.

Malatesta, M. 2021. Transmission electron microscopy as a powerful tool to investigate the interaction of nanoparticles with subcellular structures. *International Journal of Molecular Sciences*, 22(23):12789.

Malhotra, N., Ger, T.R., Uapipatanakul, B., Huang, J.C., Chen, K.H.C. & Hsiao, C.D. 2020. Review of copper and copper nanoparticle toxicity in fish. *Nanomaterials*, 10(6):1126.

Mänd, M. & Karise, R. 2015. Recent insights into sublethal effects of pesticides on insect respiratory physiology. *Open Access Insect Physiology*, 5:31–39.

Mansano, A.S., Souza, J.P., Cancino-Bernardi, J., Venturini, F.P., Marangoni, V.S. & Zucolotto, V. 2018. Toxicity of copper oxide nanoparticles to Neotropical species *Ceriodaphnia silvestrii* and *Hyphessobrycon eques*. *Environmental Pollution*, 243:723–733.

Mansouri, B., Rahmani, R., Azadi, N.A., Davari, B., Johari, S.A. & Sobhani, P. 2015. Effect of waterborne copper oxide nanoparticles and copper ions on guppy (*Poecilia reticulata*):

Bioaccumulation and histopathology. *Journal of Advances in Environmental Health Research*, 3(4):215–223.

Marciniak, L., Nowak, M., Trojanowska, A., Tylkowski, B. & Jastrzab, R. 2020. The effect of pH on the size of silver nanoparticles obtained in the reduction reaction with citric and malic acids. *Materials*, 13(23):5444.

Matsui, I. 2005. Nanoparticles for electronic device applications: a brief review. *Journal of Chemical Engineering of Japan*, 38(8):535–546.

McLaughlin, P.A. 1983. Internal anatomy. In: Mantel, L.., ed. *Internal Anatomy and Physiological Regulation*. Elsevier. pp. 1–53.

McMahon, B. & Wilkens, J. 1983. Ventilation, perfusion and oxygen uptake. *Internal Anatomy and Physiological Regulation*, 5:289–372.

Mendonça, E., Diniz, M., Silva, L., Peres, I., Castro, L., Correia, J.B. & Picado, A. 2011. Effects of diamond nanoparticle exposure on the internal structure and reproduction of *Daphnia magna*. *Journal of hazardous materials*, 186(1):265–271.

Mensah, P., Muller, W. & Palmer, C. 2011. Acute toxicity of Roundup® herbicide to three life stages of the freshwater shrimp *Caridina nilotica* (Decapoda: Atyidae). *Physics and Chemistry of the Earth*, 36(14–15):905–909.

Mensah, P., Muller, W. and Palmer, C. 2012a. Using growth measures in the freshwater shrimp *Caridina nilotica* as biomarkers of Roundup® pollution of South African freshwater systems. *Physics and Chemistry of the Earth, Parts A/B/C*, 50:262–68.

Mensah, P., Palmer, C. & Muller, W. 2012b.I Lipid peroxidation in the freshwater shrimp *Caridina nilotica* as a biomarker of Roundup® herbicide pollution of freshwater systems in South Africa. *Water Science and Technology*, 65(9):1660–1666.

Miao, L., Wang, C., Hou, J., Wang, P., Ao, Y., Li, Y., Lv, B., Yang, Y., You, G. & Xu, Y. 2015. Enhanced stability and dissolution of CuO nanoparticles by extracellular polymeric substances in aqueous environment. *Journal of Nanoparticle Research*, 17:e.404.

Min, S.H., Lee, T.H., Lee, S., Song, J.H., Lee, G.Y., Zontar, D., Brecher, C. & Ahn, S.H. 2019. Simulation of electrical conductivity for nanoparticles and nanotubes composite sensor according

to geometrical properties of nanomaterials. *Composites Part B: Engineering*, 174:107003.

Mirimin, L., Kitchin, N., Impson, D.N., Clark, P.F., Richard, J., Daniels, S.R. & Roodt-Wilding, R. 2015. Genetic and Morphological Characterization of Freshwater Shrimps (*Caridina africana* Kingsley, 1882) Reveals the Presence of Alien Shrimps in the Cape Floristic Region, South Africa. *Journal of Heredity*, 106(6):711 –718.

Mochalin, V.N., Shenderova, O., Ho, D. & Gogotsi, Y. 2012. The properties and applications of nanodiamonds. *Nature Nanotechnology*, 7(1):11–23.

Mohan, N., Chen, C.S., Hsieh, H.H., Wu, Y.C. & Chang, H.C. 2010. *In vivo* imaging and toxicity assessments of fluorescent nanodiamonds in *Caenorhabditis elegans*. *Nano Letters*. 10(9):3692–3699.

Moloi, M.S., Lehutso, R.F., Erasmus, M., Oberholster, P.J. & Thwala, M. 2021. Aquatic environment exposure and toxicity of engineered nanomaterials released from nano-enabled products: current status and data needs. *Nanomaterials*, 11(11):2868.

Muller, E.B., Lin, S. & Nisbet, R.M. 2015. Quantitative adverse outcome pathway analysis of hatching in zebrafish with CuO nanoparticles. *Environmental Science & Technology*, 49(19):11817–11824.

Muller, W., Slaughter, A., Ketse, N., Davies-Coleman, H., De Kock, E. & Palmer, C. 2011. Development of chronic toxicity test methods for selected indigenous riverine macroinvertebrates: WRC Report No. KV276/11. Pretoria: Water Research Commission.

Muneer, R., Hashmet, M.R. & Pourafshary, P. 2020. Fine migration control in sandstones: surface force analysis and application of DLVO Theory. *American Chemical Society Omega*, 5(49):31624–31639.

Muralisankar, T., Bhavan, P.S., Radhakrishnan, S., Seenivasan, C. & Srinivasan, V. 2016. The effect of copper nanoparticles supplementation on freshwater prawn *Macrobrachium rosenbergii* post larvae. *Journal of Trace Elements in Medicine and Biology*, 34:39–49.

Murugadoss, S., Vrcek, I.V., Pem, B., Jagiello, K., Judzinska, B., Sosnowska, A., Martens, M., Willighagen, E.L., Puzyn, T. & Dusinska, M. 2021. A strategy towards the generation of testable adverse outcome pathways for nanomaterials. *ALTEX-Alternatives to Animal Experimentation*, 38(4):580–594.

Mushtaq, W., Shakeel, A., Fazili, M.A., Chakrabartty, I. & Sevindik, M. 2020. Pros and Cons of Nanotechnology. In: Hakeem, K. & Pirzadah, T., eds. *Nanobiotechnology in Agriculture*. Cham: Springer. pp. 207–222.

Mwaanga, P. 2018. Risks, Uncertainties, and Ethics of Nanotechnology in Agriculture. In: Çelik, Ö., ed. *New Visions in Plant Science*. IntechOpen. pp. 143–159.

Naeemi, A.S., Elmi, F., Vaezi, G. & Ghorbankhah, M. 2020. Copper oxide nanoparticles induce oxidative stress mediated apoptosis in carp (*Cyprinus carpio*) larva. *Gene Reports*, 19:100676.

Nakatsuji, T., Lee, C.Y. & Watson, R.D. 2009. Crustacean moult-inhibiting hormone: structure, function, and cellular mode of action. *Comparative Biochemistry and Physiology Part A: Molecular and Integrative Physiology*, 152(2):139–148.

Nasser, F., Davis, A., Valsami-Jones, E. & Lynch, I. 2016. Shape and charge of gold nanomaterials influence survivorship, oxidative stress and moulting of *Daphnia magna*. *Nanomaterials*, 6(12):222.

Naz, S., Gul, A. & Zia, M. 2020. Toxicity of copper oxide nanoparticles: A review study. *The Institute of Engineering and Technology Nanobiotechnology*, 14(1):1–13.

Nei, M. & Kumar, S. 2000. Chapter 8: Phylogenetic inference: maximum likelihood methods. *Molecular evolution and phylogenetics*. Oxford University Press. pp. 147 – 164.

Neupane, G.P., Ma, W., Yildirim, T., Tang, Y., Zhang, L. & Lu, Y. 2019. 2D organic semiconductors, the future of green nanotechnology. *Nano Materials Science*, 1(4):246–259.

Nikalje, A.P. 2015. Nanotechnology and its applications in medicine. *Medicinal Chemistry*, 5(2):81–89.

Niriella, D. & Carnahan, R. 2006. Comparison study of zeta potential values of bentonite in salt solutions. *Journal of Dispersion Science and Technology*, 27(1):123–131.

Niroumand, H., Zain, M.F.M. & Jamil, M. 2013. The role of nanotechnology in architecture and built environment. *Procedia - Social and Behavioral Sciences*, 89:10–15.

Noss, C., Dabrunz, A., Rosenfeldt, R.R., Lorke, A. & Schulz, R. 2013. Three-dimensional analysis of the swimming behavior of *Daphnia magna* exposed to nanosized titanium dioxide. *Public Library of Science One*, 8(11):80960.

Nowinski, S.M., Van Vranken, J.G., Dove, K.K. & Riutter, J. 2018. Impact of mitochondrial fatty acid synthesis on mitochondrial biogenesis. *Current Biology*, 28(20):1212–1219.

Odzak, N., Kistler, D., Behra, R. & Sigg, L. 2014. Dissolution of metal and metal oxide nanoparticles in aqueous media. *Environmental Pollution*, 191:132–138.

OECD, 2004. OECD Guideline for the Testing of Chemicals. Guideline 202: *Daphnia magna* Acute Immbolisation Test: OECD Publishing. https://www.oecd-ilibrary.org/environment/test-no-202-daphnia-sp-acute-immobilisation-test_9789264069947-en.

Ojha, K.K., Mishra, S. & Singh, V.J. 2022. Computational molecular phylogeny: concepts and applications. In: Singh, D.B. & Pathak, R.K., eds. *Bioinformatics: Methods and Applications*. Academic Press. pp. 67–89.

Ovais, M., Raza, A., Naz, S., Islam, N.U., Khalil, A.T., Ali, S., Khan, M.A. & Shinwari, Z.K . 2017. Current state and prospects of the phytosynthesized colloidal gold nanoparticles and their applications in cancer theranostics. *Applied Microbiology and Biotechnology*, 101(9):3551–3565.

Ovissipour, M., Rasco, B. & Sablani, S.S. 2013. Impact of Engineered Nanoparticles on Aquatic Organisms. *Journal of Fisheries and Livestock Production*, 1(3):1000e105.

Pacheco-Torgal, F. & Jalali, S. 2011. Nanotechnology: Advantages and drawbacks in the field of construction and building materials. *Construction and Building Materials*, 25(2):582–590.

Park, S.J. 2020. Protein–Nanoparticle Interaction: Corona Formation & Conformational Changes in Proteins on Nanoparticles. *International Journal of Nanomedicine*, 15:5783–5802.

Parra-Flores, A., Ponce-Palafox, J., Spanopoulos-Hernández, M. & Martinez-Cardenas, L. 2019 Feeding behavior and ingestion rate of juvenile shrimp of the genus Penaeus (Crustacea: Decapoda). *Open Access Journal of Science,* 3(3):111–113.

Parsai, T. & Kumar, A. 2019. Understanding effect of solution chemistry on heteroaggregation of zinc oxide and copper oxide nanoparticles. *Chemosphere*, 235:457–469.

Passantino, A., Elwood, R.W. & Coluccio, P. 2021. Why Protect Decapod Crustaceans Used as Models in Biomedical Research and in Ecotoxicology? Ethical and Legislative Considerations. *Animals*, 11(1):73.

Patel, K.D., Singh, R.K. & Kim, H.W. 2019. Carbon-based nanomaterials as an emerging platform for theranostics. *Materials Horizons*, 6(3):434–469.

Patra, J.K. & Baek, K.H. 2015. Green nanobiotechnology: factors affecting synthesis and characterization techniques. *Journal of Nanomaterials*, 2014:417305.

Patra, J.K., Das, G., Fraceto, L.F., Campos, E.V.R., Rodriguez-Torres, M.D.P., Acosta-Torres, L.S., Diaz-Torres, L.A., Grillo, R., Swamy, M.K., Sharma, S. & Habtemariam. 2018. Nano based drug delivery systems: recent developments and future prospects. *Journal of Nanobiotechnology*, 16:e.71.

Phlippen, M.K., Webster, S.G., Chung, J.S. & Dircksen, H. 2000. Ecdysis of decapod crustaceans is associated with a dramatic release of crustacean cardioactive peptide into the haemolymph. *Journal of Experimental Biology*, 203(3):521–536.

Poh, T.Y., Ali, N.A.T.B.M., Mac Aogáin, M., Kathawala, M.H., Setyawati, M.I., Ng, K.W. & Chotirmall, S.H. 2018. Inhaled nanomaterials and the respiratory microbiome: Clinical, immunological and toxicological perspectives. *Particle and Fibre Toxicology*, 15:e.46.

Pooja, Rana, M. & Chowdhury, P. 2021. Modern applications of quantum dots: Environmentally hazardous metal ion sensing and medical imaging. In: Hussain, C.M. & Kailasa, S.K., eds. *Handbook of Nanomaterials for Sensing Applications: Micro and Nano Technologies*. London: Elsevier. pp. 465–503.

Pradhan, A., Seena, S., Pascoal, C. & Cássio, F. 2012. Copper oxide nanoparticles can induce toxicity to the freshwater shredder *Allogamus ligonifer*. *Chemosphere*, 89(9):1142–1150.

Prasad, R., Bhattacharyya, A. & Nguyen, Q.D. 2017. Nanotechnology in Sustainable Agriculture: Recent Developments, Challenges, and Perspectives. *Frontiers in Microbiology*, 8:1014.

Qin, J.X., Yang, X.G., Lv, C.F., Li, Y.Z., Liu, K.K., Zang, J.H., Yang, X., Dong, L. & Shan, C.X. 2021. Nanodiamonds: Synthesis, properties, and applications in nanomedicine. *Materials and Design*, 210:110091.

Rahdar, A., Amini, N., Askari, F., Susan, M. & Hasan, A.B. 2019. Dynamic light scattering: A useful technique to characterize nanoparticles. *Journal of Nanoanalysis*, 6(2):80–89.

Raj, S., Sumod, U., Jose, S. & Sabitha, M. 2012. Nanotechnology in cosmetics: Opportunities and challenges. *Journal of Pharmacy and Bioallied Sciences*, 4(3):186–193.

Ramadan, A., Abol-Noor, K., Elshiekh, A., Aboghalia, A. & El-Shafiey, S. 2020. Responses of desert locust *Schistocerca gregaria* (Orthoptera: Acrididae) to treatment with chemically synthesized zinc and copper oxides nanoparticles. *Egyptian Journal of Plant Protection Research Institute*, 3(1):339–345.

Ramskov, T., Selck, H., Banta, G., Misra, S.K., Berhanu, D., Valsami-Jones, E. & Forbes, V.E. 2014. Bioaccumulation and effects of different-shaped copper oxide nanoparticles in the deposit-feeding snail *Potamopyrgus antipodarum*. *Environmental Toxicology & Chemistry*, 33(9):1976–1987.

Raval, N., Maheshwari, R., Kalyane, D., Youngren-Ortiz, S.R., Chougule, M.B. & Tekade, R.K. 2019. Importance of physicochemical characterization of nanoparticles in pharmaceutical product development. In: Tekade, R.K., ed. *Basic Fundamentals of Drug Delivery: Advances in Pharmaceutical Product Development and Research*. Academic Press. pp. 369–400.

Rawat, R.S. 2015. Dense plasma focus - from alternative fusion source to versatile high energy density plasma source for plasma nanotechnology. *Conference proceedings* (volume 591). 15th Latin American Workshop on Plasma Phsyics (LAWPP 2014) and 21st IAEA TM on Research Using Small Fusion Devices (RUSFD), San José, Costa Rica.

Renzi, M. & Guerranti, C. 2015. Ecotoxicity of nanoparticles in aquatic environments: A review Based on multivariate statistics of meta-data. *Journal of Environmental Analytical Chemistry*, 2(4):e.1000149.

Ribas, G.S., Vargas, C.R. & Wajner, M. 2014. L-carnitine supplementation as a potential antioxidant therapy for inherited neurometabolic disorders. *Gene*, 533(2):469–476.

Roth, G.A., Tahiliani, S., Neu-Baker, N.M. & Brenner, S.A. 2015. Hyperspectral microscopy as an analytical tool for nanomaterials. *Wiley Interdisciplinary Reviews: Nanomedicine and Nanobiotechnology*, 7(4):565–579.

Rotini, A., Gallo, A., Parlapiano, I., Berducci, M., Boni, R., Tosti, E., Prato, E., Maggi, C., Cicero, A. & Migliore, L. 2018. Insights into the CuO nanoparticle ecotoxicity with suitable marine model species. *Ecotoxicology & Environmental Safety*, 147:852–860.

Russom, C.L., LaLone, C.A., Villeneuve, D.L. & Ankley, G.T. 2014. Development of an adverse outcome pathway for acetylcholinesterase inhibition leading to acute mortality. *Environmental Toxicology & Chemistry*, 33(10):2157–2169.

Sabzehmeidani, M.M., Mahnaee, S., Ghaedi, M., Heidari, H. & Roy, V.A.L. 2021. Carbon based materials: a review of adsorbents for inorganic and organic compounds. *Materials Advances*, 2(2):598–627.

Sadik, O.A. 2013. Anthropogenic nanoparticles in the environment. *Environmental Science: Processes & Impacts*, 15(1):19–20.

Sahoo, S.K. 2022. Sensing and biosensing with optically active nanomaterials: a note. In: Sahoo, S.K., ed. *Sensing and Biosensing with Optically Active Nanomaterials: Micro and Nano Technologies*. London: Elsevier. pp. 1–7.

Salgin, S., Salgin, U. & Bahadir, S. 2012. Zeta potentials and isoelectric points of biomolecules: the effects of ion types and ionic strengths. *International Journal of Electrochemical Science*, 7(12):12404–12414.

Sanhueza, F., Valdebenito, E., Udayabhaskar, R., Salvo, C., Sahlevani, S.F., Elgueta, E., Parra, M., Bello, H. & Mangalaraja, R.V. 2019. Effect of ultrasonic sonication time on the structural, optical and antibacterial properties of ceria nanostructures. *Materials Research Express,* 6(9):095055.

Saptarshi, S.R., Duschl, A. & Lopata, A.L. 2013. Interaction of nanoparticles with proteins: relation to bio-reactivity of the nanoparticle. *Journal of Nanobiotechnology*, 11(1):26.

Savage, D.T., Hilt, J.Z. & Dziubla, T.D. 2018. *In vitro* methods for assessing nanoparticle toxicity. *Methods in Molecular Biology,* 1894:1–29.

Schnackenberg, L.K., Sun, J. & Beger, R.D. 2012. Metabolomics techniques in nanotoxicology studies. In: Reinecke, J. *Nanotoxicity: Methods and Protocols.* Springer. pp. 141–156.

Shang, Y., Hasan, Md.K., Ahammed, G.J., Li, M., Yin, H. & Zhou, J. 2019. Applications of nanotechnology in plant growth and crop protection: A review. *Molecules*, 24(14):2558.

Sharifi, S., Behzadi, S., Laurent, S., Laird Forrest, M., Stroeve, P. & Mahmoudi, M. 2012. Toxicity of nanomaterials. *Chemical Society Reviews*, 41(6):2323–2343.

Shuhaimi-Othman, M., Yakub, N., Ramle, N.A. & Abas, A. 2011. Toxicity of metals to a freshwater ostracod: Stenocypris major. *Journal of Toxicology*, 2011:136104.

Siddique, S. & Chow, J.C.L. 2020. Application of Nanomaterials in Biomedical Imaging and Cancer Therapy. *Nanomaterials*, 10(9):1700.

Sim, S. & Wong, N. 2021. Nanotechnology and its use in imaging and drug delivery (Review). *Biomedical Reports*, 14(5):42.

Singh, D.S., Alkins-Koo, M., Rostant, L.V. & Mohammed, A. 2020b. The effects of acute oxygen changes on heart rate in the freshwater crab *Poppiana dentata* (Randall, 1840). *Latin American Journal of Aquatic Research*, 48(3):480–487.

Singh, V., Yadav, P. & Mishra, V. 2020a. Chapter 3: Recent advances on classification, properties, synthesis, and characterization of nanomaterials. In: Srivastava, N., Srivastava, M., Mishra, P.K. & Gupta, V.K., eds. *Green Synthesis of Nanomaterials for Bioenergy Applications*. India: Wiley & Sons. pp. 83–97.

Siregar, P., Suryanto, M.E., Chen, K.H.., Huang, J.., Chen, H.., Kurnia, K.A., Santoso, F., Hussain, A., Ngoc Hieu, B.T. & Saputra, F. 2021. Exploiting the freshwater shrimp *Neocaridina denticulata* as aquatic invertebrate model to evaluate nontargeted pesticide induced toxicity by investigating physiologic and biochemical parameters. *Antioxidants*, 10(3):391.

Sohal, I.S., Cho, Y.K., O'Fallon, K.S., Gaines, P., Demokritou, P. & Bello, D. 2018. Dissolution behavior and biodurability of ingested engineered nanomaterials in the gastrointestinal Environment. *American Chemical Society Nano,* 12(8):8115–8128.

Soltis, P.S. & Soltis, D.E. 2003. Applying the bootstrap in phylogeny reconstruction. *Statistical Science*, 18(2):256–267.

Song, Y., Feng, A., Liu, Z. & Li, D. 2020. Zeta potentials of PDMS surfaces modified with poly (ethylene glycol) by physisorption. *Electrophoresis*, 41(10–11):761–768.

Song, Y., Villeneuve, D.L., Toyota, K., Iguchi, T. & Tollefsen, K.E. 2017. Ecdysone receptor agonism leading to lethal molting disruption in Arthropods: Review and adverse outcome pathway development. *Environmental Science & Technology*, 51(8):4142–4157.

SoRelle, E.D., Liba, O., Campbell, J.L., Dalal, R., Zavaleta, C.L. & de la Zerda, A. 2016. A hyperspectral method to assay the microphysiological fates of nanomaterials in histological samples. *eLife*, 5:16352.

Sørensen, S.N., Lützhøft, H.C.H., Rasmussen, R. & Baun, A. 2016. Acute and chronic effects from pulse exposure of *D. magna* to silver and copper oxide nanoparticles. *Aquatic Toxicology*, 180:209–217.

Sousa, V.S. & Teixeira, M.R. 2013. Aggregation kinetics and surface charge of CuO nanoparticles: the influence of pH, ionic strength and humic acids. *Environmental Chemistry*, 10(4):313–322.

Spicer, J.I. 1995. Effect of water-borne copper on respiratory and cardiac function during the early ontogeny of the brine shrimp, *Artemia franciscana* Kellogg 1908 (Branchiopoda: Anostraca). *Journal of Comparative Physiology B,* 165:490–495.

Sreya, A. & Chitra, K.C. 2021. An overview of the applications and environmental risk assessment of nanomaterials in the aquatic organisms. *Journal of Biology and Nature*, 13(1):1–30.

Stanley, J.K., Laird, J.G., Kennedy, A.J. & Steevens, J.A. 2016. Sublethal effects of multiwalled carbon nanotube exposure in the invertebrate *Daphnia magna*. *Environmental Toxicology & Chemistry*, 35(1):200–204.

Stepan, T., Tété, L., Laundry-Mottiar, L., Romanovskaia, E., Hedberg, Y.S., Danninger, H. & Auinger, M. 2022. Effect of nano-particle size on the near-surface pH-distribution in aqueous and carbonate buffered solutions. *Electrochimica Acta*, 409:139923.

Stincone, A., Prigione, A., Cramer, T., Wamelink, M.M., Campbell, K., Cheung, E., Olin-Sandoval, V., Grüning, N.M., Krüger, A. & Tauqeer Alam, M. 2015. The return of metabolism: Biochemistry and physiology of the pentose phosphate pathway. *Biological Reviews*, 90(3):927–963.

Strain, J. & Lynch, S. 1990. Excess dietary methionine decreases indices of copper status in the rat. *Annals of Nutrition and Metabolism*, 34(2):93–97.

Sucahyo, D., van Straalen, N.M., Krave, A. & van Gestel, C.A.M. 2008. Acute toxicity of pesticides to the tropical freshwater shrimp *Caridina laevis*. *Ecotoxicology & Environmental Safety*. 69(3):421–427.

Sun, C., Lee, J. & Zhang, M. 2008. Magnetic nanoparticles in MR imaging and drug delivery. *Advanced Drug Delivery Reviews*, 60(11):1252–1265.

Sun, H., Zhang, A.H., Song, Q., Fang, H., Liu, X.Y., Su, J., Yang, L., Yu, M.D. & Wang, X.J. 2018. Functional metabolomics discover pentose and glucuronate interconversion pathways as promising targets for Yang Huang syndrome treatment with Yinchenhao Tang. *RSC advances*, 8(64):36831–36839.

Sun, Y., Zhang, G., He, Z., Wang, Y., Cui, J. & Li, Y. 2016. Effects of copper oxide nanoparticles on developing zebrafish embryos and larvae. *International Journal of Nanomedicine*, 11:905.

Suresh, S. 2013. Semiconductor nanomaterials, methods and applications: A review. *Nanoscience and Nanotechnology*, 3(3):62–74.

Sweet, M.J., Chessher, A. & Singleton, I. 2012. Review: Metal-based nanoparticles; size, function, and areas for advancement in applied microbiology. *Advances in Applied Microbiology Volume 80,* 80:113–142.

Takahashi, K. 2022. Changes in the anxiety-like and fearful behaviour of shrimp following daily threatening experiences. *Animal Cognition*, 25(2):319–327.

Tan, Z., Zhao, W., Yin, Y., Xu, M., Pan, W., Liu, Y., Zhang, Q., Gale, B.K., Rui, Y. & Liu, J. 2023. Insight into the formation and biological effects of natural organic matter corona on silver nanoparticles in water environment using biased cyclical electrical field-flow fractionation. *Water Research*, 228:119355.

Thit, A., Huggins, K., Selck, H. & Baun, A. 2016. Acute toxicity of copper oxide nanoparticles to *Daphnia magna* under different test conditions. *Toxicological and Environmental Chemistry*, 99(4):665–679.

Thit, A., Skjolding, L.M., Selck, H. & Sturve, J. 2017. Effects of copper oxide nanoparticles and copper ions to zebrafish (*Danio rerio*) cells, embryos and fry. *Toxicology in vitro*, 45:89–100.

Tollefsen, K.E., Scholz, S., Cronin, M.T., Edwards, S.W., de Knecht, J., Crofton, K., Garcia-Reyero, N., Hartung, T., Worth, A. & Patlewicz, G. 2014. Applying adverse outcome pathways (AOPs) to support integrated approaches to testing and assessment (IATA). *Regulatory Toxicology & Pharmacology*, 70(3):629–640.

Truter, E. 1994. Methods of estimating the Chronic Toxicity of a chemical or water sample to the Cladoceran *Daphnia pulex*, Department of Water Affairs and Forestry, Department of Water Affairs and Forestry, Pretoria.

Uddin, M.D.N., Desai, F. & Asmatulu, E. 2020. Engineered nanomaterials in the environment: bioaccumulation, biomagnification and biotransformation. *Environmental Chemistry Letters*, 18(4):1073–1083.

Untersteiner, H., Kahapka, J. & Kaiser, H. 2003. Behavioural response of the Cladoceran *Daphnia magna* Straus to sublethal Copper stress validation by image analysis. *Aquatic Toxicology*, 65(4):435–442.

Utembe, W., Potgieter, K., Stefaniak, A.B. & Gulumian, M. 2015. Dissolution and biodurability: Important parameters needed for risk assessment of nanomaterials. *Particle and Fibre Toxicology*, 12(11).

Vale, G., Mehennaoui, K., Cambier, S., Libralato, G., Jomini, S. & Domingos, R.F. 2016. Manufactured nanoparticles in the aquatic environment-biochemical responses on freshwater organisms: a critical overview. *Aquatic Toxicology*, 170:162–174.

van der Laan, K., Hasani, M., Zheng, T. & Schirhagl, R. 2018. Nanodiamonds for *in vivo* applications. *Small*, 14(19):1703838.

van Rensburg, G.J., Bervoets, L., Smit, N.J., Wepener, V. & Van Vuren, J. 2020. Biomarker responses in the freshwater shrimp Caridina nilotica as indicators of persistent pollutant exposure. *Bulletin of Environmental Contamination and Toxicology*, 104(2):193–199.

van Rensburg, G.J., Wepener, V., Horn, S. & Greenfield, R. 2022. Oxidative stress in the freshwater shrimp Caridina africana following exposure to atrazine. *Bulletin of Environmental Contamination and Toxicology*, 109(3):443–449.

Villeneuve, D.L., Crump, D., Garcia-Reyero, N., Hecker, M., Hutchinson, T.H., LaLone, C.A., Landesmann, B., Lettieri, T., Munn, S. & Nepelska, M. 2014. Adverse outcome pathway (AOP) development I: strategies and principles. *Toxicological Sciences*, 142(2):312–320.

Vinken, M. 2013. The adverse outcome pathway concept: a pragmatic tool in toxicology. *Toxicology*, 312:158–165.

Vitiello, M.S., Viti, L., Coquillat, D., Knap, W., Ercolani, D. & Sorba, L. 2015. One dimensional semiconductor nanostructures: An effective *active*-material for terahertz detection. *APL Materials*, 3(2):026104.

Walters, C., Pool, E. & Somerset, V 2016. Chapter 2: Nanotoxicity in aquatic invertebrates. Invertebrates. In. Larramendy, M.L. & Soloneski, S., eds. *Experimental Models in Toxicity Screening.* 1st ed. Zagreb, Croatia: IntechOpen. pp.13–34.

Wang, H., Zhao, X., Han, X., Tang, Z., Liu, S., Guo, W., Deng, C., Guo, Q., Wang, H. & Wu, F. 2017. Effects of monovalent and divalent metal cations on the aggregation and suspension of Fe_3O_4 magnetic nanoparticles in aqueous solution. *Science of the Total Environment*, 586:817–826.

Wang, J., Nabi, M.M., Erfani, M., Goharian, E. & Baalousha, M. 2022a. Identification and quantification of anthropogenic nanomaterials in urban rain and runoff using single particle-inductively coupled plasma-time of flight-mass spectrometry. *Environmental Science: Nano*, 9(2):714–729.

Wang, L., Huang, X., Sun, W., Too, H.Z., Laserna, A.K.C. & Li, S.F.Y. 2020c. A global metabolomic insight into the oxidative stress and membrane damage of copper oxide nanoparticles and microparticles on microalga *Chlorella vulgaris*. *Environmental Pollution*, 258:113647.

Wang, T. & Liu, W. 2022b Emerging investigator series: metal nanoparticles in freshwater: transformation, bioavailability and effects on invertebrates. *Environmental Science: Nano*, 9(7):2237–2263.

Wang, W., Yang, Y., Yang, L., Luan, T. & Lin, L. 2021a. Effects of undissociated SiO2 and TiO2 nano-particles on molting of *Daphnia pulex*: Comparing with dissociated ZnO nano particles. *Ecotoxicology & Environmental Safety*, 222:112491.

Wang, X., Liu, L., Zheng, H., Wang, M., Fu, Y., Luo, X., Li, F. & Wang, Z. 2020b. Polystyrene microplastics impaired the feeding and swimming behaviour of mysid shrimp *Neomysis japonica*. *Marine Pollution Bulletin*, 150:110660.

Wang, X., Qin, Y., Li, X., Yan, B. & Martyniuk, C.J. 2021b. Comprehensive interrogation of metabolic and bioenergetic responses of early-staged zebrafish (*Danio Rerio*) to a commercial copper hydroxide nanopesticide. *Environmental Science & Technology*, 55(19):13033–13044.

Wang, Z., Hu, T., Liang, R. & Wei, M. 2020a. Application of Zero-Dimensional nanomaterials in biosensing. *Frontiers in Chemistry*, 8:320.

Wei, K. & Yang, J. 2015. Oxidative damage induced by copper and beta-cypermethrin in gill of the freshwater crayfish *Procambarus clarkii*. *Ecotoxicology & Environmental Safety*, 113:446–453.

Wei, K. & Yang, J. 2016. Copper-induced oxidative damage to the prophenoloxidase-activating system in the freshwater crayfish *Procambarus clarkii*. *Fish and Shellfish Immunology*, 52:221–229.

Williams, O.A., Hees, J., Dieker, C., Jager, W., Kirste, L. & Nebel, C.E. 2010. Size-dependent reactivity of diamond nanoparticles. *American Chemical Society Nano*, 4(8):4824–4830.

Wolmarans, C. & Van Aardt, W. 1985. Experimental evidence that copper is taken up by the freshwater snail *Bulinus tropicus* through a process of adsorption. *African Zoology*, 20(4):258–260.

Wu, F., Bortvedt, A., Harper, B.J., Crandon, L.E. & Harper, S.L. 2017. Uptake and toxicity of CuO nanoparticles to *Daphnia magna* varies between indirect dietary and direct waterborne exposures. *Aquatic Toxicology*, 190:78–86.

Wu, F., Harper, B.J., Crandon, L.E. & Harper, S.L. 2020b. Assessment of Cu and CuO nanoparticle ecological responses using laboratory small-scale microcosms. *Environmental Science: Nano*, 7(1):105–115.

Wu, Q., Miao, W., Zhang, Y., Gao, H. & Hui, D. 2020a. Mechanical properties of nanomaterials: A review. *Nanotechnology Reviews*, 9(1):259–273.

Xu, H., Akbari, M.K. & Zhuiykov, S. 2021. 2D semiconductor nanomaterials and heterostructures: controlled synthesis and functional applications. *Nanoscale Research Letters*, 16(1):94.

Xu, L., Xu, M., Wang, R., Yin, Y., Lynch, I. & Liu, S. 2020. The crucial role of environmental coronas in determining the biological effects of engineered nanomaterials. *Small*, 16(36):2003691.

Xu, X., Shi, Y. & Yang, X.L. 2013. Crystal structure of human Seryl-tRNA synthetase and Ser-SA complex reveals a molecular lever specific to higher eukaryotes. *Structure*, 21(11):2078–2086.

Yadav, A.N., Verma, P., Kumar, S., Kumar, V., Kumar, M., Sugitha, T.C.K., Singh, B.P., Saxena, A.K. & Dhaliwal, H.S., 2018. Actinobacteria from rhizosphere: molecular diversity, distributions, and potential biotechnological applications. In: Yadav, M.K. & Singh, B.P., eds. *New and future developments in microbial biotechnology and bioengineering*. Amsterdam, Netherlands: Elsevier. pp. 13–41.

Yadwade, R., Gharpure, S. & Ankamwar, B. 2021. Nanotechnology in cosmetics pros and cons. *Nano Express*, 2(2):022003.

Yang, J.L., Hsien, L., Lee, Y.C. & Chen, H.C. 2008. Effects of fipronil on freshwater shrimp (*Caridina japonica*): Acute toxicity and acetylcholinesterase activity. *Environmental Science*, 3(2):177–180.

Yaqoob, A.A., Ahmad, H., Parveen, T., Ahmad, A., Oves, M., Ismail, I.M., Qari, H.A., Umar, K. & Mohamad Ibrahim, M.N. 2020. Recent advances in metal decorated nanomaterials and their various biological applications: A review. *Frontiers in Chemistry,* 8:341.

Yazdi, M.K., Zarrintaj, P., Bagheri, B., Kim, Y.C., Ganjali, M.R. & Saeb, M.R. 2020. Nanotechnology-based biosensors in drug delivery. In: Mozafari, M., ed. *Nanoengineered Biomaterials for Advanced Drug Delivery: Woodhead Publishing Series in Biomaterials*. Elsevier. pp. 767–779.

Yu, X., Zhang, X., Zhang, P. & Yu, C. 2009. Critical swimming speed, tail-flip speed and physiological response to exercise fatigue in kuruma shrimp, *Marsupenaeus japonicus*. *Comparative Biochemistry and Physiology Part A: Molecular and Integrative Physiology*, 153(2):120–124.

Zachariades, C., Paterson, I.D., Strathie, L.W., Hill, M.P. & Van Wilgen, B.W. 2017. Assessing the status of biological control as a management tool for suppression of invasive alien plants in South Africa. *Bothalia-African Biodiversity and Conservation*, 47(2):1–19.

Zhang, J., He, X., Zhang, P., Ma, Y., Ding, Y., Wang, Z. & Zhang, Z. 2015. Quantifying the dissolution of nanomaterials at the nano-bio interface. *Science China Chemistry*, 58(5):761–767.

Zhang, P., Zhang, X., Li, J. & Huang, G. 2006. Swimming ability and physiological response to swimming fatigue in whiteleg shrimp, *Litopenaeus vannamei*. *Comparative Biochemistry and Physiology Part A: Molecular and Integrative Physiology*, 145(1):26–32.

Zhou, B. 2015. Adverse outcome pathway: framework, application, and challenges in chemical risk assessment. *Journal of Environmental Sciences*, 35:191–193.

Zhou, C., Feng, M., Tang, Y., Yang, C., Meng, X. & Nie, G. 2021. Species diversity of freshwater shrimp in Henan province, China, based on morphological characters and COI mitochondrial gene. *Ecology and Evolution*, 11(15):10502–10514.

Zhou, P., Wang, J., Du, X., Huang, T., Nallathamby, P.D., Yang, L., Zou, W., Zhou, Y., Jault, J., Chen, M. & Ding, F. 2018. Nanoparticles in biomedicine-focus on imaging applications. *Engineered Science*, 5:1–20.

Zhu, Y., Li, J., Li, W., Zhang, Y., Yang, X., Chen, N., Sun, Y., Zhao, Y., Fan, C. & Huang, Q. 2012. The biocompatibility of nanodiamonds and their application in drug delivery systems. *Theranostics*, 2(3):302–312.

Zuo, W., Shahriari, M., Shahriari, M., Javadi, M., Mohebi, H., Abbasi, N. & Ghaneialvar, H. 2021. Synthesis and application of Au NPs-chitosan nanocomposite in the treatment of acute myeloid leukemia *in vitro* and *in vivo*. *Arabian Journal of Chemistry*, 14(2):102929.

APPENDIX A:

ETHICS CERTIFICATE AWARDED BY FNASCREC AS A NO RISK CATEGORY

Private Bag X1290, Potchefstroom
South Africa 2520

Tel: 018 299-1111/2222
Fax: 018 299-4910
Web: http://www.nwu.ac.za

Senate Committee for Research Ethics
Tel: 018 299-4849
Email: nkosinathi.machine@nwu.ac.za

ETHICS APPROVAL LETTER OF STUDY

Based on the review by the **Faculty of Natural and Agricultural Sciences Ethics Committee (FNASREC)**, the Committee hereby clears your study as no ethical risk. This implies that the FNASREC grants permission that, provided the general conditions specified below are met, the study may be initiated, using the ethics number below.

Study title: Sublethal effects of nanodiamonds and copper oxide on the freshwater shrimp, Caridina nilotica.
Study Leader/Supervisor: Prof V Wepener
Student: NS Donough

Ethics number:	N	W	U	-	0	0	5	2	8	-	2	1	-	A	9
	Institution				Study Number						Year			Status	

Status: S = Submission; R = Re-Submission; P = Provisional Authorisation; A = Authorisation

Application type: Single **Risk Category:** **No Risk**
Commencement date: 01/02/2021
Expiry date: 31/12/2023

General conditions:
The following general terms and conditions apply:

- *The commencement date indicates the date when the study may be started.*
- *In the interest of ethical responsibility, the NWU-SCRE and FNASREC reserves the right to:*
  - *request access to any information or data at any time during the course or after completion of the study;*
  - *to ask further questions, seek additional information, require further modification or monitor the conduct of your research or the informed consent process;*
  - *withdraw or postpone approval if:*
    - *any unethical principles or practices of the study are revealed or suspected;*
    - *it becomes apparent that any relevant information was withheld from the FNASREC or that information has been false or misrepresented;*
    - *submission of the annual (or otherwise stipulated) monitoring report, the required amendments, or reporting of adverse events or incidents was not done in a timely manner and accurately; and / or*
    - *new institutional rules, national legislation or international conventions deem it necessary.*
- *FNASREC can be contacted for further information or any report templates via Roelof.Burger@nwu.ac.za 018 299 4269*

The FNASREC would like to remain at your service as scientist and researcher, and wishes you well with your study. Please do not hesitate to contact the FNASREC or the NWU-SCRE for any further enquiries or requests for assistance.

Yours sincerely,

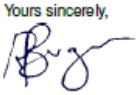

Prof Roelof Burger
Chairperson Faculty of Natural and Agricultural Sciences Ethics Committee (FNASREC)

File reference: 9.1.5.4.2

Page 1 of 1

APPENDIX B:

COMPOSITION OF FOOD FOR *C. AFRICANA* AS STATED BY DENNERLE'S WEBSITE

Shrimp King Complete

Composition: kelp, insect proteins, dandelion, stinging nettle, spinach, mulberry leaves, chlorella, montmorillonite, moringaoleifera, rosemary, mannanoligosaccarides, ß-glucans, flower pollen, turmeric, cinnamon

Analytical components: 24,6% crude protein, 6,0% crude fat, 7,7% crude fiber, 15,4% crude ash https://dennerle.com/en/products/food/invertebrates-food/shrimp-king-complete/

Shrimp Baby

Composition: insect proteins, wheat flour, wheat protein, krill meal, squid meal, spinach, corn, yeast, betaine, kale, inulin, salmon oil, Moringa oleifera, spirulina algae, garlic, mannanoligosaccarides, ß-glucans Additives per kg: Colorants: 250 mg E 161j astaxanthin Analytical components: 49,5% crude protein, 10,2% crude fat, 4,4% crude fiber, 6,4% crude ash https://dennerle.com/en/products/food/invertebrates-food/shrimp-king-baby/

Shrimp Color

Composition: insect proteins, wheat flour, wheat proteins, krill, squid meal, spinach, corn, yeast, betaine, kale, inulin, krill oil, moringa oleifera, spirulina algae, garlic, mannanoligosaccarides, ß-glucans

Additives per kg: Colorants: 500 mg 2a161j astaxanthin, 300 mg 2a161g canthaxanthin, 300 mg E 160a beta-carotene Analytical components: 48.5% crude protein, 10.0% crude fat, 4.4% crude fiber, 6.2% crude ash https://dennerle.com/en/products/food/invertebrates-food/shrimp-king-color/

Shrimp Mineral

Supplementary feed for ornamental shrimps.

Composition: kelp, insect proteins, dandelion, stinging nettle, spinach, mulberry leaves, calcium carbonate, chlorella, montmorillonite, moringa oleifera,

rosemary, mannanoligosaccarides, ß-glucans, flower pollen, turmeric, cinnamon

Analytical components: 21.0% crude protein, 6.0% crude fat, 8.0% crude fiber, 26.0% crude ash

https://dennerle.com/en/products/food/invertebrates-food/shrimp-king-mineral/

Shrimp Protein

Composition: Bacterial protein from Corynebacterium glutamicum, insect proteins, stinging nettles, dandelion, mulberry leaves, Daphnia, krill, chlorella algae, montmorillonite, moringa oleifera, rosemary, mannanoligosaccarides, ß-glucans, flower pollen, turmeric, cinnamon

Analytical components: 42,6 % crude protein, 7,5 % crude fat, 5,9 % crude fiber, 13,4 % crude ash

https://dennerle.com/en/products/food/invertebrates-food/shrimp-king-protein/

Shrimp Snow Pops

Composition: Soy bran

Analytical components: Crude protein 13.4%, crude fat 4.2%, crude fiber 32.9%, crude ash 4.8%.

https://dennerle.com/en/products/food/invertebrates-food/shrimp-king-snow-pops/

APPENDIX C:

METABOLITES AND THEIR SIGNIFICANT VALUES OBTAINED USING METABOANALYST

Control vs nCuO LC_{10}					
Compound	***p*-value**	***d*-value**	**Compound**	***p*-value**	***d*-value**
2,5-Bis((trimethylsilyl)oxy)pyrazine	0.032	1.332	d-Mannose	0.050	1.116
2'-Desoxyuridine	0.025	1.575	Gluconic acid	0.032	1.275
5-Ethyl-1-(4-[(trimethylsilyl)oxy]-3-{[(trimethylsilyl)oxy]methyl}tetrahydrofuran-2-yl)pyrimidine-2,4(1H,3H)-dione	0.009	1.878	Glucopyranose	0.008	2.010
5-Methyluridine	0.009	1.801	Glyceric acid	0.026	1.464
9H-Purin-6-ol	0.023	1.747	L-Lysine	0.010	1.651
9-Tetradecenoic acid	0.013	1.726	Putrescine	0.016	1.901
a-D-Glucopyranose	0.006	2.294	Serine	0.044	1.198
a-L-(-)-Fucopyranose	0.017	1.464	Stearic acid	0.035	1.473
Cadaverine	0.008	1.785	Uridine	0.049	1.230
D-Lyxose	0.017	1.619			
Control vs nCuO LC_{20}					
11-Eicosenoic acid	0.043	1.231	Glucopyranose	0.002	2.194
2'-Desoxyuridine	0.006	1.737	Heptadecanoic acid	0.043	1.325
4-Aminobutanoic acid	0.000	2.677	L-5-Oxoproline	0.049	1.056
5-Methyluridine	0.016	1.437	L-Lysine	0.014	1.520
9,12-Octadecadienoic acid	0.028	1.351	L-Methionine	0.000	3.151
9H-Purin-6-ol	0.019	1.683	L-Proline	0.004	1.863
9-Tetradecenoic acid	0.002	1.994	l-Prolylglycine	0.005	2.005
a-D-Allopyranose	0.040	1.120	L-Rhamnose	0.000	3.802
a-D-Glucopyranose	0.000	2.642	L-Serine	0.012	1.457
a-L-(-)-Fucopyranose	0.019	1.375	Myristic acid	0.003	2.074
Arachidonoyl amide	0.004	1.766	N-Acetyl-D-glucosamine	0.001	3.004
Benzenepropanoic acid, a-(methoxyimino)-, trimethylsilyl ester	0.003	2.320	Oleic Acid	0.042	1.081
Benzenepropanoic acid, a-(methoxyimino)-4-	0.047	1.058	Pentanedioic acid	0.019	1.443

[(trimethylsilyl)oxy]-, trimethylsilyl ester					
Cadaverine	0.000	2.934	Phosphoric acid	0.001	2.348
D-(-)-Ribofuranose	0.002	2.777	Putrescine	0.011	2.072
D-Arabinose	0.021	1.667	Ribitol	0.001	3.162
DL-Phenylalanine	0.017	1.380	Serine	0.009	1.611
D-Lyxose	0.000	3.018	Stearic acid	0.004	1.818
d-Mannose	0.004	2.148	Tyrosine	0.006	1.693
Gluconic acid	0.002	2.287	Uracil	0.000	4.661
Control vs ND LC_{10}					
D-(-)-Ribofuranose	0.023721	1.325881	Uridine	0.014778	1.627292
L-Rhamnose	0.004444	2.095552			
Control vs ND LC_{20}					
4-Aminobutanoic acid	0.048331	1.334	Myristic acid	0.036118	1.303373
9-Tetradecenoic acid	0.027707	1.331582	Phosphoric acid	0.004637	1.947964
Cadaverine	0.000792	2.588749	Tridecanoic acid	0.049338	1.161012
Methyl stearate	0.024195	1.494953	Uracil	0.023719	1.290032
nCuO LC_{10} vs nCuO LC_{20}					
2,5-Bis((trimethylsilyl)oxy)pyrazine	0.049061	1.359569	L-Threonine	0.045037	1.212389
Benzenepropanoic acid, a-(methoxyimino)-, trimethylsilyl ester	0.015024	1.667084			
ND LC_{10} vs ND LC_{20}					
9-Tetradecenoic acid	0.020678	1.37221	Methyl stearate	0.018	1.383449
Arachidic acid	0.011744	2.044485	Myo-Inositol	0.008906	1.818867
Cadaverine	0.002938	2.661466	Palmitelaidic acid	0.043976	1.426497
D-(-)-Ribofuranose	0.025926	1.653827	Putrescine	0.036161	1.525399
Glyceric acid	0.043551	1.322737	Thymidine	0.004548	2.130974
L-Rhamnose	0.020618	1.42144	Uracil	0.034923	1.453446
L-Serine	0.024072	1.44518			
nCuO LC_{10} vs ND LC_{10}					
			Glucopyranose	0.038	1.218
2'-Desoxyuridine	0.025	1.650	Glyceric acid	0.003	1.990
5-Ethyl-1-(4-[(trimethylsilyl)oxy]-3-{[(trimethylsilyl)oxy]methyl}tetrahydrofuran-2-	0.035	1.171	Heptadecanoic acid	0.006	2.204

yl)pyrimidine-2,4(1H,3H)-dione					
9H-Purin-6-ol	0.049	1.169	L-Proline	0.017	1.533
9-Tetradecenoic acid	0.011	1.680	l-Prolylglycine	0.044	1.206
a-D-Glucopyranose	0.001	2.915	L-Rhamnose	0.003	2.197
a-L-(-)-Fucopyranose	0.035	1.176	L-Serine	0.016	1.532
Butanedioic acid	0.025	1.560	Palmitelaidic acid	0.037	1.383
Cadaverine	0.025	1.623	Putrescine	0.002	2.375
D-(-)-Ribofuranose	0.016	1.815	Serine	0.031	1.217
Diethylene glycol	0.017	1.611	Stearic acid	0.039	1.453
D-Mannose	0.035	1.277	Tridecanoic acid	0.038	1.527
D-Proline	0.001	3.227	Tyrosine	0.021	1.521
Gluconic acid	0.019	1.526	Uridine	0.000	4.452
nCuO LC_{20} vs ND LC_{20}					
2'-Desoxyuridine	0.038	1.180	L-5-Oxoproline	0.038	1.372
9-Tetradecenoic acid	0.016	1.382	L-Lysine	0.026	1.307
a-D-Glucopyranose	0.042	1.105	L-Methionine	0.045	1.146
DL-Phenylalanine	0.023	1.712	Myristic acid	0.049	1.315
D-Lyxose	0.005	1.816	Palmitic Acid	0.050	1.317
D-Proline	0.044	1.082	Serine	0.013	1.591
Gluconic acid	0.048	1.172	Stearic acid	0.035	1.138
Heptadecanoic acid	0.034	1.389			
Control vs $CuCl_2$ LC_{10}					
2,5-Bis((trimethylsilyl)oxy)pyrazine	0.002	2.748	L-Methionine	0.035	1.274
2'-Desoxyuridine	0.035	1.239	l-Prolylglycine	0.016	1.506
4-Aminobutanoic acid	0.004	2.157	L-Serine	0.044	1.103
5-Dodecenoic acid	0.045	1.065	L-Tryptophan	0.030	1.360
5-Methyluridine	0.006	2.119	Myristic acid	0.023	1.568
9-Tetradecenoic acid	0.005	1.762	N-Acetyl-D-glucosamine	0.035	1.587
a-D-Glucopyranose	0.035	1.579	Oleic Acid (UM129)	0.042	1.490
a-L-(-) Fucopyranose	0.011	1.581	Putrescine	0.044	1.406
Cadaverine	0.013	1.599	Ribitol	0.011	1.972
DL-Phenylalanine	0.028	1.224	Serine	0.038	1.213
D-Lyxose	0.001	2.379	Stearic acid	0.007	1.636

Gluconic acid	0.012	1.714	Uracil	0.015	1.438
Glyceric acid	0.044	1.284			
Control vs $CuCl_2$ LC_{20}					
Gluconic acid	0.03239	1.783095			
$CuCl_2$ LC_{10} vs $CuCl_2$ LC_{20}					
11-Eicosenoic acid	0.009	2.048	D-Proline	0.018	1.403
5-Methyluridine	0.017	1.590	Gluconic acid	0.002	2.823
a-D-Allopyranose	0.046	1.211	N-Acetyl-D-glucosamine	0.015	1.563
DL-Phenylalanine	0.046	1.101	Stearic acid	0.039	1.128
D-Lyxose	0.006	1.760			
$CuCl_2$ LC_{20} vs nCuO LC_{20}					
11-Eicosenoic acid	0.002	2.492	Glucopyranose	0.050	1.092
9-Tetradecenoic acid	0.040	1.107	L-Glutamic acid	0.026	1.586
a-D-Allopyranose	0.013	1.534	L-Proline	0.018	1.373
Glucopyranose	0.039	1.126	L-Serine	0.040	1.114
DL-Phenylalanine	0.026	1.282	Methyl stearate	0.023	1.784
D-Lyxose	0.002	2.103	N-Acetyl-D-glucosamine	0.003	2.147
D-Proline	0.006	1.783	Stearic acid	0.024	1.265
Gluconic acid	0.001	3.240	Tyrosine	0.040	1.115